Universidade de Aveiro
2013
Departamento de Electrónica, Telecomunicações e Informática

Reza Holakouei

Técnicas de pré-codificação para Sistemas Multicelulares Coordenados

Precoding Techniques for Coordinated Multicell Systems

Universidade de Aveiro
2013
Departamento de Electrónica,Telecomunicações e Informática

Reza Holakouei

Técnicas de pré-codificação para Sistemas Multicelulares Coordenados

Precoding Techniques for Coordinated Multicell Systems

Dissertação apresentada à Universidade de Aveiro para cumprimento dos requisitos necessários à obtenção do grau de Doutor em Engenharia Telecomunicações realizada sob a orientação científica do Doutor Atílio Gameiro, Professor Associado do Departamento de Departamento de Electrónica, Telecomunicações e Informática da Universidade de Aveiro e co-orientações do Doutor Adão Silva e Professor Auxiliar do Departamento de Departamento de Electrónica, Telecomunicações e Informática da Universidade de Aveiro.

texto Apoio financeiro da FCT e do FSE no âmbito do III Quadro Comunitário de Apoio.

To my loved ones.

o júri

presidente

Prof. João de Lemos Pinto
professor catedrático da Universidade de Aveiro

Prof. Doutor Francisco António Bucho Cercas
professor associado com agregação do ISCTE – Instituto Universitário de Lisboa

Prof. Doutor Henrique Manuel de Castro Faria Salgado
professor associado da Faculdade de Engenharia da Universidade do Porto

Prof. Doutor Paulo Miguel Nepomuceno Pereira Monteiro
professor associado da Universidade de Aveiro

Prof. Doutor Atílio Manuel da Silva Gameiro
professor associado da Universidade de Aveiro (Orientador)

Prof. Doutor Antonio José Castelo Branco Rodrigues
professor auxiliar do Instituto Superior Técnico da Universidade Técnica de Lisboa

Prof. Doutor Marco Alexandre Carvo Gomes
professor auxiliar da Faculdade de Ciências e Tecnologia da Universidade de Coimbra

Prof. Doutor Adão Paulo Soares Silva
professor auxiliar da Universidade de Aveiro (Coorientador)

agradecimentos

Agradeço aos meus orientadores Prof. Atílio e Adão por todo o apoio e disponibilidade prestados, cujo envolvimento foi fundamental para ultrapassar as diversas dificuldades com que me deparei ao longo deste projecto.
Agradeço aos meus colegas de grupo de trabalho MOBNET pela partilha de ideias e experiências que longo deste período ajudaram a enriquecer este trabalho.
Agradeço à FCT e ao Instituto de Telecomunicações pelo suporte financeiro prestado que tornou este trabalho exequível.
Aos meus pais agradeço a confiança que em mim sempre depositaram, que por vezes me fazem pensar que realmente nada é impossível, e pelo apoio que sempre me deram não só nestes últimos anos como ao longo de toda a minha vida.
Aos meus amigos que me acompanharam nos momentos menos académicos, por estarem ao meu lado sempre que precisei.
Sem todos eles tudo teria sido mais difícil.
A todos o meu obrigado.

palavras-chave

Coordenação/Cooperação Multicelular, Pré-codificação, Alocação de Potência, MIMO, OFDM.

resumo

Coordenação Multicélula é um tópico de investigação em rápido crescimento e uma solução promissora para controlar a interferência entre células em sistemas celulares, melhorando a equidade do sistema e aumentando a sua capacidade. Esta tecnologia já está em estudo no LTE-*Advanced* sob o conceito de coordenação multiponto (COMP). Existem várias abordagens sobre coordenação multicélula, dependendo da quantidade e do tipo de informação partilhada pelas estações base, através da rede de suporte (*backhaul network*), e do local onde essa informação é processada, i.e., numa unidade de processamento central ou de uma forma distribuída em cada estação base.

Nesta tese, são propostas técnicas de pré-codificação e alocação de potência considerando várias estratégias: centralizada, todo o processamento é feito na unidade de processamento central; semi-distribuída, neste caso apenas parte do processamento é executado na unidade de processamento central, nomeadamente a potência alocada a cada utilizador servido por cada estação base; e distribuída em que o processamento é feito localmente em cada estação base. Os esquemas propostos são projectados em duas fases: primeiro são propostas soluções de pré-codificação para mitigar ou eliminar a interferência entre células, de seguida o sistema é melhorado através do desenvolvimento de vários esquemas de alocação de potência. São propostas três esquemas de alocação de potência centralizada condicionada a cada estação base e com diferentes relações entre desempenho e complexidade. São também derivados esquemas de alocação distribuídos, assumindo que um sistema multicelular pode ser visto como a sobreposição de vários sistemas com uma única célula. Com base neste conceito foi definido uma taxa de erro média *virtual* para cada um desses sistemas de célula única que compõem o sistema multicelular, permitindo assim projectar esquemas de alocação de potência completamente distribuídos.

Todos os esquemas propostos foram avaliados em cenários realistas, bastante próximos dos considerados no LTE. Os resultados mostram que os esquemas propostos são eficientes a remover a interferência entre células e que o desempenho das técnicas de alocação de potência propostas é claramente superior ao caso de não alocação de potência. O desempenho dos sistemas completamente distribuídos é inferior aos baseados num processamento centralizado, mas em contrapartida podem ser usados em sistemas em que a rede de suporte não permita a troca de grandes quantidades de informação.

keywords

Multicell Coordination/Cooperation, Precoding, Power Allocation, MIMO, OFDM, Distributed Algorithms.

abstract

Multicell coordination is a promising solution for cellular wireless systems to mitigate inter-cell interference, improving system fairness and increasing capacity and thus is already under study in LTE-A under the coordinated multipoint (CoMP) concept. There are several coordinated transmission approaches depending on the amount of information shared by the transmitters through the backhaul network and where the processing takes place i.e. in a central processing unit or in a distributed way on each base station.

In this thesis, we propose joint precoding and power allocation techniques considering different strategies: Full-centralized, where all the processing takes place at the central unit; Semi-distributed, in this case only some process related with power allocation is done at the central unit; and Full-distributed, where all the processing is done locally at each base station. The methods are designed in two phases: first the inter-cell interference is removed by applying a set of centralized or distributed precoding vectors; then the system is further optimized by centralized or distributed power allocation schemes. Three centralized power allocation algorithms with per-BS power constraint and different complexity tradeoffs are proposed. Also distributed power allocation schemes are proposed by considering the multicell system as superposition of single cell systems, where we define the average *virtual* bit error rate (BER) of interference-free single cell system, allowing us to compute the power allocation coefficients in a distributed manner at each BS.

All proposed schemes are evaluated in realistic scenarios considering LTE specifications. The numerical evaluations show that the proposed schemes are efficient in removing inter-cell interference and improve system performance comparing to equal power allocation. Furthermore, full-distributed schemes can be used when the amounts of information to be exchanged over the backhaul is restricted, although system performance is slightly degraded from semi-distributed and full-centralized schemes, but the complexity is considerably lower. Besides that for high degrees of freedom distributed schemes show similar behaviour to centralized ones.

Table of Content

List of Figures

List of Tables

List of Acronyms

3GPP	3rd Generation Partnership Project
AMPS	Advanced Mobile Phone System
AWGN	Additive White Gaussian Noise
BC	Broadcast Channel
BD	Block Diagonalization
BER	Bit Error Rate
BLAST	Bell lab Layered Space-Time
BPSK	Binary Phase Shift Keying
BS	Base Station
CDMA	Code Division Multiple Access
COFDM	Coded OFDM
CoMP	Coordinated Multipoint
CQI	Channel Quality Indicator
CSI	Channel State Information

CSIR	Channel State Information at Receiver
CSIT	Channel State Information at Transmitter
CTC	Convolutional Turbo Codes
CU	Central Unit
DAS	Distributed Antenna System
DBWS	Distributed Broadband Wireless System
DFT	Descrete Fourier Transform
DMRT	Distributed MRT
DMT	Discrete Multi Tone
DoF	Degrees of Freedom
DPC	Dirt Paper Coding
DQPSK	Differential QPSK
DSL	Digital Subscriber Line
DVSINR	Distributed Virtual SINR
DZF	Distributed ZF
EDGE	Enhanced Data Rates for GSM Evolution
EPA	Equal Power Allocation
ETSI	European Telecommunications Standards Institute
ETU	Extended Typical Urban
FCC	Federal Communication Commission
FDD	Frequency Division Duplex
FDM	Frequency Division Multiplexing
FFT	Fast Fourier Transform
FIR	Finite Impulse Response
GPRS	General Packet Radio Service
GSM	Global System for Mobile Communication
HeNB	Home enhanced Node B

HK	Han-Kobayashi
HNB	Home Node B
HSDPA	High Speed Downlink Packet Access
i.i.d	Independent Identically Distributed
ICI	Inter-Carrier Interference
IMT-2000	International Mobile Telecommunications 2000
IMT-A	IMT Advanced
IMTS	Improved MTS
IRC	Interference Rejection Combining
ISI	Inter-symbol Interference
ITU	International Telecommunication Union
JPU	Joint Processing Unit
KKT	Karush-Kuhn-Tucker
LTC	Long Term Channel
LTE	Long-Term Evolution
LTE-A	LTE-Advanced
MAC	Multiple Access Channel
CMBER	Closed-form Minimum BER
MIMO	Multiple Input Multiple Output
MISO	Multiple Input Single Output
MMSE	Minimum Mean Square Error
MRC	Maximal Ratio Combining
MRT	Maximal Ratio Transmission
MS	Multiple Stream
MTS	Mobile Telephone Service
MVBER	Minimum Virtual BER
NPA	Non Power Allocation

OFDM	Orthogonal Frequency Division Multiplexing
OFDMA	Orthogonal Frequency Division Multiple Access
OPA	Optimal Power Allocation
O-STBC	Orthogonal STBC
PAPR	Peak to Average Power Ratio
PC	Power Constraint
PDC	Personal Digital Cellular
Pdf	Probability Density Function
PMI	Precoding Matrix Indicator
PRB	Physical Resource Block
PSD	Power Spectral Density
QAM	Quadrature Amplitude Modulation
QoE	Quality of Experience
QoS	Quality of Service
QO-STBC	Quasi Orthogonal STBC
QPSK	Quadrature Phase Shift Keying
RAT	Radio Access Technology
RF	Radio Frequency
RoF	Radio over Fibre
SCME	Spatial Channel Model Extended
SER	Symbol Error Rate
SF	Space-Frequency
SFN	Single Frequency Network
SIC	Successive Interference Cancellation
SINR	Signal to Interference and Noise Ratio
SISO	Single Input Single Output
SLNR	Signal to Leakage and Noise Ratio

SM	Spatial Multiplexing
SNR	Sigal to Noise Ratio
SOCPA	Suboptimal Closed-form Power Allocation
SOIPA	Suboptimal Iterative Power Allocation
SS	Single Stream
STBC	Space-Time Block Code
STTC	Space-Time Trellis Code
SU-MIMO	Single User MIMO
SVD	Singular Value Decomposition
TACS	Total Access Communications Systems
TCM	Trellis Coded Modulation
TDD	Time Division Duplex
TDMA	Time Division Multiple Access
TD-SCDMA	Time Division SCDMA
THP	Tomlinson-Harashima Precoding
TPC	Total Power Constraint
SCDMA	Synchronous Code Division Multiple Access
UMTS	Universal Mobile Telephone System
UT	User Terminal
VBER	Virtual BER
V-BLAST	Vertical BLAST
WC	Worst Case
WiMAX	Worldwide Interoperability for Microwave Access
WLAN	Wireless LAN
WMAN	Wireless Metropolitan Area Network
ZF	Zero Forcing

List of Symbols

$a_i(t,\tau)$	Amplitude of complex channel attenuation
a_R	Channel envelop
A_k	Interference term in downlink
b	Transmit antenna index
B	Number of BSs
B_c	Coherence bandwidth
B_k	Interference term in uplink
B_x	Bandwidth of received signal
B_m	Maximum transmission bandwidth
B_{OFDM}	Total passband OFDM bandwidth
c	Velocity of light
$conv(.)$	Convex hull operator
$CN(.,.)$	Circular symmetric Gaussian distribution

$\mathbf{d}$	Non-local channel terms
d_i	Obstacle distance
$d_{\min}$	Minimum distance of separation of constellation points
d_t	Transmission distance
$d(.)$	Arbitrary manipulation of transmit symbols
e_k	Interfering signal at UT k
$E\{.\}$	Expectation
E_s	Transmit symbol energy
f_c	Carrier frequency
f_m	Magnitude of maximum Doppler shift
g_a	Array gain
$g_d^o(\rho)$	Diversity gain at ρ
g_{ki}	Linear equalizer to extract useful signal of symbol i on UT k
g_s	Multiplexing gain
$\mathbf{G}$	Decoder matrix
$h_{I_b}(t)$	Channel I quadrature component
$h_{Q_b}(t)$	Channel Q quadrature component
$h(t)$	Time variant channel impulse response
$h_b(t)$	Complex baseband representation of $h(t)$
H_e	Effective channel
$\mathbf{H}$	MIMO channel matrix
$\mathbf{H}_k^b$	Sub-portion of channel between all BSs and UT k
$\tilde{\mathbf{H}}_k$	Concatenated channel missing channel of UT k

I	Mutual information
$\mathbf{I}$	Identity matrix
$J_0(.)$	Zero order Bessel function of first kind
J_c	Lagrangian function
k	User index
k_0	Constant from Friss expression
K	Number of UTs
K_b	Set if UTs served by BS b
L	Channel taps
$\tilde{L}_k$	Rank of $\tilde{\mathbf{H}}_k$
$\mathbf{n}$	Noise vector
$\tilde{\mathbf{n}}$	Noise vector after decoding
N_c	Number of OFDM subcarriers
N_r	Total number of receive antennas in Multicell system
N_{r_k}	Number of antennas at receive equipment
N_t	Total number of transmit antennas in Multicell system
N_{t_b}	Number of antennas at transmit equipment
$\bar{N}_e$	Number of nearest neighbors in constellation
p	Transmit power
P_e	Error probablity
$p_s(s)$	Fading distribution
P_t	Total transmit power
P_{tb}	Total transmit power per-BS
Q	Number of symbols for STBC

Q_b	Active beam to serve one UT
$Q(.)$	Q function
$r(.)$	Rank of matrix
r_s	Spatial multiplexing rate of STBC
R	Capacity
$\mathbf{R}$	Correlation matrix
$R(\rho)$	Transmission rate at ρ
$\mathbf{R}_{yy,k}$	Covariance matrix of received signal
s	Channel amplitude
$S\{.\}$	Possible set selection
t	Time index
$tr(.)$	Trace of a matrix
T_c	Coherence time
T_m	Minimum signal duration which frequency dispersion become noticeable
T_U	Useful symbol duration
T_x	Duration of received signal
v	Vehicular velocity
$vec(.)$	Vector operation
$\mathbf{V}_{k,i}$	Covariance matrix of symbols received by UT k
$\mathbf{w}$	Precoder vector
$\mathbf{W}$	Precoder matrix
$\mathbf{W}_k^b$	Sub-portion of precoder between all BSs and UT k
W_0	Lambert function of index 0

$\mathbf{x}$	Transmitting symbols
$\tilde{\mathbf{x}}$	Received signal after decoding
$\mathbf{y}$	Received signal
$\mathbf{z}$	transmitted signal
τ_m	Maximum excess delay of the channel
τ_i	Delay of path i
τ_0	Delay of the first path
χ	Envelop correlation coefficient
Δf	Frequency difference
Δt	Time difference
σ_{DS}^2	Delay spread of channel
Φ	Loss in power of transmitted signal
Φ_{PL}	Path-loss of transmitted signal
Φ_{SF}	Loss in power of transmitted signal due to slow fading
ε	Path-loss exponent
$\phi_i(t,\tau)$	Argument of complex channel attenuation
λ	Carrier wavelength
η	Transmit power scaling factor
$\delta(.)$	Dirac Delta
$\otimes$	Kronecker product
ρ	Average SNR
ρ_{out}	Output SNR
$\|.\|_F$	Frebinious norm
λ	Eigen value of a matrix
Ψ	Transmit covariance

$\bigcup$	Union operator
u	Encoding order
Ω_i^b	Predefined beam set
ω	Beam set size
ζ_k	Interfering noise at UT k
β, ψ	Modulation parameters
δ	Cross-power gain
χ^2	Chi-square distribution
μ	Lagrangian multiplier
$(.)^H$	Hermitian of a vector/matrix
$(.)^T$	Transpose of a vector/matrix

1 Introduction

1.1 Perspective and Motivation

Mobile communication has gained significant importance in today's society. As of 2011, the number of mobile phone subscribers has surpassed 6 billion [1], and the global annual mobile revenue is soon expected to hit USD 1 trillion by 2013 [2].

While these numbers appear promising for mobile operators at first sight, the major game-changer that has come up recently is the fact that the market is more and more driven by the demand for mobile data traffic [3]. This requires the increase of data rates in wireless communications. Consequently the mobile communication is experiencing a rapid and steady growth. It is expected that the demand for wireless services will continue to increase in the near and medium term, asking for more capacity and putting more pressure on the usage of radio resources. This puts mobile operators under the pressure to respond to the increasing quality of experience (QoE) over the area (often referred to as improved fairness), while continuously decreasing cost per bit and addressing the more and more crucial issue of energy efficiency [4].

We have to be aware that current cellular systems are mainly limited by inter-cell interference [5], especially in urban areas where the rate demand is largest and base station (BS) deployment is dense. Hence point-to-point communication link is characterized by a certain ratio of desired receive signal power over interference and noise power, where Shannon [6] states a clear upper bound on the capacity of the link. This then translates to a maximum spectral efficiency, i.e., the maximum data rate achievable for a given bandwidth. Therefore, the increasing rate demand can surely not be met by improving point-to-point links, but requires other innovations. Using more spectrum, utilizing more antennas (multiple-input multiple-output (MIMO) techniques), increasing the degrees of sectorization, using more BSs or introducing relays and micro/femto cells are some consensual solutions.

MIMO techniques take the advantage of multipath fading in wireless communication channels, thus improving the cellular system capacity. However, there is significant correlation between channels of MIMO systems in some environments, and using an antenna array at user terminal (UT) may not be feasible due to size, cost and hardware limitations. Thus, the very high data rates envisioned for next-generation cellular communication systems in reasonably large areas do not appear feasible with the conventional cellular architecture. Another fact with the conventional cellular architecture is that inter-cell interference degrades the gain promised by the MIMO techniques, since the system is essentially interference limited.

While most previously stated options have limitations and require the deployment of new equipment, it is known from theory that interference can be overcome and even exploited if coordination or cooperation between cells is introduced. Such schemes are particularly interesting, as they require a fairly small change of infrastructure, and may lead to a more homogeneous quality of service (QoS) distribution over the area [7].

This thesis presents the results of research on precoding and power allocation schemes, and development of new algorithms to be implemented in coordinated multicell systems in order to mitigate inter-cell interference and thus improve the quality. Finally system performance of the proposed algorithms would be evaluated in realistic scenarios and over the most recent technologies.

This introductory chapter provides a survey of cellular communications, and includes the motivation and objectives of this thesis, as well as the original contributions of this research work. In the next sub-section a very brief overview of the evolution of cellular systems is given. Then, in Section 1.3, we provide a brief introduction and discussion on long-term evolution (LTE) and LTE-Advanced (LTE-A) technologies where the contributions from this thesis can be applied. Following

this system and technology overview, we then identify the objectives defined for this thesis work. Then in section 1.5 we outline the important contributions of this thesis for the advance in the area state of the art. In section 1.6 we explain how the document is organized to present the results of the research work.

1.2 Evolution of Cellular Communications

Public mobile telephone history begins in the 1940s, after World War II. On July 28, 1945, the principles of today wireless cellular systems were first described, in print, by J. K. Jett [8]. Nevertheless, the United States' Federal Communications Commission (FCC) never allocated the spectrum needed for this service. In 1946, AT&T and South Western Bell introduced the Mobile Telephone Service (MTS) [9], at Saint Louis, Missouri [8]. In MTS the traffic was manually routed by an operator, at the central office. Eighteen years later, in 1964, Bell System launched an enhanced version of MTS the Improved Mobile Telephone Service (IMTS) [10], [8]. The IMTS was a full duplex system, unlike MTS, with direct-dial and caller identification.

The first nationwide public radiotelephone system was inaugurated in 1949 by the Dutch National radiotelephone network and the first fully automatic phone system, the Mobile Telephone System A (MTA), was designed by Swedish Telecommunications Administration's Sture Lauhrén and Ragnar Berglund, in 1951, and did not become entirely operational until 1956 [8].

In 1947, at Bell Labs, D. H. Rings, with the help from W. R. Young, clearly proposed the cellular concept for mobile wireless systems in an internal company memorandum [11]. The cellular concepts is based on the divide and conquer principle, namely the main idea behind it is to replace a high-power base station, covering a large geographical area and using all available frequency channels, by a set of low powered base stations, covering a small area, called cell, and using only a subset of all frequency channels. With the help of frequency reuse, BSs in non-adjacent cells could reuse the same set of channels with little interference. However, only thirteen years later, in 1960, the final portrait of the entire wireless cellular system was drawn when two papers, discussing the handoff process, were published in the Institute of Radio Engineers Transactions on Vehicle Communications [8]. Nevertheless, the first commercial cellular radio system, the Metroliner [12], just became operational in 1969.

In Europe, the Analog cellular was also widely accepted. Namely, in 1981, Sweden, Finland, Denmark and Norway began operating the first multinational cellular system, the NMT 450, which offered roaming [8]. In the same decade, Great Britain introduced the Total Access Communications System (TACS), the West German C-Netz, the French Radiocom 2000 and the

Italian RTMI/RTMS. In the United States, the first commercial cellular services began in 1983, using Advanced Mobile Phone Service (AMPS) [13].

The main characteristics of the 1G system are: analog frequency modulation for voice transmission, digital signaling, handover and the use of frequency division multiple access (FDMA) for channel allocation. The increasing diversity of incompatible cellular systems working in Europe led the Europeans to draw a plan to create a single European wide digital mobile service with advanced features and easy roaming [8]. The Global System for Mobile Communications (GSM) [14] was born. GSM has no backward compatibility with previous existing systems and is fully digital. The move from analog to digital clearly defines another major technological step, a turning point to the 2G. The advances made within the area of micro-electronics, in the seventies, with the introduction of the microprocessor, by Intel, and also the development of low-rate digital speech coding techniques, were among the most important contributions to the full development of 2G [13], [14]. With the advent of the 2G systems, the infrastructure and handsets' cost has become lower, the spectral efficiency increased, new services have been offered (such as data, messaging, fax and roaming) and the privacy increased [15]. Unlike Europe, in the US, the newly adopted digital standard, IS-54, had backward compatibility with existing AMPS systems [8]. However, like most 2G systems, it used time division multiple access (TDMA) to separate the channels of different users [8]. Among the most important 2G systems, we have: GSM which started in Europe and is now all over the world, spread around 130 countries, IS-54 in the United States and the Personal Digital Cellular (PDC) in Japan [16].

In the nineties, we started to assist a paradigm shift. Namely, the mobile phone, a device primarily built to make voice calls started to be more and more used to access the Internet, check the email, receiving faxes, etc. Nonetheless, its effectiveness for doing that stuff was, since it and the associated network were not built for data traffic [8]. Consequently, a fundamental change was needed from circuit switching to packet switching, since unlike voice, data is not efficiently handled by circuit switching [8]. To tackle this problem two technologies were developed: General Packet Radio Service (GPRS) and its improvement, Enhanced Data Rates for GSM Evolution (EDGE), well known as 2.5G systems [8]. The 3G systems were designed to add mobility not only to voice but also to the new data applications that were emerging. This new generation of systems has been designated by the International Telecommunications Union (ITU) as International Mobile Telecommunications 2000 (IMT- 2000). In 1991, European Telecommunications Standards Institute (ETSI) standardized Universal Mobile Telecommunications System (UMTS), the European 3G system [8]. UMTS key features include the support to basic modes (frequency division duplex (FDD) and time division duplex (TDD)), variable transmission rates, inter-cell asynchronous operation, adaptive power control, increased coverage and capacity, etc. Other

examples of 3G systems are the American CDMA2000 and the Chinese Time-Division Synchronous Code Division Multiple Access (TD-SCDMA), just to name a few. All these systems were specified by the 3rd Generation Partnership Project (3GPP) [17], all use CDMA technology and offered from 144 kbps (high mobility) to 2 Mbps (low mobility). Nevertheless, with the High-Speed Downlink Packet Access (HSDPA) technology which is considered as enhanced 3G it is possible to achieve up to 42 Mbps. Further speed increases are available with HSPA+, which provides speeds of up to 337 Mbps.

The full deployment of 3G systems has been slow and expensive, since the upgrade from 2G to 3G requires a change of access technology, from time to code division, and a costly infrastructure [8]. In between, 4G has begun to see the light of the day, driven by the steady increase of user requirements unable to be met by the limitations of the current mobile communication systems. Worldwide Interoperability for Microwave Access (WiMAX) and LTE are considered as the two pre-4G technologies, sometimes called 3.9G technologies. Although these two technologies have made a great leap into the 4G world, they have failed to achieve the full vision of the ITU IMT-advanced (IMT-A) project [18]. The key features of IMT-A are [18], [19]:

- improved spectral efficiency and peak rates (100 Mbit/s for high and 1 Gbit/s for low mobility were established as targets for research);
- low latencies;
- ubiquitous Access;
- transparent mobility and worldwide roaming capability;
- low cost and low-complexity terminals;
- high quality mobile services;
- user equipment suitable for worldwide use;
- user-friendly applications, services and equipment;

To comply fully with the IMT-A project specifications LTE-Advanced, the next milestone along the evolution path of LTE, has been developed. LTE and LTE-A use orthogonal frequency division multiplexing (OFDM) as its radio access technology (RAT). The main improvements of LTE-A over LTE Release 8 are [20]:

- Wider bandwidth, enabled by carrier aggregation;
- Advanced multiple input multiple output (MIMO) techniques;
- Support for heterogeneous network;
- Relaying;

- Coordinated multipoint transmission and reception (CoMP);
- LTE Self Optimizing Networks SON enhancements;
- Home Node B (HNB) and Home enhanced Node B (HeNB) mobility enhancements;

1.3 OFDM Systems

OFDM technology was proposed for digital cellular systems in the mid-1980s and it has also been proved to be effective for digital audio and digital video broadcasting in Europe. Moreover, it has been incorporated into standards by the ETSI [21]. The IEEE 802.11 standards group also adopted OFDM modulation for WLANs operating at bit rates up to 30 Mbps at 5 GHz. OFDM has been recently used in 4G technologies such as LTE. OFDM can largely eliminate the effects of inter-symbol interference (ISI) for high-speed transmission rates in very dispersive environments, and it readily supports interference suppression and space-time coding to enhance efficiency. Dynamic packet assignment can support excellent spectrum efficiency and high peak-rate data access.

The basic idea of OFDM is that the total bandwidth is divided into a number of orthogonal tones, over which multiple data symbols are transmitted in parallel. Let us consider the construction of an OFDM signal using tones, where each of the tone signals is a modulated sinusoid at a certain frequency and the frequencies of those tone signals are properly spaced (see section 2.2.2). In this case, all the tone signals are orthogonal to each other in time duration, which is the reciprocal of the tone-frequency spacing. An OFDM symbol is the sum of the tone signals for time duration, preceded by a cyclic prefix, which is a cyclic extension of the tone signals. The introduction of the cyclic prefix ensures that, in a multipath channel, and as long as the delay spread does not exceed that of the cyclic prefix, the multipath replicas of the OFDM symbol at the receiver always have an integer number of sinusoid cycles within the time duration , thereby maintaining the orthogonality at the receiver [22], [23]. OFDM concept will be discussed in more detail in chapter 2.

1.4 Multiple Antenna Systems

In this section we briefly introduce the multiple antenna concept. First we point out the main advantages of using MIMO which are diversity and multiplexing gain, then space-time codes are introduced and finally drawbacks of MIMO channels are mentioned. These concepts will be discussed in more detail in chapter 2.

1.4.1 **Diversity versus Multiplexing Concept**

Diversity is a technique that can dramatically improve system performance, mitigating the effect of fading in a channel. This technique consists in ensuring that the information symbols pass through multiple independent signal paths. Several types of diversity can be identified, such as time, frequency, space or cooperative diversity, depending on the resource through each repetition of information is transmitted, as can be seen in more detail in chapter 2. It is possible to achieve space diversity, or antenna diversity, using multiple antennas in the transmitter and/or receptor. Wireless MIMO channels can be accomplished through systems where several antenna elements are available at the transmitter and receiver side. Seshadri and Winters [24] had proposed two signaling schemes that exploit the availability of multiple antennas at the transmitter to provide diversity benefits in the receiver. The landmark contributions by Telatar [25] and Foschini and Gans [26] have demonstrated that the capacity of a MIMO system exceeds the capacity of a single input single output (SISO) system due to multiplexing gain. They proved that when the number of transmit antennas, N_t, and receive antennas, N_r, increases, the link capacity grows in theory as $\min(N_t, N_r)$. The extra capacity of MIMO systems in comparison with SISO capacity is provided through spatially uncorrelated channels.

Due to the limited inter-antenna space in mobile terminals, caused by limitations in handset designs, the use of multiple transmitting antennas at the BS attracted attentions. Moreover, the use of multiple antennas can provide significant improvements in a system in terms of capacity or diversity, thus the research in this area has evolved in both directions. Diversity techniques, in both transmitter and receiver, can be combined in MIMO systems to improve reliability in communications, though the capacity gain is sacrificed. This leads to the classical spatial multiplexing-diversity tradeoff for multiple antennas, where the amount of diversity and multiplexing gains that can be simultaneously obtained for a richly scattered Rayleigh fading channel are analyzed [27].

1.4.2 **Space-Time Codes for MIMO Systems**

The benefits of MIMO systems led several authors to investigate and examine suitable coding and decoding methods for multi-antenna systems exploring antenna diversity. The association of MIMO concept with space-time coding is commonly used, aiming to increase robustness and flexibility in multimedia transmissions. Foschini [28], Alamouti [29] and Tarokh [30], [31] contributed to the pioneering work on the construction of suitable space-time block codes (STBCs) to apply in multi-antenna systems, so that MIMO systems could be used to achieve diversity and

combat fading using the richness of channels. In a multipath-rich wireless channel, involving multiple antennas at both the transmitter and receiver sides, it is possible to achieve high data rates without increasing the total transmission power or bandwidth.

Among the first developments to design codes that exploit the diversity provided by the use of multiple antennas, lies the work of Foschini and Gans on the Bell lab layered space-time (BLAST) system, known as vertical BLAST (V-BLAST) architecture [28], [26]. The purpose of V-BLAST architecture was to increase capacity while exploring multipath fading. Multiple transmit antennas were used to simultaneously transmit independent data, each one using the same frequency spectrum for every transmission, which leads to high spectral efficiency [28].

The issue of decoding complexity was addressed by Alamouti [29]. The concept of orthogonal space-time block code (O-STBC) emerged from this work. The code suggested by Alamouti is optimal for transmitting signals in a complex modulation alphabet over two independent fading channels. Decoding complexity is the strong point of this code. A linear decoding scheme is applied to both symbols, which estimates them by combining the two channels with maximal ratio combining (MRC). This code has rate one, as it transmits two symbols in two time phases, reaching the maximum diversity order, which is of two, for the two-antenna case. STBCs are generally used when the channel is quasi-static and the diversity achieved with transmission yields the same diversity advantage as MRC.

The concept of space-time trellis code (STTC) arose as an approach that combines ideas of trellis coded modulation (TCM) with a space-time diversity approach, in order to provide additional coding gain to STBCs. They are concatenated with a TCM outer code, which provides coding gain with a reasonable complexity [32]. STTCs were introduced by Tarokh, Seshadri and Calderbank [30] for open-loop transmit diversity, where no side of the channel state information (CSI) is provided by the receiver to the transmitter.

1.4.3 **Drawbacks of MIMO Channels**

If we increase the number of transmitters, the diversity gain for the users located on the cell edges can be increased, but at the same time the interference from the neighboring signals is also increased. High interference from the neighboring signals not only results in decoding complexity but may also reduce the performance. In order to solve this problem, schemes with selective receive antenna or feedback schemes were proposed, where the maximum diversity is only reached if the scheme is combined with the best antenna receiver selection [33], [34], [35].

MIMO channels promise to meet the required spectral efficiency of future wireless communications. However, as immediate consequences the increased transceiver complexity and the correlation between transmit and receive antennas are obtained. A high correlation between the antenna elements reduces the MIMO wireless channel towards that of a single link channel. Therefore, the main challenge that a MIMO communication engineer faces in practice is to design an antenna array with mutually decorrelated antenna elements. Correlation between the antenna elements is not only influenced by the surrounding environment but also by the transceiver hardware design. A dominant plane wave, when arriving at the receiving array, is seen to be highly correlated between array elements, whereas a field resulting from impinging waves from all directions tends to be uncorrelated at a distance approximated to one half of the wavelength of antenna elements [36]. Besides, for line-of-sight communication, the field tends to be highly correlated, thus counteracting the capacity improvement promised by MIMO channels. As for the hardware design, correlation among the antenna elements is observed if their mutual spacing is too small causing electromagnetic coupling [37]. MIMO channels hence promise an increase in capacity only if decorrelated signals are present at the antenna elements. Naturally, physical limitations within the mobile terminal will lead to mutual correlation between the elements thus jeopardizing MIMO capacity bounds [38]. It should be emphasized that interference also degrades the MIMO gains, i.e. diversity and multiplexing gains.

A solution to overcome these problems is to use multicell coordination, which is the scope of this thesis. Coordination of BSs by sharing users' data can be used to achieve better performance. The concept of multicell coordination is introduced in the next section and later will be deeply discussed in chapter 3.

1.5 Multicell Cooperation System

LTE-A has been accepted, by ITU, as beyond 4G technology, in 2010, by complying with or exceeding the ITU established criteria in all aspects. One of the main technologies introduced in LTE-A, which promises to bring increased data rates and system coverage, is CoMP [20], [39]. This concept is introduced in a scenario where BSs are geographically distributed. Every BS or a group of BSs is called a cell. All cells are linked through a backhaul network which enables them to exchange information related to channel or data for UTs. In such a scenario, a UT, at the cell-edge, may receive signals from multiple cells and can also transmit its signal, to be jointly processed, by several cells. Transmission/reception with multicell coordination is illustrated in Fig 1-1.

The way different intervening cells cooperate, and the cell coordination process influences the final performance of the system. Coordinated centralized beamforming approaches, where transmitters exchange both data and CSI for joint signal processing at the CU, promise larger spectral efficiency gains than distributed interference coordination techniques, but typically at the price of larger backhaul requirements and more severe synchronization requirements. For distributed schemes less requirement is needed, such as no or partial information exchange over the backhaul. On the other hand the overall complexity is lower than centralized case, although the performance of the system is degraded because the number of degrees of freedom is less than the centralized case.

The cooperation/coordination can go from simple interference avoidance techniques to full cooperation. In case of non-cooperative downlink transmission scheme, no or very limited explicit cooperation takes place between BSs but interference-aware transmission and reception is performed within cells using fixed beams (i.e., fixed sets of possible precoding vectors) for transmission. In this case the coordination is within a cell which is called intra-cell CoMP. On the other hand, if CoMP involves multiple cells, we deal with inter-cell CoMP [40], [41]. Intra-cell CoMP does not involve the exchange of information through the backhaul, since the communication is within a cell. However, inter-cell CoMP, does need a backhaul infrastructure to pass information between the different cell sites, for cooperation. An interesting CoMP architecture is the one where a set of geographically distributed Remote Radio Units (RRU) are connected by optical fiber to an evolved NodeB (eNB), where all the coordination/processing is done. This architecture can be considered to be in between the intra-cell and the inter-cell architecture, since the coordination process is done in the corresponding site eNB, but the transmission behaves like the inter-cell CoMP. More recently, a similar architecture has been pursued in the FUTON European project [42].

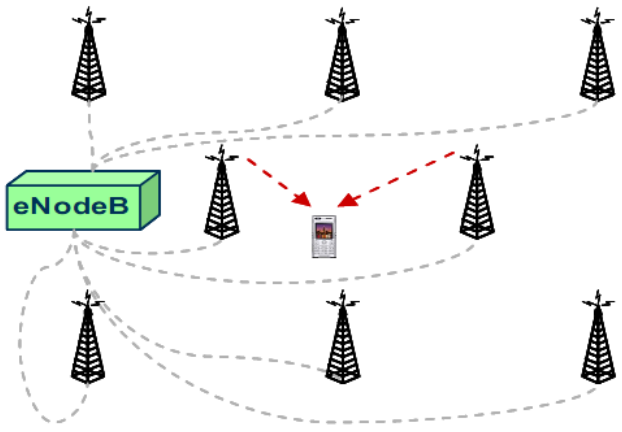

Fig 1-1 Transmission with multicell coordination **[39]**.

1.6 Thesis Objective

The multicell MIMO-OFDM based system can be considered as an ideal infrastructure for future wireless systems promising the provision of high speed and reliable internet access to the moving users of such networks which benefits from multicell coordination concept. The main challenge is such systems are inter-cell interference created by multiple transmissions of symbols from more than one BS to different UTs. Therefore the main objective of this thesis is to propose efficient transmission techniques tailored for downlink of such multicell systems in order to efficiently mitigate inter-cell interference and to further improve specific quality of services such as bit error rate (BER) and user fairness.

The proposed transmission techniques in this work have two phases. First the inter-cell interference is cancelled or mitigated by implementing centralized or distributed linear precoding techniques where the precoding vectors or matrices are computed in central unit (CU) or locally at each BS , respectively, To further improve the system performance centralized and distributed power allocation schemes are proposed based on minimizing BER or virtual BER ,respectivelywhich lead to closed-form and iterative solutions for power elements. Finally, the results from all schemes are compared together in terms of performance and complexity.

1.7 Thesis Contribution

The scientific research work developed in this thesis can be synthesized as follows:

- Proposal of joint centralized ZF precoding and power allocation for downlink of multicell systems to cancel inter-cell interference assuming that all participating BSs have full CSI and data.
- Proposal of optimum and sub-optimum centralized power allocation schemes for previous precoder matrices by minimizing BER which lead to solution based on iterative Lambert function
- Proposal of sub-optimum centralized power allocation for the mentioned precoder matrices by minimizing inverse of SNR from where a novel closed-form solution is obtained.
- Proposal of distributed ZF (DZF) precoding scheme to mitigate the interference assuming the knowledge of local CSI at BSs and full data sharing.
- Proposal of centralized power allocation schemes for previous precoder vectors using minimization of BER and minimization of inverse of SINR criteria.

- Definition the average *virtual* BER by treating the multicell system as a superposition of individual single cell systems.
- Developed a new distributed power allocation scheme for distributed precoded multicell systems that minimizes the average *virtual* BER. The solution is based on Lambert's $W(x)$ function of index 0, $W_0(x)$.
- Derivation of upper and lower bounds for the Lambert's $W_0(x)$ function for $x \geq 0$. These bounds are used to reduce the search space for the optimum solution and therefore efficiently perform the power allocation procedure.

The original publications in International Scientific Journals are listed below, from the earliest to the most recent:

- R. Holakouei, A. Silva, A. Gameiro, "Multiuser precoding techniques for a distributed broadband", *Telecommunication Systems Journal, Special Issue on Mobile Computing and Networking Technologies, Springer, 2011, online, printed version to appear.*
- R. Holakouei, A. Silva , A. Gameiro, "Power allocation strategies for distributed precoded multicell based systems", *Wireless Communications and Networking Journal, EURASIP, vol. 2011, 2011.*
- R. Holakouei, A. Silva, A. Gameiro, "Coordinated Precoding Techniques for multicell MISO-OFDM Networks", *accepted to Wireless Personal Communication (WPC) Journal,Springer 2012.*
- A. Silva, R. Holakouei, D. Castanheira, A. Gameiro and R. Dinis, "A Novel Distributed Power Allocation Scheme for Coordinated Multicell Systems", *accepted to Wireless Communications and Networking Journal, EURASIP, 2013.*

The contributions to International Conferences were the following, which are listed from the earliest to the most recent:

- R. Holakouei, A. Silva, A. Gameiro, "Precoded Multiuser Distributed MIMO OFDM Systems", *in proc. of International Symposium on Wireless Communication Systems (ISWCS), Siena, Italy, 2009*.
- R. Holakouei, A. Silva, A. Gameiro, "Multiuser Precoding and Power Allocation Techniques for Distributed MIMOOFDM Systems" *in proc. of International Conference on Advanced Information Networking and Applications (AINA), Perth, Australia, 2010.*

- R. Holakouei, A. Silva, A. Gameiro, "Power Allocation Strategies for SVD Multicell MIMO-OFDM Based Systems", *in proc. of Wireless Telecommunication Symposium (WTS), New York, USA, 2011.*
- R. Holakouei, A. Silva, A. Gameiro, "Linear Precoding for Centralized Multicell MIMO Networks", *in proc. of IEEE Symposium on Computers and Communications (ISCC), Kerkyra, Greece, 2011.*
- R. Holakouei, A. Silva, A. Gameiro, "Performance Evaluation of Distributed Precoding Schemes for Multicell OFDM Systems ", *in proc. of Vehicular Technology Conference (VTC) fall, San Francisco, USA, 2011.*
- R. Holakouei. A. Silva. A. Gameiro, "Distributed Precoding with Centralized Power Allocation for Multicell OFDM based Systems", *in proc. of Wireless Personal Multimedia Communications Conference (WPMC), Brest, France, 2011.*
- R. Holakouei, A. Silva, A. Gameiro, "Distributed Versus Centralized Zero-Forcing Precoding for Multicell OFDM Systems ", *in proc. of Globecom (GC), Workshop on Distributed Antenna System for Broadband Mobile Communications (DASBMC), Houston, USA, 2011.*
- R. Holakouei, A. Silva, R. Dinis, A. Gameiro, "Distributed Power Allocation Schemes for precoded Multicell MISO-OFDM Systems ",*in proc. of Vehicular Technology Conference (VTC) fall, Quebec, Canada, 2012.*

There is also one contribution to scientific book chapter as follows:

- R. Holakouei, A. Silva, A. Gameiro, "Multicell Cooperation for Future Wireless Systems", *chapter of book entitled* "Wireless Communications", *InTech publications, 2011.*

1.8 Thesis Organization

The main research work developed to reach the previously pointed objectives is presented in the following chapters of this thesis. Its structure is described in this section.

In Chapter 2, "The Fundamental Concepts of Cellular Systems", we present the fundamental of SISO and MIMO channel models as well as diversity and multiplexing gain promised by MIMO. Then we briefly present MIMO techniques such as space-time coding and precoding to improve the system performance. Furthermore, we introduce the concept of OFDM and it benefits to the cellular systems.

In Chapter 3, “Multicell Coordinated Transmission”, we introduce the concept of multicell coordination. Then we derive the bounds on capacity for point to point link and then extend it for MIMO considering full cooperation. Finally a simple beamforming technique with interference rejection combining is introduced where limited partial cooperation and no data sharing is considered.

In Chapter 4, “Full Centralized Cooperation for Multicell MIMO OFDM Systems”, we propose centralized precoding techniques for downlink of multicell systems assuming full CSI and data sharing at the transmitters. Then we further improve the system performance by proposing novel closed-form power allocation for such systems assuming full channel knowledge. Here both precoding and power allocation schemes require full CSI therefore; we call it full centralized transmission scheme. Finally the performance of proposed techniques are numerically evaluated considering some multiuser scenarios.

In Chapter 5, “Distributed Cooperation for Multicell MIMO OFDM Systems”, we propose distributed ZF precoding scheme for downlink of multicell systems assuming only local CSI at transmitter sides and full data sharing. Then we enhance the system performance by prospering two set of power allocation schemes, centralized and distributed which are based on minimization of BER or *virtual* BER, respectively.

Finally, in Chapter 6, “Conclusions and Future Work”, we point out the overall conclusions of this research work and briefly mention the open problems for future work. To have a more clear view of what is proposed in this thesis, table 1.1 shows all proposed techniques by chapter.

Table 1-1 Different classes of multicell cooperation techniques.

	Centralized Power Allocation	Distributed Power Allocation
Centralized Precoding	Full-centralized Schemes (full CSI sharing – full data sharing) – chapter 4	
Distributed Precoding	Semi-distributed Schemes (partial CSI sharing- full data sharing) – chapter 5	Full-distributed Schemes (partial CSI sharing-full data sharing) – chapter 5

1.9 Bibliography

[1] "Wireless subscriber forecasts," ABI Research, June 2010.

[2] "Global Mobile Forcasts to 2014, Worldwide Market Analysis, Strategic Outlook and Forecasts to 2014," Informa Telecoms and Media, 2010.

[3] Cisco, "Cisco Visual Networking Index (VNI) Global Mobile Data Trafic Forcast Update 2009-2014," Feb. 2010.

[4] A. Fehske, J. Malmodin and G. Fettweis, "The global carbon footprint of mobile communications - the ecological and economic perspective," *IEEE Comms. Magazine,* vol. 49, issue 8, p. 55-62, Nov. 2010.

[5] P. Kumar and P. Gupta, "The capacity of wireless networks," *IEEE Trans. on Inf. Theory,* vol. 46, no. 2, p. 388–404, Mar. 2000.

[6] C. Shannon, "A mathematical theory of communication," *Bell System Technical Journal,* vol. 27, p. 379–423 and 623–656, 1948.

[7] P. Marsch, S. Khattak and G. Fettweis, "A framework for determining realistic capacity bounds for distributed antenna systems," in *IEEE Inf. Theory Workshop (ITW'06)*, Oct. 2006.

[8] T. Farley, "Mobile telephone history," Teletronikk, 2005.

[9] J. A. C. Peterson, "Vehicle Radiotelephony Becomes a Bell System Practice," Bell Laboratories Record, Apr. 1947.

[10] V. A. Douglas, "The MJ Mobile Radio Telephone System," Bell Laboratories Record, Dec. 1964.

[11] D. Roessner, "The role of NSF's Support of Engineering in Enabling Technological, chapter 4: The Cell Phone. Final Report to the National Science Foundation," Bell Laboratories Record Technical Memorandum, Dec. 1947.

[12] C. Paul, "Telephones Aboard the Metroliner," Bell Laboratories Record, 77, March, 1969.

[13] J. Padgett, C. Gunther and T. Hattori, "Overview of wireless personal communications," *IEEE Communications Magazine,* vol. 33, no. 1, pp. 28-41, Jan. 1995.

[14] M. Mouly and M. Pautet, "Mobile Communications Advanced Systems and Components," *Springer,* vol. 783, pp. 13-20, 1994.

[15] R. Bekkers and J. Smits, Mobile telecommunications: standards, regulation, and applications, Artech House, 1999.

[16] T. Rappaport, Wireless Communications: Principles and Practice, Prentice Hall, 1996.

[17] "Third Generation Partnership Project," [Online]. Available: http://www.3gpp.org.

[18] "ITU, Visions, Framework and Overall Objectives of the Future Development of IMT-2000 and Systems Beyond IMT-2000," ITU-R, Rec. ITU-R M.1645, Jun. 2003.

[19] "Background on IMT-Advanced," IMT-ADV, May 2008.

[20] "Introducing LTE-Advanced," Agilent, Mar., 2011.

[21] L. J. Cimini, "Analysis and simulation of a digital mobile channel using orthogonal frequency division multiplexing," *IEEE Transactions on Communications,* vol. 33, no. 7, pp. 665-675, July 1985.

[22] R. Laroia, S. Uppala and J. Li, "Designing a mobile broadband wireless access network," *IEEE Signal Processing Magazine,* vol. 21, no. 5, pp. 20-28, Sep. 2004.

[23] H. Liu and G. Li, OFDM-based broadband wireless networks, New York, NY, USA: Wiley-Interscience, 2005.

[24] N. Seshadri and J. H. Winters, "Two signaling schemes for improving the error performance of frequency-division-duplex transmission systems using transmitter antenna diversity," in *43rd IEEE Vehicular Technology Conference (VTC'93 Spring)*, May 1993.

[25] E. Telatar, "Capacity of multi-antenna Gaussian channels.," *European Trans. on Telecomms.,* vol. 10, no. 6, p. 585–595, Nov. 1999.

[26] G. J. Foschini and M. J. Gans, "On limits of wireless communications in a fading environment when using multiple antenna," *Wireless Personal Communication Magazine,* vol. 6, no. 3, pp. 311-335, Mar. 1998.

[27] L. Zheng and D. N. C. Tse, "Diversity and multiplexing: A fundamental trade-off in multiplexing antennas," *IEEE Transactions on Information Theory,* vol. 49, no. 5, pp. 1073-1095, May 2003.

[28] G. Foschini, "Layered space–time architecture for wireless communication in a fading environment when using multi-element antennas," Bell Labs Tech. J., Autumn 1996.

[29] S. Alamouti, "A Simple Transmit Diversity Technique for Wireless Communications," *IEEE Journal on Selected Areas in Communications,* vol. 16, no. 8, p. 1451–1458, Oct. 1998.

[30] V. Tarokh, N. Seshadri and A. Calderbank, "Space–time codes for high data rate wireless communication: Performance criterion and code construction," *IEEE Trans. Inform. Theory,* vol. 44, no. 3, p. 744–765, Mar. 1998.

[31] V. Tarokh, H. Jafarkhani and A. Calderbank, "Space time block codes from orthogonal design," *IEEE Transactions on Information Theory,* vol. 45, no. 5, pp. 1456-1467, Jul. 1999.

[32] G. Ungerboeck, "Channel coding with multilevel/phase signals," *IEEE Transactions on Information Theory,* vol. 28, no. 1, pp. 55-67, Jan. 1982.

[33] L. Liu, S. Kim and M. Lim, "An efficient selective receiver for STBC scheme," in *IEEE International Conference on communications (ICC'07)*, Glasgow, Jun. 2007.

[34] J. Li, U. Park and S. Kim, "An efficient rate one STBC scheme with 3 transmit antennas," in 4th International Conference on Wireless Communications, Networking and Mobile Computing (WiCOM'08), Dallian, China, Oct. 2008.

[35] Y. Yu, S. Keroueden and J. Yuan, "Closed-loop extended orthogonal STBC for three and four transmit antennas," *IEEE Signal Processing Letters,* vol. 13, no. 5, May 2006.

[36] B. Vucetic and J. Yuan, Space-Time Coding, John Wiley & Sons, Inc., 2003.

[37] C. Balanis, Antenna Theory, John Wiley & Sons, Inc., 1997.

[38] F. H. P. Fitzek and M. D. Katz, Cooperation in Wireless Networks: Principles and Applications, Netherlands: Springer, 2006.

[39] S. Parkvall, E. Dahlman, A. Furuskar, Y. Jading, M. Olsson, S. Wanstedt and K. Zangi, "LTE-Advanced - Evolving LTE towards IMT-Advanced," in *Vehicular Technology Conference (VTC)*, 2008.

[40] M. Sawahashi, Y. Kishiyama, A. Morimoto, D. Nishikawa and M. Tanno, "Coordinated multipoint transmission/reception techniques for LTE-advanced [Coordinated and Distributed MIMO]," *IEEE Wireless Communications,* vol. 17, no. 3, pp. 26-34, Jun. 2010.

[41] R. Irmer, H. Droste, P. Marsch, M. Grieger, G. Fettweis, S. Brueck, H. P. Mayer, L. Thiele and V. Jungnickel, "Coordinated multipoint: Concepts, performance, and field trial results," *IEEE Communications Magazine,* vol. 49, no. 2, pp. 102-111, Feb. 2011.

[42] "Fibre optic networks for distributed, extendible heterogeneous radio architectures and service provisioning. FUTON project," [Online]. Available: http://www.ict-futon.eu.

2 Fundamental Concepts of Cellular Systems

In this chapter we introduce some of the basic literature concepts of wireless communications, which are needed to understand the proposed work. The chapter reviews the relevant models for channel characterization and provides the main background required for the understanding of MIMO communications, extending the basic overview provided in Chapter 1. Furthermore, the concept of OFDM is introduced and its benefits to the cellular systems are emphasized.

2.1 Introduction to Multi-antenna Communication

In this section first we present the history of array processing briefly then in section 2.1.2 relevant SISO and MIMO channel models are presented. Section 2.1.3 presents diversity and multiplexing gain obtained using MIMO system. In Section 2.1.4 open-loop techniques such as space-time coding are

introduced. After that in section 2.1.5 some closed-loop (e.g. precoding) techniques for MIMO system are presented.

2.1.1 Brief History of Array Processing

Wireless system designers are facing a number of challenges. These include the limited availability of the radio frequency spectrum and a complex space–time varying wireless environment. In addition, there is an increasing demand for higher data rates, better quality of service, and higher network capacity. In recent years, MIMO systems have emerged as almost promising technology in these measures. MIMO communication systems can be defined intuitively [1], [2] by considering that multiple antennas are used at the transmitting end as well as at the receiving end. The core idea behind MIMO is that signals sampled in the spatial domain at both ends are combined is such a way that they either create effective multiple parallel spatial data pipes (therefore increasing the data rate), and/or add diversity/multiplexing to improve the quality of the communication in terms of error probability.

Clearly, the benefits from multiple antennas arise from the use of a new dimension i.e. space. Hence, because the spatial dimension comes as a complement to time (the natural dimension of digital communication data), MIMO technology is also known as 'space–time' wireless or 'smart' antennas. Until the 1990s, the use of antenna arrays at one end of the link was mainly oriented to the estimation of directions of arrival as well as diversity, leading to beamforming and spatial diversity. Beamforming is a powerful technique which increases the link signal to noise ratio (SNR) through focusing the energy into desired directions. The concept of spatial diversity is that, in the presence of random fading caused by multipath propagation, the SNR is significantly improved by combining the output of decorrelated antenna elements. The early 1990s witnessed new proposals for using antenna arrays to increase the capacity of wireless links, creating enormous opportunities beyond just diversity. It turned out that diversity was only a first step to mitigate multipath propagation. With the emergence of MIMO systems, multi paths were effectively converted into a benefit for the communication system. MIMO indeed takes advantage of random fading, and possibly delay spread, to multiply transfer rates. Paulraj and Kailath [3] introduced a technique for increasing the capacity of a wireless link using multiple antennas at both ends. The prospect of dramatic improvements in wireless communication performance at no cost of extra spectrum was further illustrated in the now famous paper by Telatar [4]. Simultaneously, Bell Labs developed the so-called BLAST architecture [5] that achieved spectral efficiencies up to 10–20 bits/s/Hz, while the first space–time coding architectures appeared [6].The MIMO success story had begun. Today, MIMO appears as an ideal technology for large-scale commercial wireless products such as wireless local area, 3G and 4G technologies such as LTE and LTE-A.

2.1.2 Wireless Channel Models

Radio channel modeling is of extreme importance to the performance evaluation of wireless communications, thus the classification of channels in terms of time and frequency is presented in this section. Some of the main channel models that can be used in communication analysis are also described.

2.1.2.1 SISO Channel Modeling

Classification of Channels Concerning Time and Frequency

Time dispersion and frequency-selective fading are both manifestations of multipath propagation with delay spread and each one implies the presence of the other. Time dispersion extends such a signal in time that the duration of the received signal is greater than that of the transmitted signal. The minimum transmission bandwidth at which time dispersion is observable, B_m, is inversely proportional to the maximum excess delay of the channel, τ_m . Relation between both variables depends on the system. The constant of proportionality usually used is 1/4, resulting in the relation.

$$B_m = \frac{1}{4\tau_m} \tag{2.1}$$

where the maximum excess delay is obtained by

$$\tau_m = \max_i \left(\tau_i - \tau_0 \right) \tag{2.2}$$

τ_i is the delay of i^{th} path and τ_0 is the delay of the first arrival path.

Frequency-selective fading filters attenuate certain frequencies of the transmitted signal more than others. If the bandwidth of the transmitted signal is sufficiently narrow, then all the transmitted frequency components will receive about the same amount of attenuation, having no frequency selective fading [7].

A measure of the transmission bandwidth at which distortion becomes appreciable is often based on the channel coherence bandwidth. The coherence bandwidth, B_c, indicates the minimum frequency separation needed so that the attenuation of the amplitudes of two frequency components becomes decorrelated. The coherence bandwidth can also be regarded as the maximum frequency separation for which propagation conditions are strongly correlated. Formally, the coherence bandwidth is the bandwidth for which the auto co-variance of the signal amplitudes at two extreme frequencies reduces 3 dB. A measurement of decorrelation is the value of envelope correlation coefficient, $\chi\left(\Delta f, \Delta t\right)$. The

frequency components become decorrelated when this coefficient takes the target value of 0.5, that is $\chi(B_c, 0) = 0.5$ [7].

The envelope correlation coefficient for the two signals separated by Δf Hz and Δt seconds, for a Rayleigh-model and assuming that the delay profile has an exponential shape and the incident power is isotropically distributed, is equal to

$$\chi(\Delta f, \Delta t) = \frac{J_0^2(2\pi\Delta t)}{1 + (2\pi\Delta f)^2 \sigma_{DS}^2} \tag{2.3}$$

where $J_0(.)$ is the zero order Bessel function of the first kind, and σ_{DS}^2 is the delay spread of the channel. To observe the decorrelation of two signals as their frequency separation is increased, Δt is set equal to zero in (2.3), which gives the frequency correlation function in the expression that follows

$$\chi(\Delta f, 0) = \frac{1}{1 + (2\pi\Delta f)^2 \sigma_{DS}^2} \tag{2.4}$$

The correlation bandwidth is thus obtained from (2.4) for the target of 0.5 resulting in the following expression

$$B_c = \frac{1}{2\pi\sigma_{DS}} \tag{2.5}$$

Frequency dispersion and time-selective fading appear in time variant channels, due to Doppler spreading. Frequency dispersion results in the signal bandwidth being stretched, so that the received bandwidth of the signal is different from that of the transmitted signal. The minimum signal duration at which frequency dispersion becomes noticeable, T_m, is given by

$$T_m = \frac{1}{4 f_m} \tag{2.6}$$

where f_m is the magnitude of the maximum Doppler shift experienced by the signal. The maximum Doppler shift for a vehicular velocity of v is represented by $f_m = v/c$, with c representing the velocity of light. Time selective fading can cause signal distortion, because the signal may change its characteristics while the signal is being transmitted.

A signal is said to have a short duration when it is passed through the channel before any significant change in the channel characteristics can take place. As the signal duration is increased, the channel is able to change while the signal is still in transmission, thereby causing distortion. We can estimate the duration of the transmitted signal at which distortion becomes noticeable, by referring to it as the channel coherence time, T_c. Analogously to the channel coherence bandwidth, the coherence time is defined by $\chi(0,T_c)=0.5$. To observe the decorrelation of two signals as their time separation is increased, Δf is set equal to zero in (2.3), resulting in the expression

$$\chi(0,\Delta t)=J_0^2(2\pi\Delta t) \tag{2.7}$$

Setting (2.7) to 0.5 we obtain an approximation for coherence time presented as

$$T_c=\frac{J_0^2(2\pi\Delta t)}{2}\approx\sqrt{\frac{9}{16\pi f_m^2}} \tag{2.8}$$

which indicates the maximum time duration for which propagation conditions are strongly correlated [7].

The coherence time and coherence bandwidth are properties of a channel and may be used to know how a transmitted signal will be affected according to its bandwidth and time duration. These classifications, related to the bandwidth and the duration of the transmission signal are summarized in Fig 2-1. They emphasize the differences between distorting and dispersive channels. The shaded area of the figure indicates the physical restriction that limits the time-bandwidth product of a signal to be less than $1/2$. T_x is the duration of the received signal, obtained by the transmitted signal duration added to channel delay spread. Similarly, B_x is the bandwidth of the received signal. Therefore, through Fig 2-1 and according to the above explanation we easily obtain the classification of the channel in terms of time and frequency. This is made by comparing the bandwidth of transmission with B_c and B_m and the signal duration with T_c , and T_m . If the bandwidth of a transmission is less than the coherence bandwidth of the channel, the channel does not have a frequency selective fading and distortion time. The channel is viewed as having a flat response across the transmission band and is therefore referred to as being frequency-flat. Similarly, if the duration of the received signal is less than the coherence time, the channel is constant for the duration of the signal transmission. For this reason the channel is referred to as time-flat.

When a channel is flat in both frequency and time, it is called a flat-flat channel. On the other hand, if a channel is not flat either in frequency or in time, it is often referred to as non-flat channel. In another

example, if the signal duration is lower than T_c and the bandwidth of transmission is between B_m and B_c bandwidths, then the channel is characterized as frequency distorting and time flat.

More generally, the channels are often classified as narrowband or wideband. A *narrowband* channel is flat in frequency and has no dispersion in time. In the *wideband* channel models, the symbol rate is sufficiently high so that each symbol is spread over adjacent symbols causing inter-symbol interference. This happens when the bandwidth of the transmitted signal oversteps the coherence bandwidth, as well as when the signal time duration exceeds coherence time. The channel is said to be frequency selective and time dispersive.

In addition, *wideband directional* channel models deal with both temporal and angular domains. In these models, additional parameters are considered such as angle-spread, which corresponds to the maximum angle deviation between the arrival angles of the signals with which signals are correlated. The channel is considered as directional for transmissions with angles of arrival that exceed the angle-spread [7], [8].

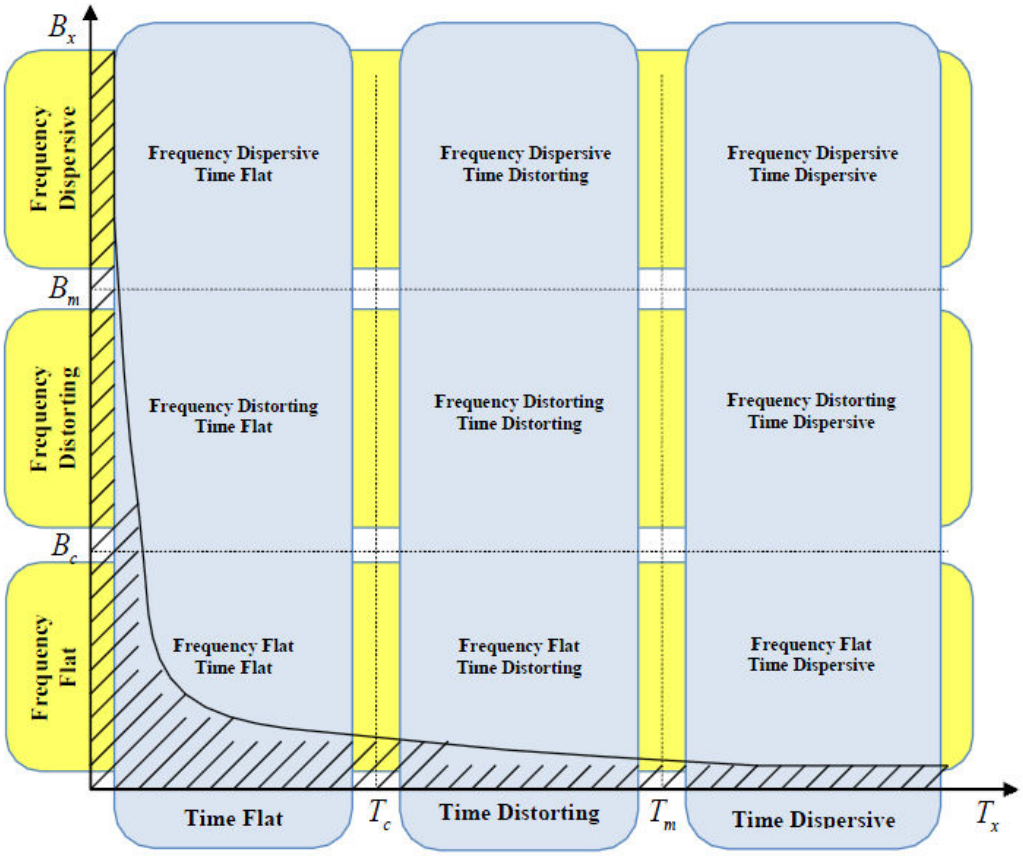

Fig 2-1 Channel classification in relation to frequency and time **[8]**.

Statistics for Channel Modeling

Through several channel measures, channel characterizations were constructed into models that are valid over a range of conditions, setting how quickly channels change and how much they vary. These models have the knowledge of their inaccuracy and dependence on external factors. They are important and are used as approaches in experiences and theoretical comparisons.

The transmitted signals can be affected by large-scale and small-scale propagation effects, which can be characterized by models. Let us consider the relation between the output signal $y(t)$ and the input given by $x(t)$ the following expression

$$y(t) = x(t)\Phi h_{iid} + n(t) \tag{2.9}$$

where $h_{iid} \sim CN(0,1)$ is the independent identically distributed channel and $\Phi = E\left\{|h_c|^2\right\}$ is loss in power of the transmitted signal:

$$\Phi = \Phi_{PL}\Phi_{SF} \tag{2.10}$$

The effects that contribute to these losses are noticeable over relatively long distances and are referred to as large-scale propagation effects. Path loss is one of these effects that contribute to signal impairment by reducing its power, as represented in (2.10) by Φ_{PL}. The path loss is the attenuation suffered by a signal as it propagates from the source to the destination. Another effect that contributes for the loss in the transmitted power is shadow fading or slow fading. This one results from the transmitted signal being obstructed by different objects as it travels to the receive antennas and is represented in (2.10) by Φ_{SF}.

The path loss factor, generally characterized by

$$\Phi_{PL} = \frac{k_0}{(d_t)^{\varepsilon}} \tag{2.11}$$

is dependent on the transmission distance, d_t , and on a constant , k_0, taken from the Friis expression. This constant includes parameters that are related to the physical setup of the transmission, such as signal wavelength and antennas height. The path loss factor also depends on the path loss exponent, ε, which is itself dependent on the environment. The path loss exponent characterizes the rate of decay of the signal power with the distance, taking values in the range of 2 (which corresponds to free space propagation) to

6 assuming far-field condition. Typical values for the path loss exponent are 4, for an urban macrocell environment, and 3, for urban microcell [9].

The slow fading or large-scale-fading factor is caused by reflections in large objects as it travels to the receiving antennas, which we call shadow effect. Since the nature and location of the obstructions that cause this effect cannot be known in advance, the loss introduced by this effect is a random variable. More specifically, it follows a log-normal distribution, according to

$$10\log_{10}\left(\Phi_{SF}\right) \sim N\left(0,\sigma_{SF}^{2}\right) \tag{2.12}$$

As a result of the random reflectors, scatterers and attenuators that a transmitted signal encounters in a wireless communication, multiple copies of the transmitted signal arrive at the destination, through different paths. The channel that characterizes such a communication is referred to as *multipath channel*. Besides the mentioned random objects, other factors influence a multipath channel. The speed of the mobile terminal or of the surrounding objects and the transmission bandwidth of the signal are some of them. The multiple copies of the transmitted signal that arrive at the destination are added, creating either constructive or destructive interference with each other.

The corresponding channel characterization, $h\left(t,\tau\right)$, for frequency and time selective channels is given by the expression

$$h\left(t,\tau\right)=\sum_{i=0}^{L-1}a_{i}\left(t,\tau\right)e^{j\phi_{i}\left(t,\tau\right)}\delta\left(\tau-\tau_{i}\left(t,\tau\right)\right) \tag{2.13}$$

with $a_{i}\left(t,\tau\right)$ and $\phi_{i}\left(t,\tau\right)$ as the amplitude and argument of complex channel attenuation values and L as the number of resolvable paths at the receiver.

The term *fading* describes the variation of the local channel due to the varying phases and amplitudes of the scatterers. *Fast fading*, also called small-scale-fading, derives from reflections in small objects and is noticeable at distances in the order of the signal wavelength.

There are an extended number of different models that characterize a fast fading channel, with different complexity degrees and specific parameters that the user can choose, as observed in the channel characteristics and classifications in the previous section. Several statistical distributions use fast fading models in the characterization of the behavior of channel envelope. They are Rayleigh, Rice, Nagakami, Weibull distributions, among others [10].

The additive white Gaussian noise (AWGN) channel is the simplest channel model. It is equivalent to having the noise generated in the receiver when the transmission path is ideal, where the noise is assumed to have a constant power spectral density (PSD) over the channel bandwidth, and a Gaussian amplitude probability density function (pdf).

It is possible to have a Gaussian channel in digital mobile radio, like in microcells having a line-of-sight with essentially no multipath. Even when there is multipath fading, but the mobile is stationary and there are no other moving objects, the mobile channel can be considered to be Gaussian, with the effects of fading represented by a local path loss.

The Gaussian channel is often used to provide an upper bound on system performance. The multipath fading effect increases BER performance of a given SNR channel. By using techniques to combat multipath fading, such as diversity, equalization, channel coding, data interleaving, and so forth, we can observe how close the BER performance approaches that of the Gaussian channel.

If each multipath component in the received signal is independent, then the pdf of its envelope is characterized as being of Rayleigh. This is the simplest probabilistic model for the channel filter taps and it is based on the assumption that there are a large number of statistically independent reflected and scattered paths with random amplitudes in the delay window corresponding to a simple tap. The phase of the i^{th} path is $2\pi f_c \tau_i$ or $2\pi d_i / \lambda$, where is the distance travelled by the i^{th} path, f_c and λ are carrier frequency and wavelength respectively. As the reflectors and scatterers are far away from the carrier wavelength ($d_i >> \lambda$), it is reasonable to assume that the phase for each path is uniformly distributed between 0 and 2π and that the phases of different paths are independent.

A path is the sum of a large number of small independent circular symmetric complex random variables. According to Central Limit Theorem, each path is in fact circular symmetric, i.e., follows $CN\left(0,\sigma^2\right)$ [11]. Its magnitude is that of a Rayleigh random variable, with a pdf given by

$$p\left(a_R\right) = \frac{a_R}{\sigma^2} e^{\frac{a_R^2}{2\sigma^2}}, a_R \geq 0 \tag{2.14}$$

and with mean and variance given respectively by

$$E\left\{a_R\right\} = \sqrt{\frac{\pi}{2}}\sigma \tag{2.15}$$

and

$$Var\{a_R\} = \frac{4-\pi}{2}\sigma^2 \tag{2.16}$$

To simplify we refer to the channel envelope as $a_R = |h(t)|$, and σ^2 represents the variance of Gaussian distributed variables. In order to have a unitary power for channels the variance should be given by $\sigma^2 = 1/2$.

A Rayleigh fading profile channel can be modeled using the arrangement shown in Fig 2-2. Basically it is formed by two quadrature channels, starting with the two Gaussian noise sources. The outputs from these blocks are applied to filters that represent the effects of Doppler frequency shifts. These filters do not change the Rayleigh envelope statistics of the channel model, but introduce the necessary correlation between frequency components in the channel. The channel is characterized by the sum of the quadrature components $h_{I_b}(t)$ and $h_{Q_b}(t)$, and can be represented as

$$h(t) = \mathrm{Re}\left\{h_b(t)e^{j\omega_c t}\right\} \tag{2.17}$$

where $h_b(t)$ is the complex baseband representation of $h(t)$. This model is quite reasonable for scattering mechanisms where there are few reflectors. It is adopted primarily due to its simplicity in typical cellular situations, with a relatively small number of reflectors.

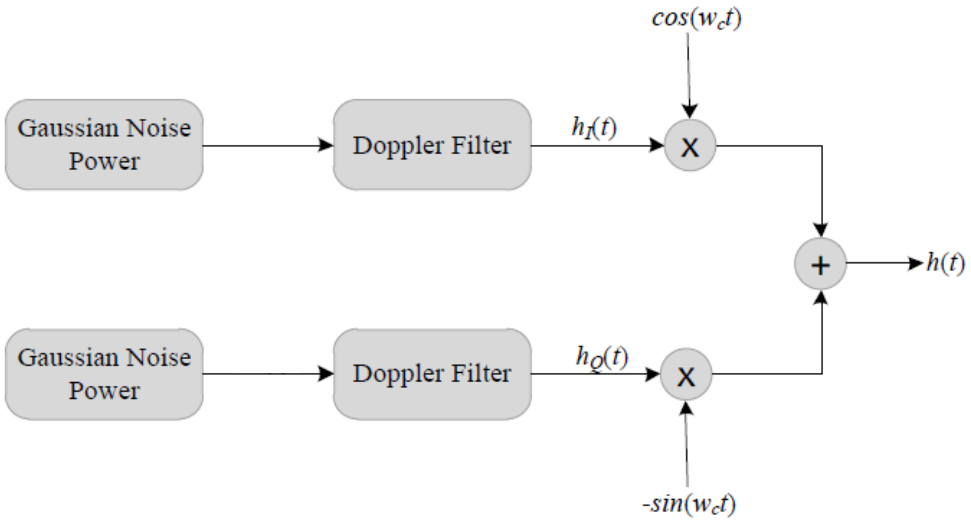

Fig 2-2 Model to generate a Rayleigh fading profile.

In the cases where there are fixed scatterers or signal reflectors in the medium, besides the randomly moving scatterers, the channel cannot be modeled as having a zero-mean. In this case the envelope can be characterized by a Rice distribution, and the channel is said to be Rician. This model has a dominant path (in general the line-of-sight path or specular path) and a large number of independent paths. This dominant path may significantly decrease the depth of fading [7], [11].

Nagakami-*m* distribution is also an alternative statistical model for the envelope of the channel model. This model can be used in conditions that are either more or less severe than Rayleigh distribution, and it includes the Rayleigh distribution as a special case. This model was shown to be the best option for data signals received in urban radio multipath channels [12].

2.1.2.2 MIMO Channel Modeling

Introduction

In multi-antenna systems, the transmitter and/or the receiver consist of arrays, i.e. they are made of several closely-spaced antennas. The fading channel between each transmit-receive antenna pair can be modeled as a SISO channel. Yet each SISO channel constituting of the MIMO channel may be characterized by a different shadowing (however, the size of the arrays is such that the path-loss is usually identical on all links).

For uni-polarized transmissions and reduced inter-element spacings, this is nevertheless a not-so-common situation. If shadowing is identical, the channel matrix $\mathbf{H}$ may be written as follows for a MIMO system with N_t antennas forming the transmit array, and N_r antennas at the receive side. Stacking all inputs and outputs in vectors $\mathbf{x}_t = \left[x_{1,t}, ..., x_{n_t,t} \right]^T$ and $\mathbf{y}_t = \left[y_{1,t}, ..., y_{n_r,t} \right]^T$, the input–output relationship at any given time instant t reads as

$$\mathbf{y}_t = \sqrt{E_s}\mathbf{H}_t\mathbf{x}_t + \mathbf{n}_t \tag{2.18}$$

where

• $\mathbf{H}_t$ is defined as the $N_r \times N_t$ MIMO channel matrix, $\mathbf{H}_t(k,b) = h_{kb,t}$ with h_{kb} denoting the narrowband channel between transmit antenna $b\left(b = 1, ..., N_t\right)$ and receive antenna $k\left(k = 1, ..., N_r\right)$.

• $\mathbf{n}_t = \left[n_{1,t}, ..., n_{N_r,t} \right]^T$ is the sampled noise vector, containing the noise contribution at each receive antenna, such that the noise is white in both time and spatial dimensions, $E\left\{ \mathbf{n}_t \mathbf{n}_{t'}^* \right\} = \sigma_n^2 \mathbf{I}_{N_r} \delta(t - t')$.

• E_s is the transmitted symbol energy, assuming that the average energy constellation is normalized to unity.

From now on, we assume that the channel remains constant over a symbol duration, and drop the time index t for better legibility. It must be clear from the context that b and k designate antennas and not sampled time instants. Using the same channel normalization as above, we also have that the average squared Frobenius norm of $\mathbf{H}$ is equal to

$$E\left\{ \left\| \mathbf{H} \right\|_F^2 \right\} = N_t N_r \tag{2.19}$$

Naturally, modeling only the individual SISO channels is not a complete representation of the multi antenna channel behavior. The statistical correlations between all matrix elements have to be characterized as well. Let us assume that the various elements of the channel matrix are circularly symmetric complex Gaussian independent variables with equal unit variances. The independent identically distributed (i.i.d.) Rayleigh assumption has been traditionally used when developing multi-antenna signal processing techniques, mostly because of its convenience and because it represents an ideal scenario.

Kronecker Model

Many signal processing techniques have been developed with very simple assumptions regarding wireless channels, including multi-antenna channels. In particular, we have so far considered that the elements of the MIMO channel matrix are uncorrelated variables. In practical scenarios, these assumptions may be far from realistic. Yet the characteristics of radio propagation environments dictate the ultimate performance of wireless systems, irrespective of the assumptions used to design the system.

Furthermore, it must be mentioned that analytical models are by essence stochastic and narrowband models. They represent the distribution of either $\mathbf{H}(t)$ or $\mathbf{H}_t$ denoted simply as $\mathbf{H}$ for better legibility. Frequency-selective representations are naturally obtained in the sampled-delay domain by combining L narrowband representations, also known as *taps*, as denoted by

$$\mathbf{H}(t,\tau) = \mathbf{H}_l\left[\tau\right] = \sum_{i=0}^{L-1} \mathbf{H}(t,\tau_i)\delta(\tau-\tau_i) \tag{2.20}$$

The l^{th} tap is then characterized on its own by a narrowband channel model, which implies that each tap is characterized by a spatial correlation matrix $\mathbf{R}_l$.

One of the simplified models, relying on specific assumptions that have been developed for Rayleigh channels, is the Kronecker model. Introduced by [13], [14], [15], the Kronecker model simplifies the expression of the full correlation matrix by using a reparability assumption

$$\mathbf{R} = \mathbf{R}_r \otimes \mathbf{R}_t \tag{2.21}$$

where $\mathbf{R}_t$ and $\mathbf{R}_r$ are the transmit and receive correlation matrices [10], respectively. Mathematically, the Kronecker model is valid if and only if two conditions are jointly met, although contradictory statements can be found in the literature [16]. The first condition is that transmit (resp. receive) correlation coefficients are (in magnitude) independent from the considered receive (resp. transmit) antenna. While this condition is easily fulfilled for most usual antenna arrays with reasonably sized antenna spacings (within the spatial stationarity region of the channel), there are cases where this condition is not met: the correlations at one end then depend on the antenna considered at the other end of the link. As an example, consider the case of mutually-coupled antennas. We know that the radiation patterns of closely located antennas are distorted because of coupling, becoming asymmetrical relative to the boresight. In such scenarios, the correlations at the other end of the link will depend on the considered antenna at the coupled end. In [16], it is claimed that the above condition is the only one required by the Kronecker assumption. However, there is an additional condition [13], [17] the cross-channel correlations must be equal to the product of corresponding transmit and receive correlations.

Finally, by some manipulations the channel matrix may be expressed as

$$\tilde{\mathbf{H}} = \mathbf{R}_r^{1/2}\mathbf{H}_w\mathbf{R}_t^{1/2} \tag{2.22}$$

where $\mathbf{H}_w$ is one realization of an i.i.d. channel matrix and $\tilde{\mathbf{H}}$ is the notation used to represent the particular case of Rayleigh fading channel matrices.

The advantage of the Kronecker model is readily apparent: operations on $vec(\mathbf{H})$ have been replaced by matrix manipulations on $\mathbf{H}$. This greatly simplifies the expressions of many parameters, such as the

mutual information, the error probability, etc. It is also easy to understand that the Kronecker model allows for separate transmit and receive optimizations.

2.1.3 Diversity Techniques

Impact of fading on system performance

The particularity of wireless links is that they are impaired by random fluctuations of the signal level not only across time, but also across space or frequency. This behavior is known as fading, and impacts the performance (in terms of symbol or bit error rate) of any wireless system. As an example, consider the simple case of binary phase shift keying (BPSK) transmission through a SISO Rayleigh fading channel [10]. In the absence of fading, the symbol-error rate (SER) in AWGN channel is given by

$$P_e = Q\left(\sqrt{\frac{2E_s}{\sigma_n^2}}\right) = Q\left(\sqrt{2\rho}\right) \tag{2.23}$$

when fading is considered, the received signal level fluctuates as $s\sqrt{E_s}$,where s is the channel magnitude. As a result, the error rate is obtained through the following integration [12].

$$P_e = \int_0^\infty Q\left(\sqrt{2\rho s}\right) p_s(s) ds \tag{2.24}$$

where $p_s(s)$ is the fading distribution and $\rho = E_s/\sigma_n^2$ is average SNR. In Rayleigh fading, the integration in (2.24) yields

$$P_e = \frac{1}{2}\left(1 - \sqrt{\frac{\rho}{1+\rho}}\right) \tag{2.25}$$

At large SNR, the error rate in (2.25) simplifies to

$$P_e \cong \frac{1}{4\rho} \tag{2.26}$$

Strikingly, the error rate decreases only inversely with the SNR (with an asymptotic slope of one). By contrast, the decrease in error rate in non-fading AWGN channels is exponential with the SNR (see(2.23)).

Principle of diversity

To combat the impact of fading on the error rate, diversity techniques are usually employed. The principle of diversity is to provide the receiver with multiple versions of the same transmitted signal. Each of these versions is defined as a diversity branch. If these versions are affected by independent fading conditions, the probability that all branches are in a fade at the same time reduces dramatically. Hence, diversity helps stabilize the link through channel hardening which leads to improved performance in terms of error rate.

Because fading may take place in time, frequency and space, diversity techniques may similarly be exploited in each of these domains. As an example, time diversity can be obtained via appropriate coding and interleaving. Frequency diversity exploits the temporal spreading of the channel (in the τ domain) through equalization techniques [12] or multi-carrier modulations. Naturally, both time and frequency diversity techniques incur a loss in time or bandwidth to allow for the introduction of redundancy. By contrast, spatial or polarization diversity does not sacrifice time and bandwidth, since it is provided by the use of multiple antennas at one or both sides of the link. Yet the spatial dimensions are increased by the use of antenna arrays.

Array and diversity gains

When discussing diversity schemes, two gains are classically introduced. It is important to make a clear distinction between these two gains, as they characterize two different improvements obtained from diversity. One way of characterizing the merits of a diversity scheme is to evaluate the increase in average output SNR (i.e. at the input of the detector) relative to the single-branch average SNR ρ. Denoting the output SNR as ρ_{out}, we define the array gain as

$$g_a = \frac{\rho_{out}}{\rho} \tag{2.27}$$

which translates by a decrease of the error rate for a fixed transmit power. A second figure of merit is the increase in the error rate slope as a function of the SNR. We define the diversity gain as the negative slope of the log–log plot of the average error probability $\overline{P}$ versus SNR

$$g_d^o(\rho) = -\frac{\log(\overline{P})}{\log(\rho)} \tag{2.28}$$

Note that classically, the diversity gain is taken as the asymptotic slope, i.e. for $\rho \to \infty$. Both gains are illustrated in Fig 2-3 and Fig 2-4. Note that the only difference between both graphs is the SNR reference. In Fig 2-3, the error probability is plotted against the output average SNR, whereas in Fig 2-4, it is plotted against the single-branch SNR. The diversity curves have exactly the same shape (the slope is the diversity gain) but are shifted from one another by a SNR difference equal to the array gain.

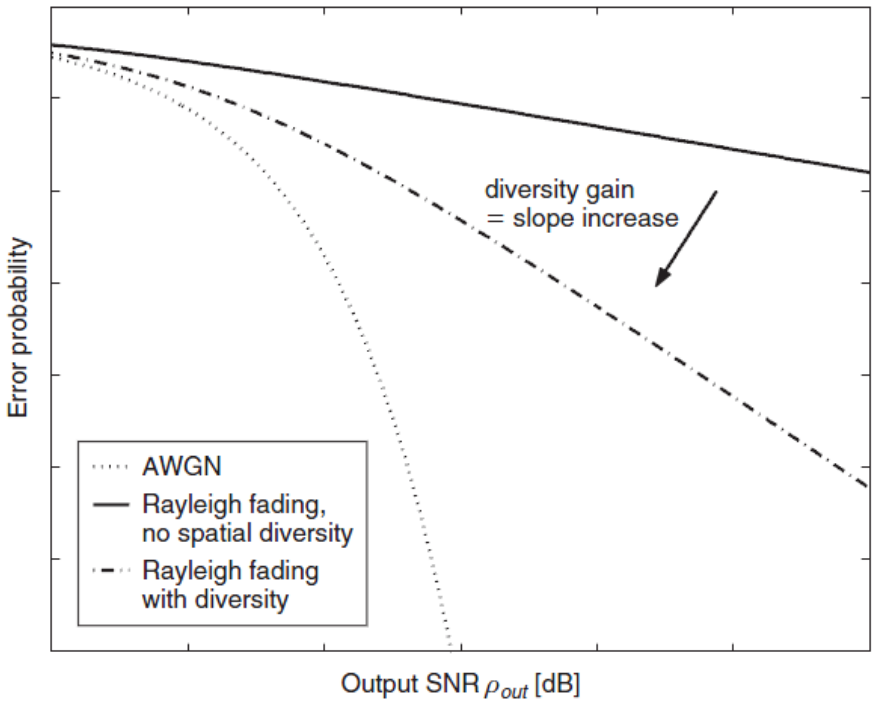

Fig 2-3 Diversity gain in Rayleigh fading channels **[10]**.

Furthermore, it is important to note that the array gain does not depend on the degree of correlation between the branches, whereas the diversity gain is maximal for independent branches and decreases as the correlation between branches increases. A third gain which should be differentiated with the above gains is known as the coding gain. The latter manifests itself by a shift of the error curve (error rate vs. SNR) to the left. By contrast, we have observed that the diversity gain increases the slope of the error rate curve. Yet it may seem that the coding gain is very similar to the array gain. There is, however, a fundamental difference. If the error rate is plotted against the average receive SNR ρ_{out}, any variation of the array gain is invisible, as already observed in Fig 2-3. This is not the case with the coding gain, as two schemes with different coding gains will yield different (yet parallel) error curves: for a given SNR level ρ_{out} at the input of the detector, the error rates will differ.

2.1.4 Multiplexing Capability

When employed at both sides of the link, multiple antennas may also be used to increase the transmission rate (or the capacity) of communication systems. In favorable channels, we will show how the rate may be increased proportionally to the minimum number of antenna elements, $\min\{N_t, N_r\}$.

This leverage of multi-antenna systems is known as spatial (or polarization) multiplexing. It is characterized by a so-called multiplexing gain g_s. Asymptotically (at high SNR), this gain is defined as

$$g_s = \lim_{\rho\to\infty} \frac{R(\rho)}{\log_2(\rho)} \tag{2.29}$$

where $R(\rho)$ is the transmission rate.

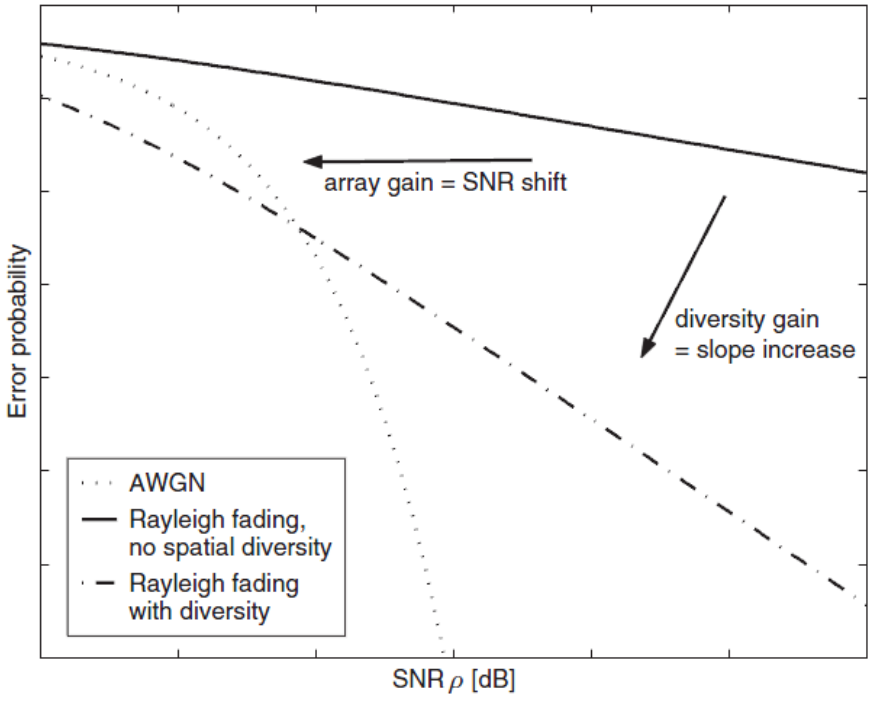

Fig 2-4 Diversity and array gains in Rayleigh fading channels **[10]**.

2.1.5 MIMO Precoding Techniques

With multiple antennas at both ends of the link comes the ability to exploit other leverages than diversity and array gains. It is now possible to increase the transmission throughput via the spatial

multiplexing capability of MIMO channels. However, we will also observe that it is not possible to maximize both the spatial multiplexing and the diversity gains. Similarly, we will show that the array gain in Rayleigh channels is also limited and is actually smaller than $N_t N_r$. In this section, we classify MIMO techniques with respect to the quality of channel knowledge at the transmitter.

2.1.5.1 MIMO with perfect transmit channel knowledge

Dominant eigenmode transmission

Let us first focus on maximizing the diversity gain of a $N_r \times N_t$ MIMO system. Intuitively, this can be done through transmitting the same signal from all transmit antennas after weighting by a $N_t \times 1$ vector $\mathbf{w}_t$. At the receive array, the antenna outputs are combined into a scalar signal x through a weighted summation according to a $N_r \times 1$ vector $\mathbf{w}_r$. Subsequently, the transmission is described by

$$\mathbf{y} = \sqrt{E_s}\mathbf{H}\mathbf{w}_t x + \mathbf{n} \tag{2.30}$$

$$\tilde{x} = \mathbf{w}_r^H \mathbf{y} = \sqrt{E_s}\mathbf{w}_r^H \mathbf{H}\mathbf{w}_t x + \mathbf{w}_r^H \mathbf{n} \tag{2.31}$$

Maximizing the receive SNR comes to maximizing $\left\|\mathbf{w}_r^H \mathbf{H}\mathbf{w}_t\right\|_F^2 / \left\|\mathbf{w}_r\right\|_F^2$. To solve this problem, we need to use the singular value decomposition (SVD) of $\mathbf{H}$ as

$$\mathbf{H} = \mathbf{U}\boldsymbol{\Sigma}\mathbf{V}^H \tag{2.32}$$

where $\mathbf{U}$ and $\mathbf{V}$ are $N_r \times r(\mathbf{H})$ and $N_t \times r(\mathbf{H})$ unitary matrices, $r(\mathbf{H})$ being the rank of $\mathbf{H}$ and

$$\boldsymbol{\Sigma} = \operatorname{diag}\left\{\sqrt{\lambda_1}, \sqrt{\lambda_2}, ..., \sqrt{\lambda_{r(\mathbf{H})}}\right\} \tag{2.33}$$

is the diagonal matrix containing the singular values of $\mathbf{H}$. Using this particular decomposition of the channel matrix, it is easily shown [2] that the receive SNR is maximized when $\mathbf{w}_t$ and $\mathbf{w}_r$ are the transmit and receive singular vectors corresponding to the maximum singular value of $\mathbf{H}$, $\sqrt{\lambda_{\max}} = \max\left\{\sqrt{\lambda_1}, \sqrt{\lambda_2}, ..., \sqrt{\lambda_{r(\mathbf{H})}}\right\}$. This technique is known as the dominant eigenmode transmission, and (2.31) may be rewritten as

$$\tilde{x} = \sqrt{E_s}\sqrt{\lambda_{\max}}x + \tilde{n} \tag{2.34}$$

where $\tilde{n} = \mathbf{w}_r^H \mathbf{n}$ has a variance equal to σ_n^2.

From (2.34), it is easily observed that the array gain is equal to $E\{\lambda_{\max}\}$, where $\lambda_{\max}$ is the largest eigenvalue of $\mathbf{H}\mathbf{H}^H$. The array gain for i.i.d. Rayleigh channels is thus bounded as follows

$$\max(N_t, N_r) \le g_a \le N_t N_r \tag{2.35}$$

Furthermore, the results in [10] indicate that in the i.i.d. Rayleigh case, the asymptotic array gain of a dominant eigenmode transmission (i.e., for large N_t, N_r) is given by

$$g_a = \left(\sqrt{N_t} + \sqrt{N_r}\right)^2 \tag{2.36}$$

Finally, the diversity gain is obtained by upper and lower-bounding the error rate $\overline{P}$ at high SNR [2] (assuming that the Chernoff bound is a good approximation of the SER at high SNR)

$$\overline{N}_e \left(\frac{\rho d_{\min}^2}{4 \min\{N_t, N_r\}} \right)^{-N_t N_r} \ge \overline{P} \ge \overline{N}_e \left(\frac{\rho d_{\min}^2}{4} \right)^{-N_t N_r} \tag{2.37}$$

where $\overline{N}_e$ and $d_{\min}$ are, respectively, the number of nearest neighbors and minimum distance of separation of the underlying constellation The above equation implies that the error rate maintains a slope of $N_t N_r$ as a function of the SNR: the dominant eigenmode transmission extracts a full diversity gain of $N_t N_r$.

Dominant eigenmode transmission with antenna selection

The dominant eigenmode transmission introduced above may be generalized to include a selection algorithm at either the transmitter or the receiver. We focus in the following on transmit selection, but all considerations remain valid if the receiver performs the selection (remember that both the transmitter and the receiver have a perfect channel knowledge).

The dominant eigenmode transmission with antenna selection [18] works as follows. We define a set of matrices $\mathbf{H}'$ created by removing $N_t - N_t'$ columns from $\mathbf{H}$. The set of all possible $\mathbf{H}'$ is denoted as

$S\{\mathbf{H}'\}$ and its cardinality is $\binom{N_t}{N_t'}$. At each time instant, the scheme comes to perform a dominant eigenmode transmission using the matrix $\mathbf{H}'$ offering the largest $\lambda'_{out} = \max\{\lambda'_1, \lambda'_2, ..., \lambda'_{r(\mathbf{H}')}\}$. The output SNR thereby reads as

$$\rho_{out} = \rho \max_{s\{\mathbf{H}'\}} \{\lambda'_{\max}\} \tag{2.38}$$

The average SNR can be calculated as described in [19]. Analogous to the classical dominant eigenmode transmission, it is shown in [19] that antenna selection extracts the same diversity gain as if all N_t transmit antennas were used, i.e. the diversity gain is equal to $N_t N_r$.

Multiple eigenmode transmission

The dominant eigenmode transmission naturally achieves no multiplexing gain as the same symbol is sent over all transmit antennas. As an alternative, one may desire to increase the system throughput by maximizing the spatial multiplexing gain. To this end, symbols are spread over all non-zero eigenmodes of the channel. We assume in the following that $N_r \geq N_t$ and that the channel matrix is i.i.d. Rayleigh with an SVD given by (2.32). If the transmitter multiplies the input vector $\mathbf{x}(N_t \times 1)$ using $\mathbf{V}$ as a precoding matrix, and the receiver multiplies the received vector by $\mathbf{U}^H$, the effective input–output relationship reads as

$$\mathbf{y} = \sqrt{E_s}\mathbf{U}^H\mathbf{H}\mathbf{V}\mathbf{x} + \mathbf{U}^H\mathbf{n} = \sqrt{E_s}\boldsymbol{\Sigma}\mathbf{x} + \tilde{\mathbf{n}} \tag{2.39}$$

We observe that the channel has been decomposed into N_t parallel SISO channels given by $\left\{\sqrt{\lambda_1}, ..., \sqrt{\lambda_{N_t}}\right\}$. What should be noticed is that all these channels are totally decoupled as if N_t virtual data pipes had been created. The mutual information of the MIMO channel is therefore the sum of the SISO channel capacities

$$I = \sum_{b=1}^{N_t} \log_2\left(1 + \rho p_b \sigma_b^2\right) \tag{2.40}$$

where $\{p_1, ..., p_{N_t}\}$ is the power allocation on each of the channel eigenmodes, normalized such that

$\sum_{b=1}^{N_t} p_b = 1$. The MIMO capacity is obtained by finding the optimal power allocation maximizing the mutual information of (2.40), and the capacity scales linearly in N_t , hence the spatial multiplexing gain is equal to N_t. By contrast, this transmission does not necessarily achieve the full diversity gain of $N_t N_r$ but does at least provide N_r-fold array and diversity gains (still assuming $N_t \leq N_r$).

In general, the capacity scales linearly with the rank of $\mathbf{H}$ in arbitrarily correlated channels. One consequence is that in highly correlated channels, only the dominant eigenmode is used for transmission, reducing the spatial multiplexing gain to one. In such channels, there is of course no available diversity gain, though a MIMO array gain of $E\{\lambda_{\max}\}$ is obtained.

Naturally, the multiple eigenmode transmission may be combined with antenna selection at the receiver. As long as $N_r' \geq N_t$, the multiplexing gain remains equal to N_t , but the array and diversity gains are reduced.

Finally, hybrid schemes based on both multiple and dominant eigenmode transmissions can also be used. As an example, it is always possible to achieve some diversity by grouping antennas subsets for diversity gain and operate a multiplexing on the new channel with reduced dimension [20].

2.1.5.2 MIMO without transmit channel knowledge

When the transmitter has no channel knowledge, the presence of multiple antennas at both sides may allow extracting diversity and/or increasing the capacity. This is achieved through the use of so-called space–time codes, which expand symbols over the antennas (i.e. over space) and over time [21], [6].

Space–time block coding

Let us start with a simple example of MIMO 2×2 transmissions. Consider that two symbols x_1 and x_2 are transmitted simultaneously from transmit antennas 1 and 2 during the first symbol period, while symbols $-x_2^*$ and x_1^* are transmitted from antennas 1 and 2 during the next symbol period.

Assume that the flat fading channel remains constant over the two successive symbol periods, and that the 2×2 channel matrix reads as

$$\mathbf{H} = \begin{bmatrix} h_{11} & h_{12} \\ h_{21} & h_{22} \end{bmatrix} \tag{2.41}$$

Note that the subscripts here denote receive and transmit antenna index and not the symbol period. The vector signal received at the receive array at the first symbol period is

$$\mathbf{y}_1 = \sqrt{E_s}\mathbf{H}\begin{bmatrix} x_1/\sqrt{2} \\ x_2/\sqrt{2} \end{bmatrix} + \mathbf{n}_1 \tag{2.42}$$

and the vector signal received at the second symbol period is

$$\mathbf{y}_2 = \sqrt{E_s}\mathbf{H}\begin{bmatrix} -x_2^*/\sqrt{2} \\ x_1^*/\sqrt{2} \end{bmatrix} + \mathbf{n}_2 \tag{2.43}$$

where $\mathbf{n}_1$ and $\mathbf{n}_2$ are the additive noise contributions at each symbol period over the receive antenna array (so the subscripts here denote the symbol periods, and not the antennas). The receiver forms a combined signal vector $\mathbf{y}$ as

$$\mathbf{y} = \begin{bmatrix} \mathbf{y}1 \\ \mathbf{y}_2^* \end{bmatrix} = \underbrace{\begin{bmatrix} h_{11} & h_{12} \\ h_{21} & h_{22} \\ h_{12}^* & -h_{11}^* \\ h_{22}^* & -h_{21}^* \end{bmatrix}}_{\mathbf{H}_e} \underbrace{\begin{bmatrix} x_1/\sqrt{2} \\ x_2/\sqrt{2} \end{bmatrix}}_{\mathbf{x}} + \begin{bmatrix} \mathbf{n}_1 \\ \mathbf{n}_2^* \end{bmatrix} \tag{2.44}$$

Analogous to the MISO system, both symbols x_1 and x_2 are spread over the two transmit antennas and over the two symbol periods. Furthermore, $\mathbf{H}_e$ is orthogonal for all channel realizations, i.e. $\mathbf{H}_e^H\mathbf{H}_e = \|\mathbf{H}\|_F^2\,\mathbf{I}_2$. If we compute $\mathbf{z} = \mathbf{H}_e^H\mathbf{y}$, we get

$$\tilde{\mathbf{x}} = \begin{bmatrix} x_1 \\ x_2 \end{bmatrix} = \mathbf{H}_e^H\mathbf{y} = \|\mathbf{H}\|_F^2\,\mathbf{I}_2\mathbf{x} + \mathbf{n}' \tag{2.45}$$

The above equation illustrates that the transmission of x_1 and x_2 is fully decoupled, i.e.

$$\tilde{x}_i = \sqrt{E_s/2}\,\|\mathbf{H}\|_F^2\,x_i + \tilde{n}_i \quad i = 1,2 \tag{2.46}$$

with the average output SNR given by

$$\rho_{out} = \frac{1}{\sigma_n^2} \mathrm{E}\left\{ \frac{E_s \left[\|\mathbf{H}\|_F^2 \right]^2}{2\|\mathbf{H}\|_F^2} \right\} = 2\rho \tag{2.47}$$

illustrating that the Alamouti scheme in a 2×2 configuration provides a receive array gain ($g_a = N_r = 2$) but no transmit array gain (since the transmitter has no channel knowledge).

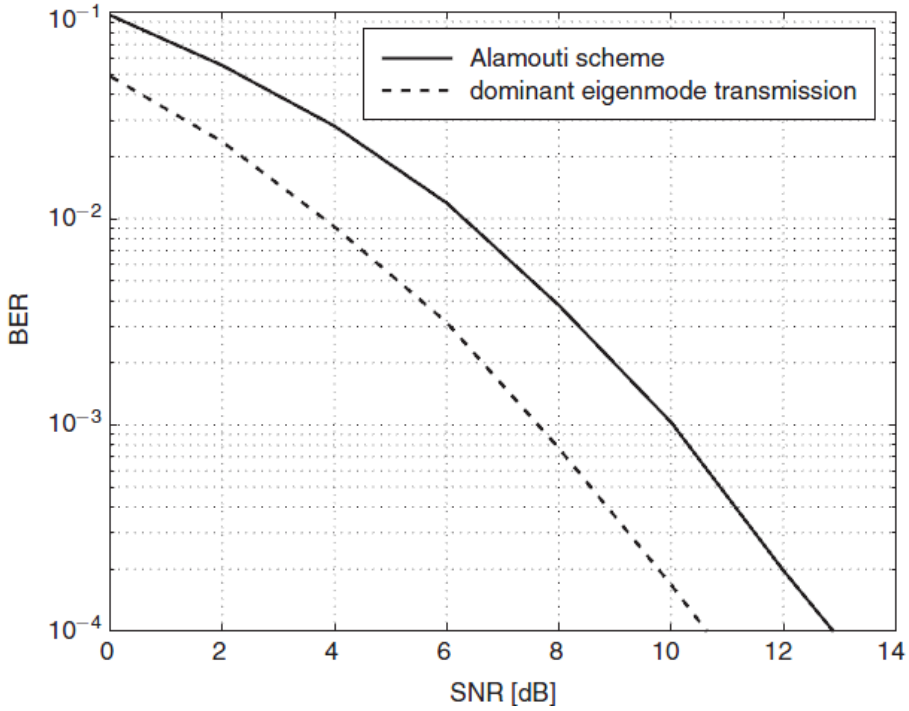

Fig 2-5 Performance of dominant eigenmode and Alamouti transmission in a 2×2 i.i.d. Rayleigh fading channel (with quadrature PSK (QPSK) modulation) **[10]**.

However, it may extract the full diversity ($g_d^o = N_t N_r = 4$) as shown in [2],

$$\overline{P} \le \overline{N}_e \left(\frac{\rho d_{\min}^2}{8} \right)^{-4} \tag{2.48}$$

A comparison between the Alamouti scheme and the dominant eigenmode transmission is depicted in Fig 2-5 as a function of the SNR. Clearly, the diversity gain is equal to 4 in both cases, but the array gain is larger by 3 dB for the dominant eigenmode transmission. Note that the Alamouti scheme may also be

used with any number of receive antennas ($g_a = N_r$ and $g_d^o = 2N_r$), but cannot be applied to systems with more than two transmit antennas.

Fig 2-5 has illustrated the possibility of extracting the full diversity of the MIMO channel without transmit channel knowledge. The principle of spreading symbols over space and time is generalized through the concept of STBCs. In general, these map Q symbols onto a codeword $\mathbf{X}$ of size $N_t \times T$, where T is thus the duration of the codewords. The codeword $\mathbf{C}$ is usually normalized such that $\mathrm{E}\left\{Tr\left\{\mathbf{X}\mathbf{X}^H\right\}\right\} = T$. As an example, the 2×2 Alamouti scheme ($T = 2, N_t = 2, Q = 2$) is represented by the following codeword matrix

$$\mathbf{X} = \frac{1}{\sqrt{2}}\begin{bmatrix} x_1 & -x_2^* \\ x_2 & x_1^* \end{bmatrix} \tag{2.49}$$

The spatial multiplexing rate of a space–time block code is then defined as $r_s = Q/T$ and a space–time block code is full-rate when $r_s = N_t$. The Alamouti scheme is therefore characterized by $r_s = 1$.

A first class of STBCs is constituted by the O-STBCs, which include the Alamouti scheme described above. O-STBCs transmit one or less independent symbol per symbol period over the N_t transmit antennas. They provide an array gain of N_r and extract the full diversity gain of $N_t N_r$. Furthermore, they allow for a direct detection since vector detections are converted into much less complex scalar detections, as illustrated by (2.46). However, for complex constellations, O-STBCs with $r_s = 1$ only exist for $N_t = 2$. Otherwise, complex O-STBCs for arbitrary N_t offer spatial multiplexing rates $r_s < 1$.

Instead of extracting the full diversity with O-STBCs, it is possible to transmit N_t independent symbols per symbol period, achieving a spatial multiplexing rate of N_t. Such full-rate schemes are known as spatial multiplexing (SM). For uncoded SM (a.k.a. V-BLAST), each codeword expands onto one symbol duration (there is no temporal encoding): the achievable array and diversity gains with ML decoding are equal to N_r, while the spatial multiplexing gain equals $\min\left\{N_t, N_r\right\}$. By contrast, coded SM transmissions such as D-BLAST may deliver the full diversity ($g_d^o = N_t N_r$) by optimally coding over time. Note however that these gains are extremely sensitive to the detection algorithm. As an example the diversity gain of uncoded SM with zero-forcing or minimum mean square error (MMSE)

detection is only $N_r - N_t + 1$ (assuming $N_r \geq N_t$) [10]. Naturally, it is also possible to combine SM with receive antenna selection (assuming $N_r \geq N_t$).

So far, we have seen that O-STBCs exploit the full diversity but with a limited spatial multiplexing rate. On the other hand, uncoded Spatial Multiplexing enables higher throughput but does not succeed in leveraging transmit diversity. If an increase of the receiver complexity is authorized, it is possible to improve the data rates while still providing transmit diversity. A first step was made in that direction by D-BLAST. Alternatively, this can be realized by so-called linear dispersion codes, which appear as an intermediate solution between O-STBCs and SM. Finally, codes known as algebraic codes have been developed with the same objective in mind.

A final remark: because space–time codes do not require the channel knowledge at the transmitter, they should be designed in such a way that their performance is not too sensitive to the actual channel state (at any time instant).

Space–time trellis coding

STTCs were actually proposed in [6] before STBCs. They are an extension of classical convolutional codes to multi-antenna transmit arrays. The difference with STBCs lies in the fact that the encoder output in space–time trellis coding is not only a function of the input bits but also of the state of the encoder, which is related to the previous input bits. This memory is inherent to the trellis approach and provides an additional coding gain.

Space-frequency coding

In frequency selective channels, it is possible to exploit the additional frequency diversity by coding not only across space (i.e. across antennas) but also across the frequency band, e.g. using OFDM. This technique is known as space-frequency (SF) MIMO-OFDM.

2.1.5.3 MIMO with partial transmit channel knowledge

The exploitation of the array gain may also be possible if the transmitter has only partial channel knowledge. Perfect channel knowledge at the transmitter has been covered before, but requires a feedback link between the receiver and the transmitter to keep the latter continuously informed about the channel state. By contrast, exploiting only the channel statistics or a quantized version of the channel at the transmitter requires a much lower rate feedback link.

Precoding techniques generally consist in combining a multi-mode beamformer spreading the codewords in orthogonal directions related to the channel distribution with a constellation shaper, or more simply, a power allocation scheme. There are naturally many similarities with the various eigenmode transmissions discussed, the difference being that the eigenbeams are now based on the statistics of $\mathbf{H}$ rather than on the instantaneous value of $\mathbf{H}$.

Similarly, antenna selection techniques may rely only on partial channel knowledge, choosing transmit or receive antennas based on the first and second-order statistics of $\mathbf{H}$ [19]. Intuitively, this comes to choose the antenna pairs with the lowest correlation. Naturally, such a technique does not minimize the instantaneous error performance, but only the average error rate. As a result, it leads mostly to a coding gain and small diversity advantage.

A generalization of antenna selection consists of exploiting a limited amount of feedback at the transmitter through quantized precoding. This technique relies on a codebook of precoding matrices, i.e. a finite set of precoders, designed off-line and known to both the transmitter and receiver. The receiver estimates the best precoder as a function of the current channel and then feeds back the index of the best precoder in the codebook.

2.1.6 Multiple Antenna Techniques in Commercial Wireless Systems

In this section, we briefly examine current or future commercial implementations of MIMO techniques. Specifically, multiple antennas have been integrated into 3G, cellular systems, broadband fixed/mobile wireless access networks (IEEE 802.16e) also known as WiMax and IEEE 802.11n release. Besides, the concept considered for 4G and beyond 4G cellular architectures such as LTE and LTE-A.

Regarding 3G systems, the current CDMA 2000 standard provides transmit diversity options, via an extension of the Alamouti scheme. The wideband CDMA UMTS and its future versions developed by the 3GPP also allow for implementing space–time transmit diversity schemes; in combination with transmit beamforming at the base station.

In wireless metropolitan area network (WMAN), the IEEE 802.16d/e standard also known as WiMax makes use of MIMO-OFDMA techniques, combining multiple antennas with OFDM modulation. The IEEE 802.16e standard operates in non line-of-sight between 2 and 11GHz. Data rates of around 40 and 15 Mbps will be available for fixed and mobile users respectively.

In wireless local area network (WLAN), the IEEE802.11n (Wi-Fi) standard considers peak data rates of 150Mbps, with 500Mbps as an option. MIMO technology is implemented in the standard using three different techniques: antenna selection, space–time coding (e.g. the Alamouti scheme) and possibly beamforming (though advanced beamforming techniques requiring transmit channel knowledge are likely to be introduced only in medium-term products).

LTE-A technology aims at very high peak data rates such as 1 Gbps in local areas and 100 Mbps in wide areas. To meet these targets, evolved MIMO techniques along with access techniques such as OFDMA and SC are required.

2.2 Orthogonal Frequency Division Multiplexing

2.2.1 Introduction

OFDM is a method of encoding digital data on multiple carrier frequencies. OFDM has developed into a popular scheme for wideband digital communication, whether wireless or over copper wires, used in applications such as digital television and audio broadcasting, digital subscriber line (DSL) broadband internet access, wireless networks, and 4G mobile communications.

OFDM is essentially identical to coded OFDM (COFDM) and discrete multi-tone (DMT), and is a frequency division multiplexing (FDM) scheme used as a digital multi carrier modulation method. A large number of closely spaced orthogonal sub-carrier signals are used to carry data. The data is divided into several parallel data streams or channels, one for each sub-carrier. Each sub-carrier is modulated with a conventional modulation scheme (such as quadrature amplitude modulation or phase-shift keying) at a low symbol rate, maintaining total data rates similar to conventional *single-carrier* modulation schemes in the same bandwidth.

The primary advantage of OFDM over single-carrier schemes is its ability to cope with severe channel conditions (for example, attenuation of high frequencies in a long copper wire, narrowband interference and frequency-selective fading due to multipath) without complex equalization filters. Channel equalization is simplified because OFDM may be viewed as using many slowly modulated narrowband signals rather than one rapidly modulated wideband signal. The low symbol rate makes the use of a guard interval between symbols affordable, making it possible to eliminate ISI and utilize echoes and time-spreading (that shows up as ghosting on analogue TV) to achieve a diversity gain, i.e. a signal-to-noise ratio improvement. This mechanism also facilitates the design of single frequency networks (SFNs), where several adjacent transmitters send the same signal simultaneously at the same

frequency, as the signals from multiple distant transmitters may be combined constructively, rather than interfering as would typically occur in a traditional single-carrier system. The most recent example is coordinated multipoint concept which is used in LTE-A technology.

2.2.2 Characteristic and Principles of Operation

Orthogonality

Conceptually, OFDM is a specialized FDM, the additional constraint being: all the carrier signals are orthogonal to each other. In OFDM, the sub-carrier frequencies are chosen so that the sub-carriers are orthogonal to each other, meaning that cross-talk between the sub-channels is eliminated and inter-carrier guard bands are not required. This greatly simplifies the design of both the transmitter and the receiver; unlike conventional FDM, a separate filter for each sub-channel is not required.

The orthogonality requires that the sub-carrier spacing is $\Delta f = b/T_U$ Hertz, where T_U seconds is the useful symbol duration (the receiver side window size), and b is a positive integer, typically equal to 1. Therefore, with N_c sub-carriers, the total passband bandwidth will be $B_{OFDM} \approx N_c.\Delta f$ (Hz). The orthogonality also allows high spectral efficiency, with a total symbol rate near the Nyquist rate for the equivalent baseband signal (i.e. near half the Nyquist rate for the double-side band physical passband signal). Almost the whole available frequency band can be utilized. OFDM generally has a nearly 'white' spectrum, giving it benign electromagnetic interference properties with respect to other co-channel users.

OFDM requires very accurate frequency synchronization between the receiver and the transmitter; with frequency deviation the sub-carriers will no longer be orthogonal, causing inter-carrier interference (ICI) (i.e., cross-talk between the sub-carriers). Frequency offsets are typically caused by mismatched transmitter and receiver oscillators, or by Doppler shift due to movement. While Doppler shift alone may be compensated for by the receiver, the situation is worsened when combined with multipath, as reflections will appear at various frequency offsets, which is much harder to correct. This effect typically worsens as speed increases, and is an important factor limiting the use of OFDM in high-speed vehicles. Several techniques for ICI suppression are suggested, but they may increase the receiver complexity.

Implementation Using the Fast Fourier Transform (FFT) Algorithm

The orthogonality allows for efficient modulator and demodulator implementation using the FFT algorithm on the receiver side, and inverse FFT on the sender side. Although the principles and some of the benefits have been known since the 1960s, OFDM is popular for wideband communications today by

way of low-cost digital signal processing components that can efficiently calculate the FFT [22], [23], [24].

Guard Interval for Elimination of Intersymbol Interference

One key principle of OFDM is that since low symbol rate modulation schemes (i.e., where the symbols are relatively long compared to the channel time characteristics) suffer less from intersymbol interference caused by multipath propagation, it is advantageous to transmit a number of low-rate streams in parallel instead of a single high-rate stream. Since the duration of each symbol is long, it is feasible to insert a guard interval between the OFDM symbols, thus eliminating the intersymbol interference.

The guard interval also eliminates the need for a pulse-shaping filter, and it reduces the sensitivity to time synchronization problems.

The cyclic prefix, which is transmitted during the guard interval, consists of the end of the OFDM symbol copied into the guard interval, and the guard interval is transmitted followed by the OFDM symbol. The reason that the guard interval consists of a copy of the end of the OFDM symbol is so that the receiver will integrate over an integer number of sinusoid cycles for each of the multipaths when it performs OFDM demodulation with the FFT.

Simplified Equalization

The effects of frequency-selective channel conditions, for example fading caused by multipath propagation, can be considered as constant (flat) over an OFDM sub-channel if the sub-channel is sufficiently narrow-banded (i.e., if the number of sub-channels is sufficiently large). This makes frequency domain equalization possible at the receiver, which is far simpler than the time-domain equalization used in conventional single-carrier modulation. In OFDM, the equalizer only has to multiply each detected sub-carrier (each Fourier coefficient) in each OFDM symbol by a constant complex number, or a rarely changed value.

If differential modulation such as DPSK or differential QPSK (DQPSK) is applied to each sub-carrier, equalization can be completely omitted, since these non-coherent schemes are insensitive to slowly changing amplitude and phase distortion.

In a sense, improvements in finite impulse response (FIR) equalization using FFTs or partial FFTs leads mathematically closer to OFDM, but the OFDM technique is easier to understand and implement, and the sub-channels can be independently adapted in other ways than varying equalization coefficients, such as switching between different quadrature amplitude modulation (QAM) constellation patterns and error-correction schemes to match individual sub-channel noise and interference characteristics.

Some of the sub-carriers in some of the OFDM symbols may carry pilot signals for measurement of the channel conditions (i.e., the equalizer gain and phase shift for each sub-carrier). Pilot signals and training symbols (preambles) may also be used for time synchronization (to avoid ISI) and frequency synchronization (to avoid ICI caused by Doppler shift).

OFDM Extended with Multiple Access

OFDM in its primary form is considered as a digital modulation technique, and not a multiuser channel access method, since it is utilized for transferring one bit stream over one communication channel using one sequence of OFDM symbols. However, OFDM can be combined with multiple access using time, frequency or coding separation of the users.

In OFDMA, frequency-division multiple access is achieved by assigning different OFDM sub-channels to different users. OFDMA supports differentiated quality of service by assigning different number of sub-carriers to different users in a similar fashion as in CDMA, and thus complex packet scheduling or Media Access Control schemes can be avoided.

2.2.3 Idealized System Model

This section describes the main blocks of OFDM system as shown in Fig 2-6 and Fig 2-7.

Transmitter

An OFDM carrier signal is the sum of a number of orthogonal sub-carriers, with baseband data on each subcarrier being independently modulated commonly using some type of QAM or PSK. This composite baseband signal is typically used to modulate a main radio frequency (RF) carrier.

First a Serial stream of binary digits is demultiplexed into N_c parallel streams, and each one mapped to a (possibly complex) symbol stream using some modulation constellation (QAM, PSK, etc.). Note that the constellations may be different, so some streams may carry a higher bit-rate than others.

An inverse FFT is computed on each set of symbols, giving a set of complex time-domain samples. These samples are then quadrature-mixed to passband in the standard way. The real and imaginary components are first converted to the analogue domain using DACs; the analogue signals are then used to modulate cosine and sine waves at the carrier frequency, f_c, respectively. These signals are then summed to give the transmission signal $x(t)$.

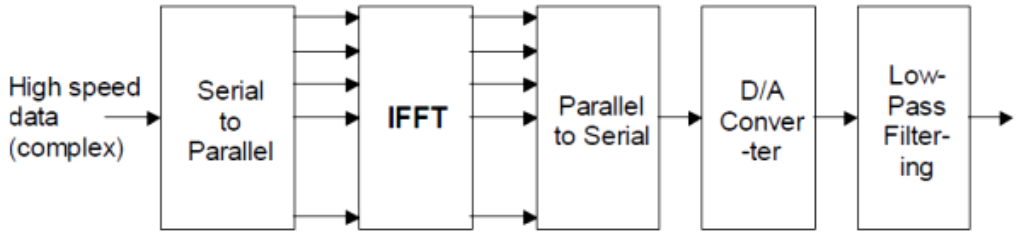

Fig 2-6 OFDM transmitter block diagram.

Receiver

The receiver picks up the signal $y(t)$, which is then quadrature-mixed down to baseband using cosine and sine waves at the carrier frequency. This also creates signals centered on $2f_c$, so low-pass filters are used to reject these. The baseband signals are then sampled and digitized using ADCs, and a forward FFT is used to convert back to the frequency domain.

This returns N_c parallel streams, each of which is converted to a binary stream using an appropriate symbol detector. These streams are then re-combined into a serial stream, which is an estimate of the original binary stream at the transmitter.

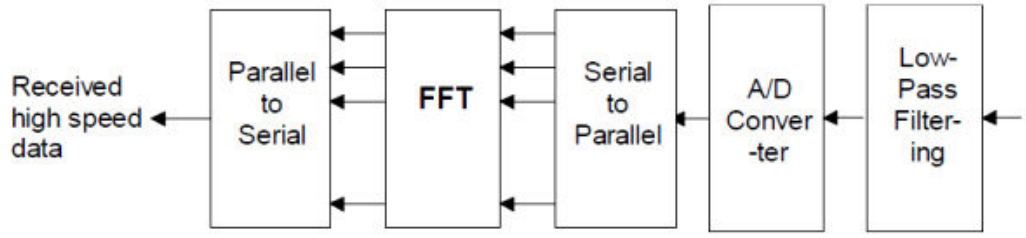

Fig 2-7 OFDM receiver block diagram.

2.3 Conclusion

In this chapter we introduced some of the fundamental concepts of wireless communications in order to understand the rest of the thesis. First we reviewed the relevant models for wireless channel characterization for SISO and MIMO. Then we provided the main background required for understanding of MIMO advantages and precoding techniques. Furthermore, the concept of OFDM was introduced and its benefits to the cellular systems were indicated.

2.4 Bibliography

[1] D. Gesbert, M. Shafi, D. Shiu, P. Smith and A. Naguib, "From theory to practice: an overview of MIMO space–time coded wireless systems," *IEEE J. Select. Areas Commun.,* vol. 21, no. 3, p. 281–302, April 2003.

[2] A. Paulraj, R. Nabar and D. Gore, Introduction to Space–Time Wireless Communications, Cambridge University Press, 2003.

[3] A. Paulraj and T. Kailath, "Increasing capacity in wireless broadcast systems using distributed transmission/directional reception". U.S. Patent Patent 5,345,599, 1994.

[4] E. Telatar, "Capacity of multiantenna Gaussian channels," AT&T Bell Labs, 1995.

[5] G. Foschini, "Layered space–time architecture for wireless communication in a fading environment when using multi-element antennas," Bell Labs Tech. J., Autumn 1996.

[6] V. Tarokh, N. Seshadri and A. Calderbank, "Space–time codes for high data rate wireless communication: Performance criterion and code construction," *IEEE Trans. Inform. Theory,* vol. 44, no. 3, p. 744–765, March 1998.

[7] R. Steele, Mobile Radio Communications, New York, NY, USA: Wiley-Pentech Publication, IEEE Press, 1992.

[8] W. C. Jakes, Microwave Mobile Communications, New York, NY, USA: IEEE Press, 1974.

[9] K. J. R. Liu, A. K. Sadek, W. Su and A. Kwasinski, Cooperative Communications and Networking, New York, USA: Cambridge University Press, 2009.

[10] C. Oestges and B. Clerckx, MIMO Wireless Communications, Elsevier academic press, 2007.

[11] D. Tse and P. Viswanath, Fundamentals of Wireless Communications, New York, NY, USA: Cambridge University Press, 2005.

[12] J. Proakis, Digital communications, McGraw-Hill, 2001.

[13] C. Chuah, J. Kahn and D. Tse, "Capacity of multi-antenna array systems in indoor wireless environment," in *Proc. Globecom 1998– IEEE Global Telecommunications Conf.*, Sydney, Australia, 1998.

[14] D. Shiu, G. Foschini, M. Gans and J. Kahn, "Fading correlation and its effect on the capacity of multielement antenna systems," *IEEE Trans. Commun.,* vol. 48, no. 3, p. 502–513, March 2000.

[15] K. Yu, M. Bengtsson, B. Ottersten, D. McNamara, P. Karlsson and M. Beach, "Second order statistics of NLOS indoor MIMO channels based on 5.2 GHz measurements," in *Proc. Globecom 2001 – IEEE Global Telecommunications Conf.*, San Antonio, TX, USA, November 2001.

[16] J. Kermoal, L. Schumacher, K. Pedersen, P. Mogensen and F. Frederiksen, "A stochastic MIMO radio channel model with experimental validation," *IEEE J. Select. Areas Commun.,* vol. 20, no. 6, p. 1211–1226, June 2002.

[17] C. Chuah, D. Tse, J. Kahn and R. Valenzuela, "Capacity scaling in MIMO wireless systems under correlated fading," *IEEE Trans. Inform. IEEE Trans. Inform.,* vol. 48, no. 3, p. 637–650, March 2002.

[18] A. Molisch, M. Win, Y. Choi and J. Winters, "Capacity of MIMO systems with antenna selection," *IEEE Trans. Wireless Commun.,* vol. 4, no. 4, p. 1759–1772, July 2005.

[19] A. Paulraj and D. Gore, "MIMO antenna subset selection with space-time coding," *IEEETrans. Signal Processing,* vol. 50, no. 10, p. 2580–2588, October 2002.

[20] D. Love and R. Heath, "Multimode antenna selection for spatial multiplexing systems with linear receivers," *IEEE Trans. Signal Processing,* vol. 53, no. 6, p. 3042–3056, August 2005.

[21] S. Alamouti, "A Simple Transmit Diversity Technique for Wireless Communications," *IEEE Journal on Selected Areas in Communications,* vol. 16, no. 8, p. 1451–1458, Oct. 1998.

[22] R. VanNee, "New high-rate wireless LAN standards," *IEEE Communications Magazine,* vol. 40, p. 140–147, Jan. 2002.

[23] R. Prasad and R. VanNee, OFDM for Wireless Multilmedia Communications, Artech House Publishers, 2000.

[24] R. VanNee, "A new OFDM standard for high rate wireless LAN in the 5 GHz band," in *Proceedings of the IEEE Vehicular Technology Conference*, 1999.

3 Introduction to Multicell Coordination

In chapter 1 we introduced the concept of multicell coordination as a new and efficient technique for broadband wireless communication systems which improves the network capacity and spectral efficiency and fully benefits from MIMO techniques. Here we introduce some recent scenarios for multicell coordination and then we derive theoretical bounds on capacity for point to point downlinks and extend it to MIMO case considering full cooperation. Finally a simple beamforming technique with limited cooperation among the cells is presented.

3.1 Coordinated Multipoint Communication

The wireless communications field is experiencing a rapid and steady growth. It is expected that the demand for wireless services will continue to increase in the near and medium term, asking for more capacity and putting more pressure on the usage of radio resources. The conventional cellular architecture considers co-located MIMO technology, which is a very promising technique to mitigate the channel fading and to increase the cellular system capacity [1]. On the other hand, OFDM is a simple technique to mitigate the effects of inter-symbol interference in frequency selective channels [2], [3]. However, the problems inherent to these systems such as shadowing,

significant correlation between channels in some environments and inter-cell interference significantly degrade the capacity gains promised by MIMO techniques [4]. Although theoretically attractive, the deployment of MIMO in commercial cellular systems is limited by interference between neighbouring cells, and the entire network is essentially interference-limited [5], [6].

Conventional approaches to mitigate multi-cell interference, such as static frequency reuse and sectoring, are not efficient for MIMO-OFDM networks as each has important drawbacks [4]. Universal frequency reuse (UFR), meaning that all cells/sectors operate on the same frequency channel, is mandatory if we would like to achieve spectrally-efficient communications. However, as it is pointed out in [5], this requires joint optimization of resources in all cells simultaneously to boost system performance and to reduce the radiated power. Such systems have the advantage of macro-diversity that is inherent to the widely spaced antennas and more flexibility to deal with inter-cell interference, which fundamentally limits the performance of user terminals (UTs) at cell edges [4]. Different transmit strategies can be considered, depending on the capacity of the backhaul channel that connects the coordinated BSs. Coordinated multiple point transmission and reception is considered as a main tool to improve the coverage of high data rates, the cell-edge throughput and/or to increase system throughput [7], [8] and thus is already under study in LTE-A under CoMP concept [9].

Recently, an enhanced cellular architecture with a high-speed backhaul channel has been proposed and implemented, under the European FUTON project [10], [11]. This project aims at the design of a distributed broadband wireless system (DBWS) by carrying out the development of a radio over fibre (RoF) infrastructure transparently connecting the BSs to a central unit (CU) where centralized joint processing can be performed. The centralized distributed architecture proposed in the FUTON DBWS system is novel and extends the concepts that are being under discussion in the IMT-Advanced proposal forums. Some similarities exist between the systems, for example a concept of multi-cell MIMO is proposed for IEEE802.16m and coordinated multiple point transmission and reception is considered in LTE-A. However, it is clear that none of the candidate systems aim to exploit the benefits offered by the centralized processing in truly distributed environment in the extent of what has been proposed in the FUTON. In the following section two main scenarios discussed by FUTON namely, *Enhanced* and *Advanced* scenarios; are presented.

3.2 FUTON Coordinated Multicell Scenarios

Multicell architectures that assume a global coordination can eliminate the inter-cell interference completely. However, in practical cellular scenarios, issues such as the complexity of joint signal processing of all the BSs, the difficulty in acquiring full CSI from all UTs at each BS,

and synchronization requirements will make global coordination difficult. Scenarios proposed by FUTON address those issues.

3.2.1 Enhanced Scenario

The first scenario to be tackled within the FUTON project is an enhanced cellular scenario, following a conventional cellular planning, but where there is cooperation between the BSs associated with each cell. The area covered by the set of cooperating BSs is termed supercell. The specific terminologies for such a scenario are:

- **Cell**: The geographical area associated with a given BS. This means that over this area the path loss from the given BS to any point is lower than the path loss from any other BS. In some scenarios where the BS is not omni-directional, it may be more convenient for the cell to be defined as the geographical area associated with a sector of a BS. Such an example is the Manhattan scenario.

- **Supercell**: The area defined by the cells of cooperating BSs (three in Fig 3-1)

- **Serving area**: The area defined by all the cells of the BSs that are linked to the same CU. This is illustrated in Fig 3-1 that considers the overall infrastructure.

For simplicity, Fig 3-1 assumes that the BS is located at the centre of the cell, but, in practice, it can be sectored and each BS may have several antenna elements. Furthermore the number of cooperating BSs in the figure is 3, but this is for illustrative purposes only. From an architecture point of view, the scenario of Fig 3-1 is identical to a classical cellular network, the sole exception being the fact that the base station is not localized, but distributed, consisting of several BSs placed at different locations. The BSs are linked to a CU (e.g., by optical fibre) as proposed in [11], [12]. The BSs corresponding to a supercell are processed jointly by a joint processing unit (JPU) not depending on the utilized technique. Furthermore, one could allow some overlapping between the BSs processed by different JPUs to facilitate handovers. The rationale for such a scenario is one of evolution. If a cellular network is deployed with towers for the base stations, the operators could increase the network capacity and improve coverage by replacing the legacy equipment (but using the same sites), with new equipment where cooperation is allowed between BSs.

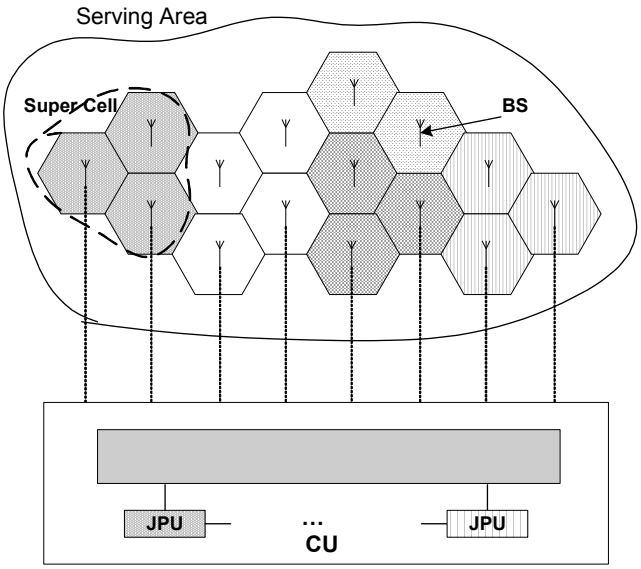

Fig 3-1 Enhanced cellular architecture **[10]**.

3.2.2 Advanced Scenario

In this scenario, the objective is to have simplified BSs that can be deployed in public facilities without the need to acquire sites and install large towers. Furthermore, in order to be easily upgradeable and reconfigurable, there should be no need of very precise static a priori planning. It should be possible to add BSs to accommodate additional traffic demand without the need of a complete re-planning of the network. The configuration of the network would be handled dynamically at the CU.

The architecture for the advanced scenario is shown in Fig 3-2. The terminology is identical to the one used in the enhanced cellular scenario, except for the concepts of the cell and the supercell. Since there is no precise static a priori planning, these concepts are no longer as precise as in the case of Section 3.1.2.1, and, therefore, we use the concept of *joint processing area*, which is the area covered by the set of BSs that are processed by the same JPU.

As there is no precise static a priori planning, the definition of the joint processing areas is dynamic and dependent on the long-term conditions of the environment. For example, if new buildings are built affecting the propagation characteristics of BSs that were originally processed by the same JPU, the BSs could be assigned to different JPUs after reconfiguration.

Illustrated also in Fig 3-2 is the possibility of overlapping between the BSs processed by different JPUs to facilitate handover, similar to the enhanced cellular scenario. However, this figure does not strictly define the scenario but gives an overall picture of the principle behind the scenario definition. The rationale for such a scenario can be briefly summarized as the answer that must be provided to address the needs of future wireless networks. It is expected that, in future wireless

networks, one should be able to receive and accommodate multiple services/requirements. Therefore,

• The system should be able to handle dynamic patterns, and

• The system should have the capacity to accommodate new services as they emerge.

All these aspects combined result in a highly evolvable and dynamic operating environment, making it difficult to use a priori static planning aiming at a horizon of several years. The following will be needed:

• The ability to reconfigure the system on the fly in order to meet dynamic patterns, and

• The implementation of simple ways to upgrade/reconfigure the network without requiring new planning.

These requirements will have implications in terms of the FUTON concept:

• The system should be able to handle dynamic patterns, and

• The BSs must be quite simple; it should be possible to deploy them in public facilities in order to provide easy upgrade paths.

• The "planning" in the advanced scenario should consist of dynamic allocation of resources to be performed real-time at the CU. Some a priori pre-planning will be, of course, needed.

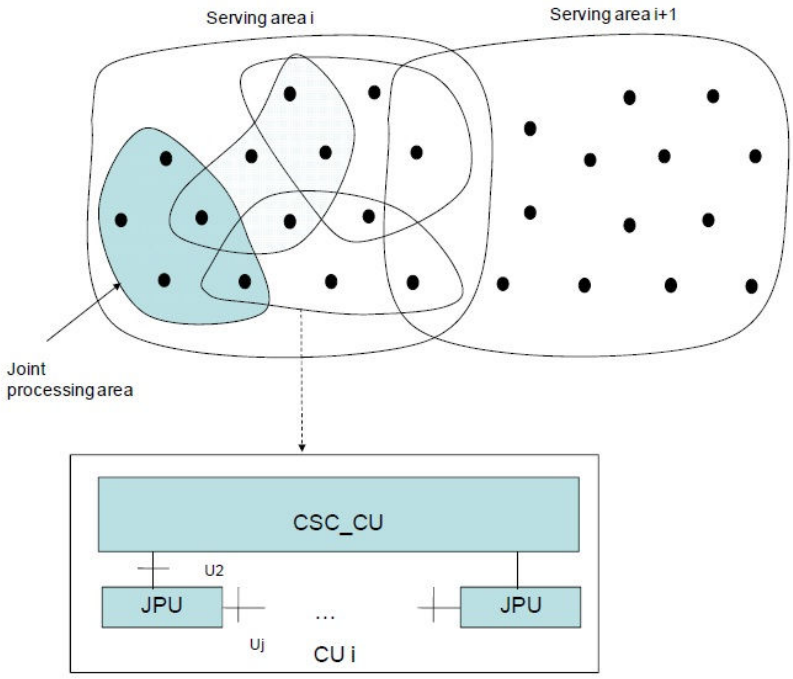

Fig 3-2 Advanced cellular architecture **[10]**.

3.3 Multi-Point Frequency-Flat Baseband Model

Three fundamental challenges in mobile communications are the fact that transmission takes place over *a) a shared medium*, which is often subject to *b) rich scattering*, and to which we desire *c) simple and flexible access* of many communicating entities. The first aspect implies that any transmission must be band limited in order not to disturb other transmissions on adjacent bands, which requires the design of particular transmit and receive filters. The second aspect implies that any receiver may observe a superposition of multiple differently delayed and attenuated copies of originally transmitted signals, which in the context of broadband transmission may lead to inter-symbol interference (ISI) that has to be dealt with. The third aspect means that we need a low-cost and efficient signal processing solution that can divide a mobile communications system into a large number of flexible bit pipes according to many users' or the applications' needs.

Therefore OFDM is a proper approach to address all aspects stated above. It also has the advantage that it enables a simple mathematical notation and analysis, as it is often sufficient to observe the baseband transmission on a single frequency-flat sub-carrier, which can be seen as a transmission over an additive white Gaussian noise (AWGN) channel. The assumption of an AWGN channel also implicitly requires the OFDM systems of all communicating entities to be perfectly synchronized in time and frequency. When observing the transmission on a single frequency-flat OFDM subcarrier, typically N_t antennas are considered at transmitter side and N_r antennas at receiver side.

In this thesis we focus on downlink transmission of multicell cooperation systems. Because we are interested in cooperation on transmission side while for uplink there is no cooperation among UTs. In the following section we will present the general downlink model for the system and then we will derive the capacity bound for point to point scenario and finally extend it to multicell case.

3.4 Downlink Transmission

We consider a multicell scenario where symbols intended for UTs, independently precoded and sent over each OFDM sub-channel. At the receivers' side the signals are equalized and the decision variables are obtained in order to extract the symbols.

$$\tilde{\mathbf{x}} = \mathbf{G}^H \mathbf{y} = \mathrm{diag}\left(\begin{bmatrix} \mathbf{G}_1^H & \cdots & \mathbf{G}_K^H \end{bmatrix}\right)\left(\mathbf{H}^H \mathbf{W}\mathbf{x} + \mathbf{n}\right) \tag{3.1}$$

where $\mathbf{x}$ of size $N_r \times 1$ are the symbols to be transmitted to the UTs, and $\mathbf{W}$ of size $N_t \times N_r$ is a precoding matrix applied at the BS side. The transmit covariance is now given as

$\Psi = \mathrm{E}\left\{\mathbf{W}\mathbf{x}\left(\mathbf{x}\right)^{H}\mathbf{W}^{H}\right\}$, which is subject to either a *sum*, *per-BS* power constraint. The reason for the latter case is that each BS has a separate power amplifier with a limited linear range. However issues such as peak to average power ratio (PAPR) should be considered in case of OFDM. The channel matrix $\mathbf{H}$ of size $N_t \times N_r$ is the channel matrix. $\mathbf{G}$ of size $N_r \times N_r$ is the global equalization matrix on the receiver side, which is block-diagonal, as we assume that no cooperation takes place between UTs. $\mathbf{n}$ of size $N_r \times 1$ is zero-mean Gaussian noise present at UTs, with covariance $\mathrm{E}\left\{\mathbf{n}\mathbf{n}^{H}\right\} = \sigma^2\mathbf{I}$. Each UT finally obtains estimated symbols $\tilde{\mathbf{x}}$ of size $N_r \times 1$.

3.4.1 Basic Downlink Capacity Bounds

To derive the information-theoretic bounds, we assume that the signals $\mathbf{x}$ are zero-mean Gaussian and each symbol sees the same channel realization $\mathbf{H}$. For point-to-point link in the downlink the upper-bound for transmission rate in bits per channel use is given by [13]

$$R \le I\left(X;Y\right) = \max_{\Psi} \log_2 \left|\mathbf{I} + \frac{1}{\sigma^2}\mathbf{H}\Psi\mathbf{H}^{H}\right| \tag{3.2}$$

And can be used to state capacity. $I\left(X;Y\right)$ denotes the mutual information between transmitter and receiver side. Point-to-point capacity under perfect channel knowledge at transmitter and receiver can be achieved with linear precoding and equalization.

Now we assume that there are one BS and multiple UTs. In this case the downlink channel follows the broadcast model (BC). In this case all the symbols are transmitted by BS to UTs. On the UT side the right symbols is extracted and the rest are considered as noise. Note that the capacity region of the BC is only known for special cases. In general, the capacity is only known for the case of Gaussian noise [14]. To tackle the inter-user interference, dirty paper coding [15] which is a nonlinear precoding can be used which allows a UT to receive signals free of interference, if this interference is known non-causally to the transmitter. So in general precoding can be used for such a system to cancel or at least mitigate the interference. There is a duality between this method and successive interference cancellation (SIC) in the uplink: If the SIC *decoding* order is $1\cdots K$ in the uplink, UT k only sees interference from UTs $k+1\cdots K$, as the others have already been decoded and their signals removed. Equivalently, if the downlink DPC *encoding* order is $1\cdots K$, UT k only sees interference from UTs $k+1\cdots K$, as the previously encoded streams can be considered as known interference and be pre-cancelled at the transmitter side. However there are some issues with nonlinear precoding comparing to decoding techniques

which are the complexity and the need for transmit channel knowledge. That is why the research community has resorted to more practical and less complex precoding methods for the downlink such as Tamlinson-Harashima precoding (THP) [16], [17] and sphere-precoding [18], but these generally require highly precise channel knowledge at the transmitter-side. To further simplify the precoding methods linear techniques also introduced with lower complexity where there is less need for information to be shared and exchanged over the backhaul. Here we consider both BC capacity (i.e. dirty paper coding (DPC) performance) and the rates achievable with linear precoding, where residual interference between streams is simply accepted as noise as sated before, knowing that a practical transmission scheme may then perform somewhere in between.

The capacity region of the BC can be stated as

$$R_{BC} = conv\left\{ \bigcup_{\mathbf{W},u} \left\langle R_1\left(\mathbf{W},u\right),...,R_K\left(\mathbf{W},u\right)\right\rangle \right\} \tag{3.3}$$

where $\bigcup$ and $\mathrm{conv}(.)$ are the *union* of multiple rate regions and *convex hull* operation, respectively [19], in this case over all choices of precoding matrix $\mathbf{W}$ and encoding order u, where for each fixed parameter choice the UT rates are bounded as

$$R_k\left(\mathbf{W},u\right) \le \log_2 \left| \mathbf{I} + \left(\sigma^2\mathbf{I} + \sum_{u(j)>u(k)} \mathbf{H}_k^H \mathbf{W}_j \mathbf{W}_j^H \mathbf{H}_k \right)^{-1} \mathbf{H}_k^H \mathbf{W}_k \mathbf{W}_k^H \mathbf{H}_k \right| \tag{3.4}$$

It is not easy to find optimal precoder $\mathbf{W}$ to maximize a particular weighted sum rate of UTs as any sum of UT rates as given in (3.4) is typically non-convex in $\mathbf{W}$ [20]. However as stated in [21], there a duality between uplink and downlink which we will discuss shortly. Let us state $\mathbf{C}_k = \sigma^2\mathbf{I} + \sum_{u(j)>u(k)} \mathbf{H}_k^H \mathbf{W}_j \mathbf{W}_j^H \mathbf{H}_k$ and $\mathbf{D}_k = \sigma^2\mathbf{I} + \sum_{u(j)<u(k)} \mathbf{H}_j \mathbf{G}_j \mathbf{G}_j^H \mathbf{H}_j^H$ as the interference terms in downlink and uplink, respectively. Then we can rewrite the upper bound for the rate in (3.4) for BC as

$$R_k\left(\mathbf{W},u\right) \le \log_2 \left| \mathbf{I} + \mathbf{C}_k^{-1} \mathbf{H}_k^H \mathbf{W}_k \mathbf{W}_k^H \mathbf{H}_k \right| \tag{3.5}$$

$$= \log_2 \left| \mathbf{I} + \mathbf{D}_k^{-1} \mathbf{H}_k \mathbf{G}_k \mathbf{G}_k^H \mathbf{H}_k^H \right| \tag{3.6}$$

which is equivalent to the uplink rate bound for a MAC, given fixed transmit filters $\mathbf{G}_k$ and opposite decoding order $\overline{u}$. Also as shown in [22], (3.5) is given by (3.6). The authors in [21] have

also shown that the above equations hold for all UTs if and only if the sum power is the same in both cases, i.e. if $\mathrm{tr}\left\{\sum_k \mathbf{G}_k \mathbf{G}_k^H\right\} = \mathrm{tr}\left\{\sum_k \mathbf{W}_k \mathbf{W}_k^H\right\}$. Hence, we can conclude that the capacity regions of the MIMO BC and MIMO MAC under the same sum power constraint are equivalent. In order to obtain the BC capacity, we can take convex hull around many MAC regions with different per-UT powers summing up to the same overall power. This is illustrated in Fig 3-3 for an example channel mentioned in the figure legend. It was shown in [14] that obtained BC rate region corresponds to the *Sato upper bound* [23], proving that there can be no other scheme that performs better. Hence, capacity has been obtained for the BC case of Gaussian noise.

By observing equations (3.5) - (3.6) we find out that it is possible to calculate the optimal precoding matrix $\mathbf{W}$ if the dual uplink transmit filters $\mathbf{G}$ are known. This is possible by calculating $\forall k\ \mathbf{D}_k$ directly from $\mathbf{G}_1..\mathbf{G}_k$, and then determining $\mathbf{C}_k$ and $\mathbf{W}_k = \mathbf{D}_k^{-1/2}\mathbf{C}_k^{1/2}\mathbf{G}_k$ iteratively, starting with UT K [21]. The calculation of $\mathbf{G}_k$ requires not only the optimization of each UT's individual transmit covariance, but also the power distribution among UTs since the dual uplink is subject to a sum power constraint. This is a convex optimization problem under the assumption of non-linear precoding (DPC) and can be solved via numerical methods [24].

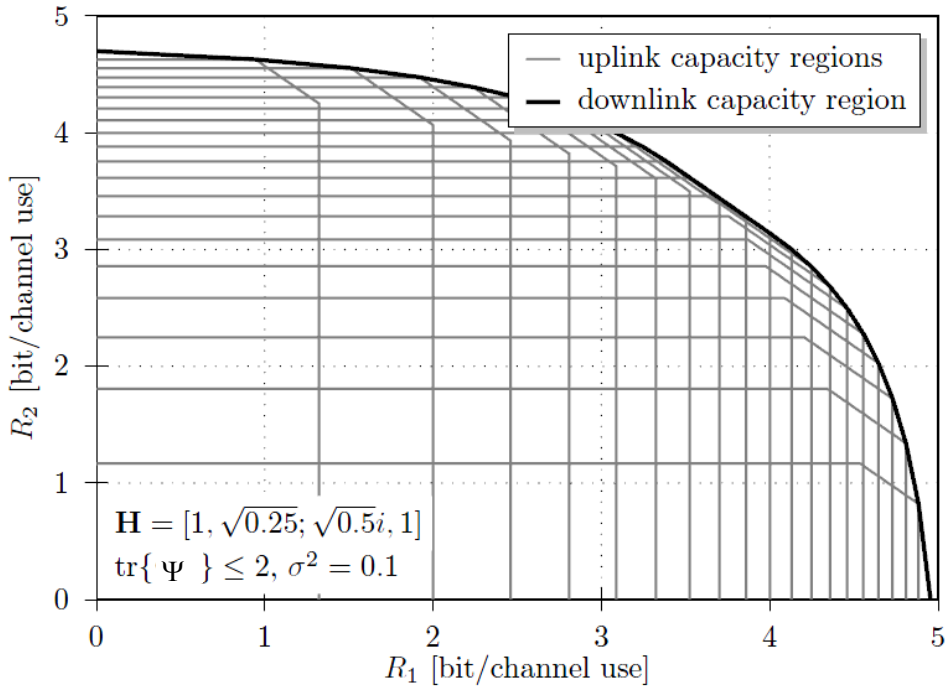

Fig 3-3 Illustration of uplink/downlink duality **[22]**.

3.4.2 Extended Downlink Capacity Bound for Cooperative Multicell Architecture

Now we assume a multicell scenario where a set of B BSs comprising a super-cell is considered; each BS is equipped with N_{t_b} antennas, transmitting to K UTs. The total number of transmitting antennas per-super-cell is $N_t = \sum_{b=1}^{B} N_{t,b}$. User k an antenna array of N_{r_k} elements and the total number of receive antennas per-super-cell is $N_r = \sum_{k=1}^{K} N_{r,k}$.

As mentioned in previous section, all existing duality results in the literature depend crucially on the sum-power constraint across all transmit antennas but in a physical implementation of a Multicell transmission system, the powers are constrained on a per-BS basis which is more realistic, i.e. $\mathrm{E}\left[\mathbf{x}_i\right]^2 \le P_{t_b}$.

Similar to previous section, uplink/downlink duality can also be used to calculate capacity regions and the precoding matrix $\mathbf{W}$ for a BC under per-BS power constraints [25], [26]. The formulation of the dual of the per-BS constrained downlink problem as an uplink problem with an uncertain noise also gives rise to numerical methods for solving the per-BS downlink problem. Capacity region calculation then becomes more complex, as the update of dual uplink transmit covariances and uplink noise covariance have to be performed iteratively [26], and convergence may become an issue. Toward this end, we first define a beamforming achievable rate region for the multiple receive-antenna channel (general case), then extend the results to the capacity region [26].

3.4.2.1 Achievable Rate Region Duality

Consider the general multi-antenna downlink channel model as

$$\mathbf{y}_i = \mathbf{H}_i \mathbf{s} + \mathbf{n}_i, \qquad i = 1,...K \tag{3.7}$$

We define the *beamforming achievable rate region* of the downlink as follows. In a beamforming design, each receiver employs a set of N_{r_k} receive filters $\mathbf{G}_{i,m}$ to create N_{r_k} independent data streams

$$y_{i,m} = \mathbf{G}_{i,m}^H \mathbf{y}_i, \qquad m = 1,..., N_{r_k} \tag{3.8}$$

where the receive filters $\mathbf{G}_{i,m}$'s are $N_{r_k} \times 1$ unit-norm vectors. The transmitter employs $N_{r_k} K$ precoders, denoted as $\mathbf{w}_{i,m}$

$$\mathbf{s} = \sum_{i=1}^{K} \sum_{m=1}^{N_{T_k}} x_{i,m} \mathbf{w}_{i,m} \tag{3.9}$$

where $x_{i,m}$ is a scalar denoting the information signal for the i th user m th data stream. Let $\mathrm{E}\left[x_{i,m}^2 \right] = 1$.

Without interference subtraction, the SINR for the i th user and m th data stream is

$$SINR = \frac{\left| g_{i,m}^2 \mathbf{H}_i \mathbf{w}_{i,m} \right|^2}{\sum_{(j,k) \neq (i,m)} \left| g_{i,m}^2 \mathbf{H}_i \mathbf{w}_{j,k} \right|^2 + \sigma^2} \tag{3.10}$$

The achievable rate for user i is then

$$R_i = \sum_{m=1}^{N_{T_k}} \log\left(1 + \frac{SINR_{i,m}}{\Gamma} \right). \tag{3.11}$$

where Γ is the SINR gap to capacity. The *beamforming achievable rate region* for the downlink is the set of $\left(R_1, ..., R_k \right)$ satisfying the power constraint.

According to theorem 2 in [26], the beamforming achievable rate region of a downlink channel under a fixed set of per-BS power constraints is identical to the achievable rate region of a dual uplink channel with a sum power constraint, P_{tb} across all the users and with an uncertain noise whose covariance matrix is diagonal and satisfies the total power constraint. This uplink–downlink duality holds either with or without dirty-paper coding and successive interference subtraction. This uplink–downlink duality holds for channels with an arbitrary number of transmit and receive antennas, and for any SINR gap Γ.

3.4.2.2 Capacity Region Duality

For a multiuser channel, boundary points of the capacity region are not necessarily achieved with water-filling covariance matrices. In this case, the information theoretically optimal transmission strategy is not a diagonalization of the effective channel by each user. Nevertheless, transmit and receive beamforming with interference cancellation and zero gap is still capacity achieving. This is true because of the following. First, any arbitrary transmit covariance matrix can be synthesized using the eigenvectors of the covariance matrix as the transmit beamformers, i.e., $\mathbf{s} = \mathbf{G}\mathbf{x}$, where $\mathbf{x}$ contains the information bits. Second, information in $\mathbf{x}$ can be recovered at the

receiver via a set of MMSE receive beamformers with interference subtraction. This is because, $I(\mathbf{s};\mathbf{y}) = I(\mathbf{x};\mathbf{y}) = I(\mathbf{x}_1;\mathbf{y}) + I(\mathbf{x}_2;\mathbf{y}\,|\,\mathbf{x}_1) + \cdots + I\left(\mathbf{x}_{N_t};\mathbf{y}\,|\,\mathbf{x}_1,...,\mathbf{x}_{N_t-1}\right)$, and each of $I(\mathbf{x}_k;\mathbf{y}\,|\,\mathbf{x}_1,...,\mathbf{x}_{k-1})$ is achievable with MMSE receiver beamforming and interference subtraction. Therefore, beamforming with interference subtraction and with scalar zero-gap error correcting codes is capacity achieving. A similar argument can be made for dirty-paper coding. This fact provides a link between information theoretical capacity region and the beamforming region for the downlink channel.

According to corollary 4 in [26], the capacity region of a downlink channel under a fixed set of per-antenna power constraints, is identical to the capacity region of a dual uplink channel with a sum power constraint across all the users and with an uncertain noise whose covariance matrix is diagonal and satisfies total power constraint. This capacity region duality holds for channels with an arbitrary number of transmit and receive antennas.

3.4.2.3 Extension to Multicell Scenario

The per-BS power constraint is also motivated by future wireless systems in which BSs can be connected via high-speed links and are capable of joint processing and cooperatively transmitting information to and receiving information from UTs. In this case, an individual power constraint must be applied to a group of antennas on each BS. A similar situation is applicable for downlink wireline systems in which joint transmission may be done at the central office by coordinating multiple modems. In this case, an individual power constraint is again applicable to each modem. In both scenarios the only difference is on the channel model used

It is straightforward to generalize the capacity analysis to per-BS power constraint for multicell scenarios since the duality for this case holds similarly. Under certain idealistic assumptions, multiple BSs can be modeled as one *virtual* BS with N_t antennas. The capacity region is similar to per-antenna case but only differs in channel specifications such as dimension (more transmitting antennas $N_t = \sum_b N_{tb}$) and different path loss and coefficient for antennas belong to different BSs. As opposed to the single-BS case, we have now obtained a*rray gain* of at most $10\log_{10}(N_{t_b})$ dB, and *spatial multiplexing gain*, as the larger channel dimensionality improves the eigenvalue distribution and hence orthogonality between BSs. Considering multiple fading realizations, cooperation may also yield spatial macro diversity gain.

3.5 Downlink Multiuser Beamforming with Interference Rejection Combing

To finalize this chapter we present and evaluate a non-cooperative downlink transmission scheme where no significant cooperation takes place between BSs (very limited, no data sharing), but where interference-aware transmission and reception is performed within BS's. The BSs or different antennas of a single BS perform precoding based on limited feedback from the UTs, while at the receiver side interference-aware scheduling and interference rejection combining (IRC) is performed [27].

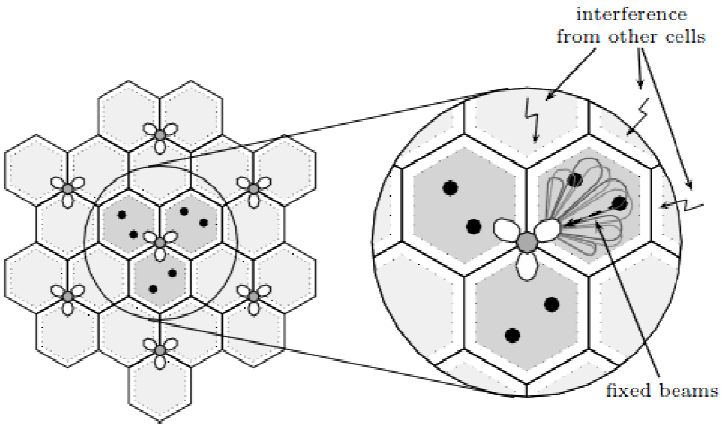

Fig 3-4 Concept of intra-cell beamforming **[22]**.

Here we present a realistic solution for decentralized interference management. Predicting interference at the receiver side also is the key fact that helps to improve the link adaptation process. Therefore fixed sets of possible precoding vectors are considered for transmission as depicted in Fig 3-4. In this scenario UTs are assumed to send their preferred precoder matrix indicators (PMIs) in combination with corresponding SINRs after equalization via a low-rate feedback channel. For the equalization at the UT, comprehensive channel knowledge required, which may be obtained by multicell channel estimation based on pilot symbols. This requires synchronization of downlink transmission [28]. With this approach considerable throughput gains for MIMO systems in multicell environments is achieved similar to those known for point-to-point links.

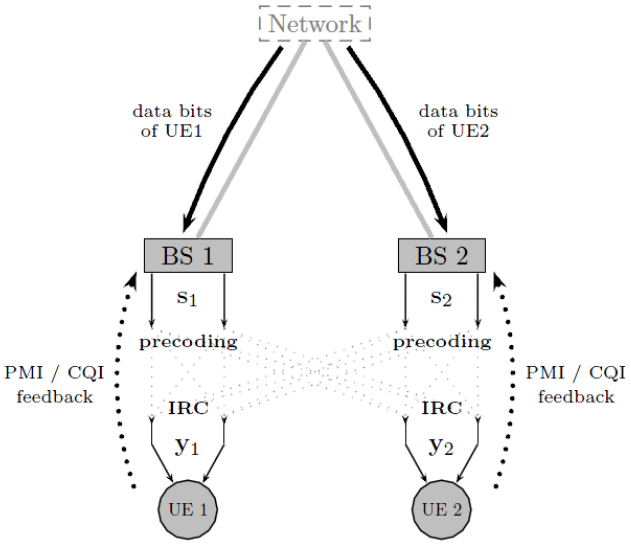

Fig 3-5 Non.cooperative transmission and PMI/channel quality indicator (CQI) feedback concept **[22]**.

3.5.1 Downlink System Model

Here we extend the multi-antenna downlink model from [22], observing an OFDM transmission on a single subcarrier from B BSs to K UTs that are scheduled to the same resource in time and frequency. The BSs and UTs are equipped with N_{t_b} and N_{r_k} antennas, respectively, leading to an total number of $N_t = BN_{t_b}$ transmit antennas and $N_r = KN_{r_k}$ receive antennas. Therefore, each BS can transmit up to N_{t_b} streams simultaneously on the same resource, while each UT can receive up to N_{r_k} such streams simultaneously. Clearly, a BS can serve less UT's with more receiving streams or more UT's with less receiving streams. As non-cooperative downlink transmission is assumed, this means different streams should be sent via different BS's and there is no data sharing as illustrated for a setup with $B = K = 2$ in Fig 3-5. Consequently, the overall precoding matrix $\mathbf{W}$ of size $N_t \times N_r$ is sparse, as each column connected to one UT and one stream may only have non-zero entries connected to the antennas of one BS.

We consider UT k which is served by BS $b = k$ and define K_b as the set of all UTs served by BS b simultaneously on the same resource, which is limited to the number of antennas on a BS, e.g. $|K_b| \leq N_{t_b}$. Finally the received signal at UT k can be expressed as

$$\mathbf{y}_k = \underbrace{\left(\mathbf{H}_k^b\right)^H \mathbf{W}_k^b}_{H_k^{eq}} \mathbf{x}_k + \underbrace{\sum_{\substack{j\in\{\mathrm{K_b}\}\\ j\neq k}} \left(\mathbf{H}_k^b\right)^H \mathbf{W}_j^b \mathbf{x}_j}_{\text{Intra-cell intfr. term } (\alpha_k)} + \underbrace{\sum_{\substack{j\in\{\mathrm{K}\}\\ j\notin\{\mathrm{K_b}\}}} \left(\mathbf{H}_k^b\right)^H \mathbf{W}_j^b \mathbf{x}_j + \mathbf{n}_j}_{\text{Intr-cell intfr. and noise term } (\beta_k)} \tag{3.12}$$

where $\mathbf{H}_k$ is the channel between UT k and all BSs and $\mathbf{H}_k^b$ and $\mathbf{W}_k^b$ are the channel matrix and precoding vectors connected to BS b and UT k. We write as $\mathbf{H}_k^{eff}$ the equivalent channel between UT k and its serving BS after precoding, which consists of one column for each of the N_{r_k} streams the UT may potentially receive. The corresponding data streams located in $\mathbf{x}_k$ with $\mathbf{x} \sim NC(\mathbf{0},\mathbf{I})$ are distorted by the intra-cell and inter-cell interference and noise in α_k and β_k, respectively. Each BS b may select a limited number $Q_b \leq N_{t_b}$ of active beams to serve one user with multiple streams or multiple users simultaneously. This is done by choosing the corresponding columns of BS b-related precoding matrix $\mathbf{W}_b$ from the columns of a pre-defined beam set Δ_i^b. In the case of $N_{t_b} = 2$, beam set size $\omega = 2$ and DFT-based precoding, this can be either

$$\Delta_1^b = \frac{1}{\sqrt{2}}\begin{bmatrix} 1 & 1 \\ i & -i \end{bmatrix} \quad or \quad \Delta_2^b = \frac{1}{\sqrt{2}}\begin{bmatrix} 1 & 1 \\ 1 & -1 \end{bmatrix} \tag{3.13}$$

Columns in $\mathbf{W}_b$ which represents the unused streams, are simply substitute with zeros. Note that $\mathbf{W}_b$ has to be scaled depending on the choice of Q_b in order to satisfy a per-BS power constraint, i.e. $\mathrm{tr}\left\{\mathbf{W}_b\left(\mathbf{W}_b\right)^H\right\} \leq P_b$. with only one active beam, i.e. $Q_b = 1$, we call it single stream (*SS)* mode, while for $Q_b > 1$, we refer to it as multiple stream (*MS)* mode [27].

3.5.2 Linear Receivers

Here we present the structure of the receiver. Assuming that a linear equalizer g_{ki} is used to extract the useful symbol from $\mathbf{y}_k$ connected to stream i, we obtain the SINR after equalization given by

$$\mathrm{SINR}_{\mathrm{k,i}} = \frac{\mathbf{g}_{k,i}^H \bar{\mathbf{h}}_{k,i} \bar{\mathbf{h}}_{k,i}^H \mathbf{g}_{k,i}}{\mathbf{g}_{k,i}^H \mathbf{V}_{k,i} \mathbf{g}_{k,i}} \tag{3.14}$$

where $\mathbf{V}_{ki}$ is the covariance matrix of the streams received by UT k (except stream i) and the interfering signals and noise in α_k and β_k, i.e $\mathbf{V}_{k,u} = \sum_{v \neq u} \bar{\mathbf{h}}_{k,v} \left(\bar{\mathbf{h}}_{k,v} \right)^H + E\left\{ \left(\alpha_k + \beta_k \right) \left(\alpha_k + \beta_k \right)^H \right\}$. For IRC [29], the interference-aware MMSE receiver is used, i.e.

$$\mathbf{g}_{k,i}^{\mathrm{MMSE}} = \mathbf{R}_{yy,k}^{-1} \bar{\mathbf{h}}_{k,i} \tag{3.15}$$

where $\mathbf{R}_{yy,k}$ represents the covariance matrix of the received signal $\mathbf{y}_k$, i.e.

$$\mathbf{R}_{yy,k} = E\left\{ \mathbf{y}_k \left(\mathbf{y}_k \right)^H \right\} = \bar{\mathbf{H}}_k \bar{\mathbf{H}}_k^H + E\left\{ \left(\alpha_k + \beta_k \right) \left(\alpha_k + \beta_k \right)^H \right\} \tag{3.16}$$

The MMSE receiver yields SINR after equalization as

$$\mathrm{SINR}_{k,i}^{\mathrm{MMSE}} = \bar{\mathbf{h}}_{k,i}^H \mathbf{V}_{k,i}^{-1} \bar{\mathbf{h}}_{k,i} \tag{3.17}$$

considering MRC receiver

$$\mathbf{g}_{k,i}^{\mathrm{MRC}} = \bar{\mathbf{h}}_{k,i} \tag{3.18}$$

the receiver yields the following SINR after equalization

$$\mathrm{SINR}_{k,i}^{\mathrm{MMSE}} = \frac{\left\| \bar{\mathbf{h}}_{k,i}^H \bar{\mathbf{h}}_{k,i} \right\|^2}{\bar{\mathbf{h}}_{k,i}^H \mathbf{V}_{k,i}^{-1} \bar{\mathbf{h}}_{k,i}} \tag{3.21}$$

3.5.3 Single-cell Performance

To evaluate the performance of the mentioned schemes a fixed system setting in an isolated cell (i.e., $\mathbf{z}_k = \mathbf{n}_k$ in (3.12)) is considered, where K UTs, each equipped with $N_{r_k} = 2$ receive antennas, communicate with a dual-antenna BS ($N_{t_b} = 2$). The spatial channel model extended (SCME) [9] used and full channel state information at the receiver (CSIR) is assumed. The probabilities of mode selection depending on the average SNR conditions are presented, which are depicted in Fig 3-6 for 2 or 10 users, respectively. Note that resources where a rate cannot be supported by any user are not assigned by the scheduler. For that reason, the selection probability of SS mode drops down to 75% at $P_s / N_0 = -5dB$ in the first case. Three different configurations of the adaptive mode switching system are considered here:

1. **SU-MIMO**: MU-MIMO option is switched off, this means that MS mode reduces to single-user MIMO (SU MIMO). Now only one user is served per physical resource block (PRB) either in diversity or SU-MIMO mode.

2. **MU-MIMO** system as described in [27] with the first beam set Δ_1^b from (3.13) being available. Simultaneously active beams can be assigned independently to different users. The mode per user is selected per PRB, i.e.va user may be served in different modes simultaneously.

3. **MU-MIMO, 2 beam sets**: Adaptive MU-MIMO system with both beam sets from (3.13) being available.

The points where the curves in Fig 3-6 cross the median indicate the SNR regions where the MS mode becomes the dominantly selected one. From both figures, we observe that going from SU-MIMO to MU-MIMO improves choosing the MS mode significantly, as the crossing point is shifted by 5 dB in case of 2 users and by more than 10 dB in case of 10 users down towards the low SNR regime. For 10 users, the crossing point falls below an SNR of 0 dB. Running in MU-MIMO mode also results in significant improvement of spectral efficiencies (refer to [27]). Finally, these results show that MU-MIMO is the best and most efficient criteria in using spatial multiplexing transmission even at low SNR.

It can be seen by adding another beam set the crossing point is shifted further down, which can be attributed to the finer granularity in the quantization of the transmit vector space. For 10 users, the crossing point in Fig 3-6 (b) can be shifted down to about -1.5 dB now. Further, it can be observed that the shape of the probability curves approach that of a step function, emphasizing that the system behavior tends towards a hard mode switching at a fixed SNR value.

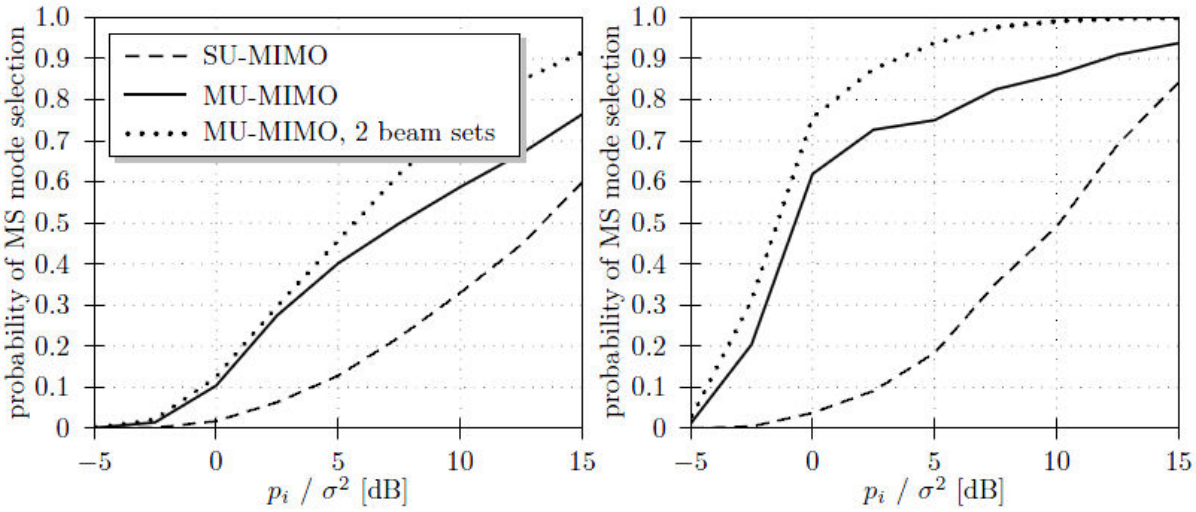

K=2 K=10

Fig 3-6 Probability of the selection of MS mode vs. SNR [22].

3.5.4 Multicell Performance under Perfect CSI

Now we assume a multicell system where the performance is evaluated in a triple-sectorized hexagonal cellular network with $B = 57$ BSs in total, i.e. a center site with three sectors or cells surrounded by two tiers of interfering sites. Simulation parameters are given in [27]. We also assume full and perfect CSIR for Initial evaluations. The SCME with urban macro scenario parameters is used, resulting in user geometry. The UTs are always served by the BS whose signal is received with highest average power over the entire frequency band. For capacity evaluation, only UTs being placed inside the three central cells are evaluated. In this way, BS signals transmitted from the 1st and 2nd tier of sites model the inter-cell interference. Performance is evaluated for both the sum-throughput in a sector and the throughput for individual users. Both values are normalized to the signal bandwidth, yielding a sector's overall spectral efficiency and normalized user throughput, respectively. The achievable rates are determined from the SINRs calculated according to expression (3.17) by using a quantized rate mapping function [30], representing achievable rates in a practical system. From these results, cumulative distribution function (CDF) plots are obtained.

Case 1: All BSs provide one fixed unitary beam set. With respect to SISO reference case, Fig 3-7 (solid lines) indicates a capacity increase of the median sector's spectral efficiency by a factor of $\alpha = 1.95$, $\alpha = 2.88$ and $\alpha = 3.43$ for the MIMO 2×2 ($N_{t_b} \times N_{r_k}$), 2×4 and 4×4 system.

By observing the results it is found out that only small additional capacity gain is obtained for systems with $N_{t_b} > N_{r_k}$ compared to a system with $N_{t_b} = N_{r_k}$. The reason is the constraint of DFT-based precoding, where the total transmit power is distributed evenly over all antennas. In contrast, the system with $N_{t_b} < N_{r_k}$ benefits from added capabilities for interference suppression and higher receive diversity. This enables the system to achieve larger scaling factors, e.g. $\alpha = 2.88$ for MIMO 2×4. The 5th percentile of normalized user throughput, which may serve as a measure to represent the throughput of cell-edge users, shows similar scaling.

Case 2: All BSs provide multiple fixed unitary beam sets. Fig 3-7 (dashed lines) further indicates the potential capacity gains for enabling the users to choose from multiple different beam sets. In this case the system may benefit from an improved channel quantization, yielding a capacity increase of $\alpha = 2.11$ for MIMO 2×2 with two beam sets. However, we shouldn't forget the fact that by assuming this PMI feedback overhead also doubles from 1 bit to 2 bit.

Interference prediction: Note that considering independent adaptation of beam sets for all BSs does not influence the received interference covariance matrix $\mathbf{V}_{k,i}$, since the Wishart product $\mathbf{W}_b \left(\mathbf{W}_b\right)^H$ equals the scaled identity matrix if we assume $\mathbf{W}_b$ to be unitary. However, changing the power allocation for different MIMO transmission modes results in a multi-cell system where $\mathbf{V}_{k,i}$ cannot be predicted at the receiver side. In order to support cell-edge UTs, it is better to arrange e.g. SS with full BS power with the access scheme which is known to the UTs.

3.6 Conclusions

In this chapter we introduced the concept of multicell coordination as a new and efficient technique for broadband wireless communication systems which improves the network capacity and spectral efficiency and system reliability. The enhanced and advanced cooperative multicell scenarios proposed by FUTON were presented then theoretical bounds on capacity for point to point downlinks were derived and extend it BC and cooperative multicell case. Finally a simple beamforming technique with limited cooperation among the cells was presented where data was not shared among BSs and single or multiple streams modes could be chosen to serve UTs.

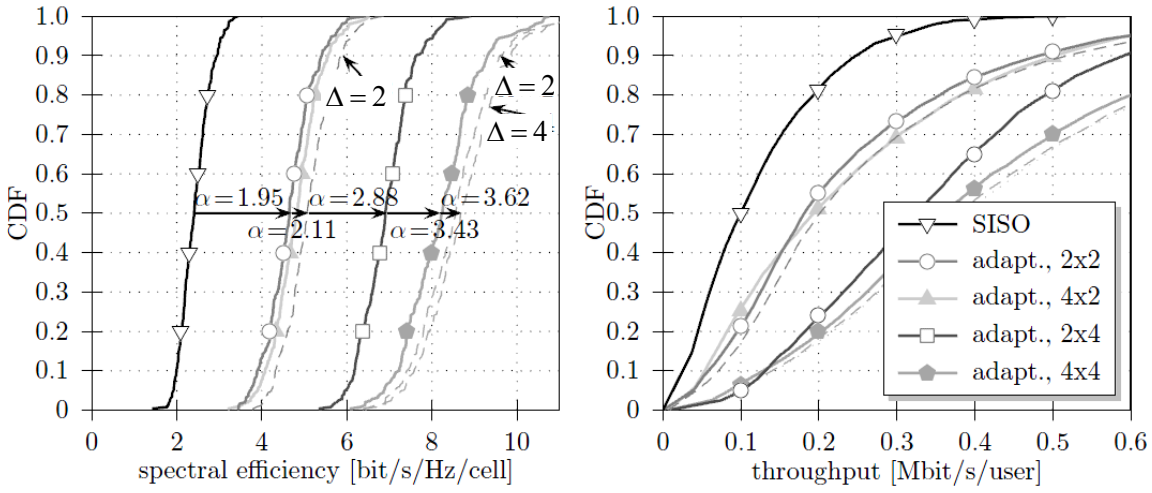

(a) Spectral efficiency. (b) User throughput

Fig 3-7 Idealistic system performance for the SISO, MIMO 2×2 ($N_{t_b}\times N_{r_k}$), 4×2, 2×4 and 4×4 system for 20 users per cell or sector. Dashed lines indicate the performance achievable with $\omega=\{2,4\}$ beam set Δ_i^b [22]

3.7 Bibliography

[1] G. J. Foschini and M. J. Gans, "On limits of wireless communications in a fading environment when using multiple antenna," *Wireless Personal Communication Magazine,* vol. 6, no. 3, pp. 311-335, 1998.

[2] L. S. Uppala and J. Li, "Designing a mobile broadband wireless access network," *IEEE Signal Processing Magazine,* vol. 21, no. 5, pp. 2120-28, 2004.

[3] A. R. S. Bahai, B. R. Saltzberg and M. Ergen, Multi-carrier digital communications theory and applications of OFDM, New York: Springer, 2004.

[4] J. G. Andrews, W. Choi and R. W. Heath, "Overcoming interference in spatial multiplexing MIMO cellular networks," *IEEE Wireless Communication Magazine,* vol. 47, no. 6, pp. 95-104, 2007.

[5] G. J. Foschini, "Coordinating multiple antenna cellular networks to achieve enormous spectral efficiency," *IEEE Proceedings on Communications,* vol. 153, no. 4, pp. 548-555, Aug. 2006.

[6] T. R. Mudumbai, D. R. Brown, U. Madhow and H. V. Poor, "Distributed transmit beamforming: challenges and recent progress," *IEEE Communication Magazine,* vol. 47, no. 2, pp. 102-110, 2009.

[7] D. Gesbert, S. Hanly, S. Shamai, O. Simeone and W. Yu, "Multi-cell MIMO cooperation networks: A new look at interference," *IEEE J. Sel. Areas Commun.,* vol. 28, no. 9, pp. 1380-1408, Dec. 2010.

[8] D. Castanheira and A. Gameiro, "Distributed antenna system capacity scaling," *IEEE Commun. Mag.- Special issue on Coordinated and Distributed MIMO,* vol. 17, no. 3, pp. 75-78, Jun. 2010.

[9] "3GPP, “Coordinated multi-point operation for LTE physical layer aspects," Technical Report 3GPP TR 36.819, 2011.

[10] "FUTON, European ICT project," 2007. [Online]. Available: https://www.ict-futon.eu..

[11] F. Diehm, P. Marsch and G. Fettweis, "The FUTON prototype: proof of concept for coordinated multi-point in conjunction with a novel integrated wireless/optical architecture," in *Proceeding of IEEE WCNC'10*, 2010.

[12] "Web: https://www.ict-futon.eu," European ICT FUTON project. [Online].

[13] T. Cover and J. Thomas, Elements of Information Theory, Wiley, 2006.

[14] H. Weingarten, Y. Steinberg and S. Shamai, "The Capacity Region of the Gaussian," *IEEE Trans. on Inf. Theory,* vol. 52, no. 9, p. 3936–3964, Sept. 2006.

[15] M. Costa, "Writing on dirty paper," *IEEE Trans. on Inf. Theory,* vol. 29, p. 439–441, May 1983.

[16] M. Tomlinson, "New automatic equaliser employing modulo arithmetic," *Electronics Letters,* vol. 7, no. 5,6, pp. 138-139, Mar. 1971.

[17] H. Harashima and H. Miyakawa, "Matched-Transmission Technique for Channels With Intersymbol Interference," *IEEE Trans. on Comms.,* vol. 20, no. 4, pp. 774-780, Aug. 1972.

[18] R. Habendorf, I. Riedel and G. Fettweis, "Reduced Complexity Vector Precoding for the Multiuser Downlink," in *IEEE Global Telecomms. Conf. (GLOBECOM'06)*, Nov. 2006.

[19] S. Boyd and L. Vandenberghe, Convex optimization, Cambridge: Cambridge University Press, 2004.

[20] H. Boche and M. Schubert, "A general duality theory for uplink and downlink beamforming," in *IEEE Vehicular Technology Conf. (VTC'02 Fall)*, Sept. 2002.

[21] N. Jindal, S. Vishwanath and A. Goldsmith, "On the duality of Gaussian multiple-access and broadcast channels," *IEEE Trans. on Inf. Theory,* vol. 50, no. 5, p. 768–783, May 2004.

[22] P. Marsch and G. P. Fettweis, Coordinated Multi-Point in Mobile Communications, Cambridge University Press, 2011.

[23] H. Sato, "An outer bound to the capacity region of broadcast channels," *IEEE Trans. on Inf. Theory,* vol. 24, no. 3, p. 374–377, May 1978.

[24] H. Viswanathan, S. Venkatesan and H. Huang, "Downlink capacity evaluation of cellular networks with known-interference cancellation," *IEEE Journal on Selected Areas in Comms.,* vol. 21, no. 5, p. 802–811, June 2003.

[25] P. Marsch, "Coordinated Multi-point under a Constrained Backhaul and Imperfect Channel Knowledge," Technische Universitat Dresden, 2010.

[26] W. Yu and T. Lan, "Transmitter optimization for the multi-antenna downlink with per-antenna power constraints," *IEEE Trans. on Signal Proc.,* vol. 55, p. 2646–2660, June 2007.

[27] L. Thiele, M. Schellmann, T. Wirth and V. Jungnickel, "Interference-aware scheduling in the synchronous cellular multi-antenna downlink," in *IEEE Vehicular Technology (VTC)*, Apr. 2009.

[28] V. Jungnickel, T. Wirth, M. Schellmann, T. Haustein and W. Zirwas, "Synchronization of cooperative base stations," in *IEEE Int. Symp. on Wireless Comms. Systems (ISWCS'08)*, Oct. 2008.

[29] J. Winters, "Optimum Combining in Digital Mobile Radio with Cochannel Interference," *IEEE Journal on Selected Areas in Comms.,* vol. 2, no. 4, pp. 528-539, July 1984.

[30] "Modulation and coding schemes for the WINNER II system," IST-4-027756 WINNER II. D2.2.3., Nov. 2007.

4 Full Centralized Cooperation for Multicell MIMO OFDM Systems

In this chapter we propose centralized precoding and power allocation schemes for downlink of multicell cellular systems. The aim is to propose a practical centralized technique to remove the inter-cell interference and improve the user's fairness at the cell-edges. The precoder is designed in two phases: first the inter-cell interference is removed by applying a set of centralized precoding vectors; then the system is further optimized through power allocation. Three centralized power allocation algorithms with per-BS power constraint and different complexity tradeoffs are proposed. The results show that the proposed schemes improve the system performance significantly and are ideal when there is a high speed backhaul network. This chapter is based on contributions from [1], [2], [3], [4], [5] *which are the publications from the thesis author where full-centralized schemes were proposed and evaluated for different conditions.*

4.1 Introduction

Multicell cooperation is a promising solution for cellular wireless systems to mitigate inter-cell interference, improve system fairness and increase capacity. In recent years, relevant works on centralized multi-cell precoding techniques have been proposed in [6], [7], [8], [9], [10], [11], [12],

[13], [14]. The multi-cell downlink channel is closely related to the MIMO broadcast channel (BC), where the optimal precoding is achieved by the dirty paper coding (DPC) principle [15]. However, the significant amount of processing complexity required by DPC prohibits its implementation in practical multi-cell processing. Some suboptimal multi-cell linear precoding schemes have been discussed in [6], where analytical performance expressions for each scheme were derived considering nonfading scenario with random phases. The comparison of the achievable rates by the different proposed cooperative schemes showed a trade-off between performance improvement and the requirement for BS cooperation, signal processing complexity and channel state information (CSI) knowledge. In [7] the impact of joint multi-cell processing was discussed through a simple analytically tractable circular multi-cell model. The potential improvement in downlink throughput of cellular systems using limited network coordination to mitigate intercell interference has been discussed in [8], where zero forcing (ZF) and DPC precoding techniques under distributed and centralized architectures have been studied. In [9] a clustered BS coordination is enabled through a multi-cell block diagonalization (BD) scheme to mitigate the effects of interference in multi-cell MIMO systems. Three different power allocation algorithms were proposed with different constraints to maximize the sum rate. A centralized precoder design and power allocation was considered. In [10], the inner bounds on capacity regions for downlink transmission were derived with or without BS cooperation and under per-antenna power or sum-power constraint. The authors showed that under imperfect CSI, significant gains are achievable by BS cooperation using linear precoding. Furthermore the type of cooperation depends on channel conditions in order to optimize the rate/backhaul trade-off. Two multi-cell precoding schemes based on the waterfilling technique have been proposed in [11]. It was shown that these techniques achieve a performance, in terms of weighted sum rate, very close to the optimal. A new BD cooperative multi-cells scheme has been proposed in [13], to maximize the weighted sum-rate achievable for all the UTs. An overview of the theory for multi-cell cooperation in networks has been presented in [16].

In this chapter we propose and evaluate centralized linear precoding and power allocation techniques for multicell MIMO OFDM cooperative systems with a high-speed backhaul channel, where it is assumed that full CSI and data are available at the CU. The precoder design aims at two goals: allow spatial users separation and optimize the power allocation. The two problems can be decoupled leading to a two step design: the centralized precoder vectors design and power allocation algorithms. In this chapter we propose three centralized power allocation algorithms with different complexities and per-BS power constraint: one optimal to minimize the average BER, for which the powers can be obtained numerically by using convex optimization, and two suboptimal. In this latter approach, the powers are computed in two phases. First the powers are derived under total power constraint (TPC). Two criterions are considered, namely minimization of the average

BER, which leads to an iterative approach and minimization of the sum of inverse of signal-to-noise ratio for which closed form solution is achieved. Then, the final powers are computed to satisfy the individual per-BS power constraint.

Most of the proposed power allocation algorithms for multicell based systems have been designed to maximize the sum rate. In this thesis, the criteria used to design power allocation are minimization of the average BER and the sum of inverse of SINR, which essentially lead to a redistribution of powers among users and subcarriers, and therefore provide users fairness mainly at the cell edges, which in practical cellular systems may be for the operators a goal as important as throughput maximization.

The remainder of this chapter is organized as follows: Section 4.2 presents the considered multicell system models. Section 4.3 describes centralized precoder vectors design. In Section 4.4 centralized power allocation schemes are derived for the different precoder vectors. Section 4.5 presents the main simulation results. The conclusions will be drawn in Section 4.6.

4.2 System Model

We consider a multicell system based on the scenario depicted in Fig 4-1 where the BSs are transparently linked by optical fibre to a joint processing unit (JPU) since here joint processing is needed. Thanks to the high speed backhaul, we can assume that all the information of all BSs, i.e., full CSI and data, belonging to the same supercell are available at the JPU. Thus, to remove the multicell multiuser interference we can use a similar centralized linear precoding algorithm designed for single cell systems. The major difference between multicell and single cell systems is that the power constraints have to be considered on a per-BS basis instead. The proposed schemes are considered in two phases: centralized SVD based precoding and centralized power allocation.

To build up the mathematical model we consider that user $k, k = 1,...,K$ can receive up to N_{r_k} data symbols on subcarrier $l, l = 1,...,N_c$ i.e., $\boldsymbol{x}_{k,l} = \begin{bmatrix} x_{k,1,l} & \dots & x_{k,N_{r_k},l} \end{bmatrix}^T$ and the global symbol vector, comprising all user symbol vectors, is $\boldsymbol{x}_l = \begin{bmatrix} \boldsymbol{x}_{1,l}^T & \dots & \boldsymbol{x}_{K,l}^T \end{bmatrix}^T$ of size $N_r \times 1$. The data symbol of user k on subcarrier l, is processed by the transmit precoder $\mathbf{W}_{k,l} \in C^{N_t \times N_{r_k}}$ in JPU, before being transmitted over BSs antennas. These individual precoders together form the global transmit precoder matrix on subcarrier l, $\mathbf{W}_l = \begin{bmatrix} \mathbf{W}_{1,l} & \cdots & \mathbf{W}_{K,l} \end{bmatrix}$ of size $N_t \times N_r$. Let the downlink transmit power over the N_t distributed transmit antennas for user k and data symbol

$i, i = 1,...,N_{r_k}$ on subcarrier l, be $p_{k,i,l}$, with $\mathbf{p}_{k,l} = \left[p_{k,1,l} \quad \cdots \quad p_{k,N_{r_k},l} \right]$ and the global power matrix $\mathbf{P}_l = \text{diag}\left\{ \left[\mathbf{p}_{1,l} \quad \cdots \quad \mathbf{p}_{K,l} \right] \right\}$ is of size $N_r \times N_r$.

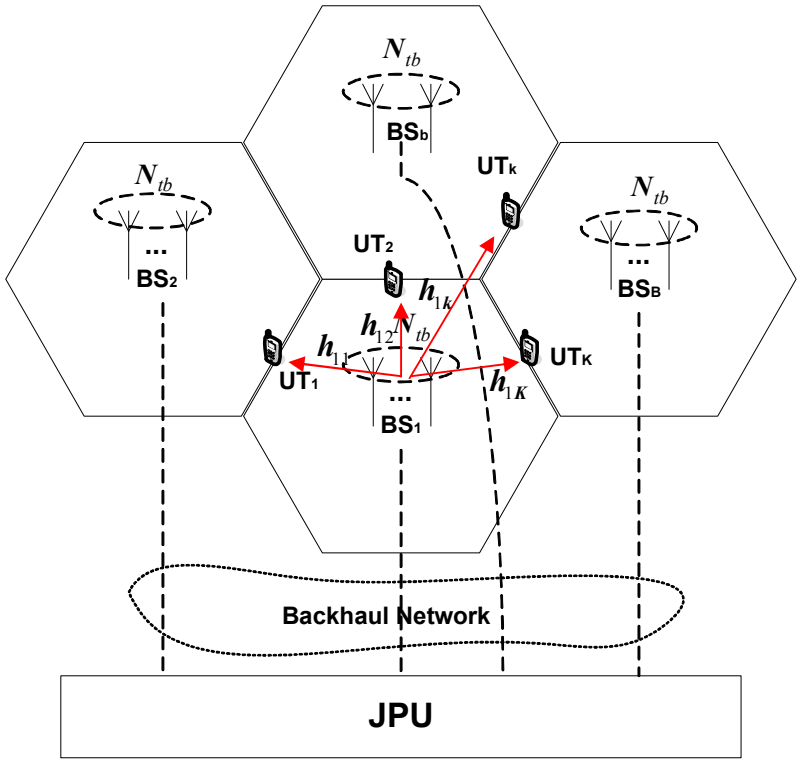

(Precoding and power allocation computation at JPU)

Fig 4-1 Multicell system model with K UTs (illustrated for $B = 4$ base stations equipped with N_{t_b} antennas) and with JPU, the subcarrier script is omitted for simplicity.

Under the assumption of linear precoding, the signal transmitted by the JPU on subcarrier l is given by $\mathbf{z}_l = \mathbf{W}_l \mathbf{P}_l^{1/2} \mathbf{x}_l$ and the global received signal vector on subcarrier l can be expressed by,

$$\mathbf{y}_l = \mathbf{H}_l \mathbf{W}_l \mathbf{P}_l^{1/2} \mathbf{x}_l + \mathbf{n}_l \tag{4.1}$$

where $\mathbf{H}_l = \left[\mathbf{H}_{1,l}^T \quad \cdots \quad \mathbf{H}_{K,l}^T \right]^T$ of size $N_r \times N_t$ is the global frequency flat fading MIMO channel on subcarrier l. The channel of user k is represented by $\mathbf{H}_{k,l} = \left[\mathbf{H}_{1,k,l} \quad \cdots \quad \mathbf{H}_{b,k,l} \quad \cdots \quad \mathbf{H}_{B,k,l} \right]$ of size $N_{r_k} \times N_t$, and $\mathbf{H}_{b,k,l}$ of size $N_{r_k} \times N_{t_b}$ represents the channel between user k and BS $b, b = 1,...,B$ on subcarrier l. The channel $\mathbf{H}_{b,k,l}$ can be decomposed as the product of the fast fading $\mathbf{H}_{b,k,l}^c$ and slow fading $\Phi_{PL_{b,k}}$ components,

i.e., $\mathbf{H}_{b,k,l}=\mathbf{H}^{c}_{b,k,l}\Phi_{PL_{b,k}}$, where $\mathbf{H}^{c}_{b,k,l}$ represents correlation and fast fading and can be further decomposed as $\mathbf{H}^{\mathrm{c}}_{\mathrm{b,k,l}}=\mathbf{R}^{1/2}_{\mathrm{r,b,k,l}}\left(\mathbf{H}^{\mathrm{c}}_{\mathrm{b,k,l}}\right)_{\mathrm{iid}}\mathbf{R}^{1/2}_{\mathrm{t,b,k,l}}$, where $\left(\mathbf{H}^{\mathrm{c}}_{\mathrm{b,k,l}}\right)_{iid}$ contains the fast fading coefficients with i.i.d. $CN(0,1)$ entries, $\boldsymbol{R}_{r,b,k}=\mathrm{E}\left\{\boldsymbol{h}_{b,k,l,i}\boldsymbol{h}^{H}_{b,k,l,i}\right\}$ and $\boldsymbol{R}_{t,b,k}=\mathrm{E}\left\{\boldsymbol{h}^{H}_{b,k,l,j}\boldsymbol{h}_{b,k,l,j}\right\}$ are the normalized receiver and transmitter correlations matrixes, respectively [17].

Vector $\boldsymbol{h}_{b,k,l,i}$ is the i^{th} column of $\mathbf{H}^{\mathrm{c}}_{\mathrm{b,k,l}}$ of size $N_{r_k}\times 1$ and represents the channel from the i^{th} transmit antenna of BS b to the correlated receiver antenna array of user k. Vector $\boldsymbol{h}_{b,k,l,j}$ is the j^{th} row of $\mathbf{H}^{\mathrm{c}}_{\mathrm{b,k,l}}$ of size $1\times N_{t_b}$ and represents the channel from the j^{th} receiver antenna of UT k to the correlated transmitter antenna array of BS b. The transmission links between the BSs and a given UT are assumed to be uncorrelated, thanks to distributed antenna system (DAS) concept, but the transmit antennas channels seen by a single BS to each UT may be correlated and $\rho_{b,k}$ represents the long-term power gain between BS b and user k

$$\Phi_{PL_{b,k}}=\mathrm{diag}\left(\left[\underbrace{\Phi_{PL_{1,k}}\ \cdots\ \Phi_{PL_{1,k}}}_{N_{t,b}}\cdots\underbrace{\Phi_{PL_{B,k}}\ \cdots\ \Phi_{PL_{B,k}}}_{N_{t,b}}\right]\right) \tag{4.2}$$

where all the transmitting signals from a single BS to user k, experience the same path loss. $\Phi_{PL_{b,k}}$ is defined in chapter 2 equation (2.11).

From a channel point of view, the centralized DBWS can be represented with a virtual MIMO model. The inputs and outputs of this system are the antennas of the UT on one side and the antennas of all BSs that communicate with the given UT on the other side. This channel looks like a typical MIMO channel. The main differences in the distributed antenna context resides in two main issues: the channel matrix does not have the same variance on all coefficients and as mentioned before, there are only correlations between antenna elements belonging to the same BS and not among all transmit antennas.

Vector $\mathbf{n}_l=\left[\mathbf{n}^{T}_{1,l}\ \cdots\ \mathbf{n}^{T}_{K,l}\right]^{T}$ represents the global AWGN vector and $\mathbf{n}_{k,l}=\left[n_{k,1,l}\ \ \ldots\ \ n_{k,N_{r_k},l}\right]^{T}$ is the noise at the user k terminal on subcarrier l with zero mean and power σ^2, i.e., $\mathrm{E}\left\{\mathbf{n}_{k,l}\mathbf{n}^{H}_{k,l}\right\}=\sigma^2\mathbf{I}_{N_{r_k}}$.

The signal transmitted by the BS b on subcarrier l can be written as $\boldsymbol{z}_{b,l}=\mathbf{W}_{b,l}\mathbf{P}_l^{1/2}\mathbf{x}_l$, where $\mathbf{W}_{b,l}$ of size $N_{t_b}\times N_r$ represents the global precoder at BS b on subcarrier l. The average transmit power of BS b is then given by,

$$\mathrm{E}\left\{\left\|\mathbf{z}_b\right\|^2\right\}=\sum_{k=1}^{K}\sum_{i=1}^{N_{r_k}}\sum_{l=1}^{N_c}p_{k,i,l}\left[\mathbf{W}_{b,k,l}^H\mathbf{W}_{b,k,l}\right]_{i,i} \tag{4.3}$$

where $\mathbf{z}_b$ is the signal transmitted over the N_c subcarriers and $\mathbf{W}_{b,k,l}$ of size $N_{t_b}\times N_{r_k}$ represents the precoder of user k on subcarrier l at BS b.

4.3 Centralized Precoding Schemes

In this section, we present BD scheme for single-antenna UTs and a generalization of that for multi-antenna UTs known as SVD based precoding. The latter scheme is similar to the one proposed in [17].

4.3.1 BD Precoding

Assuming that we have K single-antenna UTs and $N_t\geq K$, the global transmit precoder matrix on subcarrier *l* will have the following form,

$$\mathbf{W}_l=\mathbf{H}_l^H\left(\mathbf{H}_l\mathbf{H}_l^H\right)^{-1} \tag{4.4}$$

By substituting the precoder matrix of (4.4) in (4.1), we have,

$$\mathbf{y}_l=\mathbf{P}_l^{1/2}\mathbf{x}_l+\mathbf{n}_l, \tag{4.5}$$

From equation (4.5) it is easy to see that the instantaneous SNR of data symbol intended for user k on subcarrier l can be written as,

$$\mathrm{SNR}_{k,l}=\frac{p_{k,l}}{\sigma^2}, \tag{4.6}$$

4.3.2 Singular Value Decomposition (SVD) Precoding

Assumming $N_t\geq N_r$,we briefly define $\tilde{\mathbf{H}}_{k,l}$ as the following $\left(N_r-N_{r_k}\right)\times N_t$ matrix,

$$\tilde{\mathbf{H}}_{k,l}=\left[\mathbf{H}_{1,l}\ldots\mathbf{H}_{k-1,l},\mathbf{H}_{k+1,l}\ldots\mathbf{H}_{K,l}\right]^T \tag{4.7}$$

If we denote rank of $\tilde{\mathbf{H}}_{k,l}$ as $\tilde{L}_{k,l}$ then the null space of $\tilde{\mathbf{H}}_{k,l}$ has dimension of $N_t - \tilde{L}_{k,l} \geq N_{r_k}$. The SVD of $\tilde{\mathbf{H}}_{k,l}$ is partitioned as follows,

$$\tilde{\mathbf{H}}_{k,l}=\tilde{\mathbf{U}}_{k,l}\tilde{\mathbf{\Sigma}}_{k,l}\left[\tilde{\mathbf{V}}_{k,l}^{(0)}\ \tilde{\mathbf{V}}_{k,l}^{(1)}\right]^H \tag{4.8}$$

where $\tilde{\mathbf{V}}_{k,l}^{(0)}$ holds the $N_t - \tilde{L}_{k,l}$ singular vectors in the null space of $\tilde{\mathbf{H}}_{k,l}$. The columns of $\tilde{\mathbf{V}}_{k,l}^{(0)}$ are candidate for user k precoding matrix $\mathbf{W}_{k,l}$, causing zero gain at the other users, hence result in an effective single-user MIMO (SU-MIMO) system. Since $\tilde{\mathbf{V}}_{k,l}^{(0)}$ potentially holds more precoders than the number of data streams user can support, an optimal linear combination of these vectors must be found to build matrix $\mathbf{W}_{k,l}$, which can have at most N_{r_k} columns. To do this, the following SVD is formed,

$$\mathbf{H}_{k,l}\tilde{\mathbf{V}}_{k,l}^{(0)}=\mathbf{U}_{k,l}\mathbf{\Sigma}_{k,l}\left[\mathbf{V}_{k,l}^{(0)}\ \mathbf{V}_{k,l}^{(1)}\right]^H \tag{4.9}$$

where $\mathbf{\Sigma}_{k,l}$ is $L_{k,l}\times L_{k,l}$ and $\mathbf{V}_{k,l}^{(1)}$ represents the $L_{k,l}$ singular vectors with non-zero singular values. The $L_{k,l} \leq N_{r_k}$ columns of the product $\tilde{\mathbf{V}}_{k,l}^{(0)}\mathbf{V}_{k,l}^{(1)}$ represent precoders that further improve the performance subject to producing zero inter-cell interference. The transmit precoder matrix will thus have the following form,

$$\bar{\mathbf{W}}_l = \left[\tilde{\mathbf{V}}_{1,l}^{(0)}\mathbf{V}_{1,l}^{(1)} \quad \ldots \quad \tilde{\mathbf{V}}_{K,l}^{(0)}\mathbf{V}_{K,l}^{(1)}\right]\mathbf{P}_l^{1/2} = \mathbf{W}_l\mathbf{P}_l^{1/2} \tag{4.10}$$

The global precoder matrix with power allocation, $\bar{\mathbf{W}}_l = \left[\mathbf{W}_{1,l} \quad \ldots \quad \mathbf{W}_{K,l}\right]\mathbf{P}_l^{1/2}$ as computed above, block-diagonalizes the global equivalent channel $\mathbf{H}_l$, i.e., $\mathbf{H}_l\bar{\mathbf{W}}_l = \mathrm{diag}\left\{\left[\mathbf{H}_{e,1,l},\ldots,\mathbf{H}_{e,K,l}\right]\right\}$ and the interference is completely removed considering perfect CSI.

Let us define $\mathbf{H}_{e,k,l}=\mathbf{H}_{k,l}\bar{\mathbf{W}}_{k,l} = \mathbf{H}_{k,l}\mathbf{W}_{k,l}\mathbf{P}_{k,l}^{1/2}$ of size $N_{r_k}\times N_{r_k}$ as the equivalent enhanced channel for user on subcarrier l, where $\mathbf{P}_{k,l}=\mathrm{diag}\{\mathbf{p}_{k,l}\}$ is of size $N_{r_k}\times N_{r_k}$. Rewriting equation (4.1) for this user, we have,

$$\mathbf{y}_{k,l}=\mathbf{H}_{e,k,l}\mathbf{x}_{k,l}+\mathbf{n}_{k,l} \tag{4.11}$$

To estimate $\mathbf{x}_{k,l}$, user k processes $\mathbf{y}_{k,l}$ by doing Maximal Ratio Combining (MRC) [18], and the soft decision variable $\hat{\mathbf{x}}_{k,l}$ is given by

$$\hat{\mathbf{x}}_{k,l}=\mathbf{H}_{e,k,l}^{H}\mathbf{y}_{k,l}=\mathbf{H}_{e,k,l}^{H}\mathbf{H}_{e,k,l}\mathbf{x}_{k,l}+\mathbf{H}_{e,k,l}^{H}\mathbf{n}_{k,l} \tag{4.12}$$

Transmission in Multiplexing mode

In multiplexing mode each UT can receive $N_{r,k}$ different data symbols. For this case channel $\mathbf{H}_{e,k,l}$ can be easily estimated at UT k. It can be shown that,

$$\mathbf{H}_{e,k,l}^{H}\mathbf{H}_{e,k,l}=\operatorname{diag}\left\{\left[p_{k,1,l}\lambda_{k,1,l},\ldots,p_{k,N_{r,k},l}\lambda_{k,N_{r_k},l}\right]\right\} \tag{4.13}$$

where $\sqrt{\lambda_{k,i,l}}$ is the i^{th} singular value of matrix $\mathbf{H}_{k,l}\mathbf{W}_{k,l}$. From equations (4.12) and (4.13) is easy to see that the instantaneous SNR of data symbol i of user k on subcarrier l can be written as

$$\mathrm{SNR}_{k,i,l}=\frac{p_{k,i,l}\lambda_{k,i,l}}{\sigma^2} \tag{4.14}$$

Transmission in Diversity mode

In diversity mode each UT receives only one data symbol and thus $N_{r,k}$ copies are received on each UT. In this case, the system benefits from diversity gain. Rewriting equation (4.13) assuming this mode we have

$$\mathbf{H}_{e,k,l}^{H}\mathbf{H}_{e,k,l}=\frac{1}{N_{r_k}}\operatorname{diag}\left\{\left[p_{k,1,l}\lambda_{k,1,l},\ldots,p_{k,N_{r,k},l}\lambda_{k,N_{r_k},l}\right]\right\} \tag{4.15}$$

Similarly it is easy to see that the instantaneous SNR of user k can be written as

$$\mathrm{SNR}_{k,l}=\frac{p_{k,l}\sum_{i=1}^{N_{r_k}}\lambda_{k,i,l}}{N_{r_k}\sigma^2}=\frac{p_{k,l}\alpha_{k,l}}{\sigma^2} \tag{4.16}$$

From (4.6),(4.14) or (4.16) assuming a M-ary QAM constellations, the instantaneous probability of error of data symbol i of user k on subcarrier l is given by [19],

$$P_{e,k,i,l}=\psi Q\left(\sqrt{\beta SNR}\right) \tag{4.17}$$

Where $SNR = \left\{ SNR_{k,i,l}, SNR_{k,l} \right\}$ $Q(x) = \left(1/\sqrt{2\pi}\right)\int_{x}^{\infty} e^{-\left(t^2/2\right)} dt$, $\beta = 3/\left(M-1\right)$ and $\psi = \left(4/\log_2 M\right)\left(1-1/\sqrt{M}\right)$.

4.4 Centralized Power Allocation Strategies

Once the multicell multiuser interference removed, the power loading elements of $\mathbf{P}_l$ can be computed in order to minimize or maximize some metrics. Most of the proposed power allocation algorithms for precoded multicell based systems have been designed to maximize the sum rate, (e.g., [6], [14]). In this section, the criteria used to design centralized power allocation are minimization of the average BER (MBER) and sum of inverse of SNRs, which essentially lead to a redistribution of powers among users and therefore provide users fairness (which in practical cellular systems may be for the operators a goal as important as throughput maximization). The latter has a closed form expression with low complexity comparing MBER scheme. The aim of these power allocation schemes is to improve the user's fairness at the cell edge.

To realize that goal two approaches can be considered: optimizing transmit power elements individually on each subcarrier, i.e. the power per subcarrier is constrained to P_{tb}/N_c or alternatively the cost functions can be minimized jointly over all the available subcarriers and the overall power of each BS is constrained to P_{tb}. Clearly, the latter approach is more efficient since we have more degrees of freedom (DoF) to minimize the cost functions so it is used in the following sections.

4.4.1 Optimal Minimum BER Power Allocation Approach

We minimize the instantaneous average probability under the per-BS power constraint P_{tb}, i.e., $\sum_{k=1}^{K}\sum_{i=1}^{N_k}\sum_{l=1}^{N_c} p_{k,i,l}\left[\mathbf{W}_{b,k,l}^{H}\mathbf{W}_{b,k,l}\right]_{i,i} \le P_{tb}$, $b = 1,...,B$. Without loss of generality, we assume a 4-QAM constellation, and thus the optimal power allocation problem with per-BS power constraint can be formulated as,

$$\min_{\{p_{k,i,l}\}}\left(\frac{1}{KN_{r_k}N_c}\sum_{k=1}^{K}\sum_{i=1}^{N_{r_k}}\sum_{l=1}^{N_c}Q\left(\sqrt{\frac{p_{k,i,l}\lambda_{k,i,l}}{\sigma^2}}\right)\right)$$
$$\text{s.t.}\begin{cases}\sum_{k=1}^{K}\sum_{i=1}^{N_{r_k}}\sum_{l=1}^{N_c}p_{k,i,l}\left[\mathbf{W}_{b,k,l}^{H}\mathbf{W}_{b,k,l}\right]_{i,i}\le P_{tb}\ ,b=1,..,B\\ p_{k,i,l}\ge 0,\ k=1,..,K,i=1,..,N_{r_k},l=1,..,N_c\end{cases} \tag{4.18}$$

Since the objective function is convex in $p_{k,i,l}$, and the constraint functions are linear, this is a convex optimization problem. Therefore, it may be solved numerically by using for example the interior-point method [20].

In diversity mode (4.18) can be written as

$$\min_{\{p_{k,l}\}}\left(\frac{1}{KN_c}\sum_{k=1}^{K}\sum_{l=1}^{N_c}Q\left(\sqrt{\frac{p_{k,l}\alpha_{k,l}}{\sigma^2}}\right)\right)$$
$$\text{s.t.}\begin{cases}\frac{1}{N_{r_k}}\sum_{k=1}^{K}\sum_{l=1}^{N_c}p_{k,l}\sum_{i=1}^{N_{r_k}}\left[\mathbf{W}_{b,k,l}^{H}\mathbf{W}_{b,k,l}\right]_{i,i}\le P_{tb}\\ p_{k,l}\ge 0,\ \forall k,l\end{cases} \tag{4.19}$$

This scheme is referred as centralized per-BS optimal power allocation (Cent. per-BS OPA).

4.4.2 Suboptimal MBER Power Allocation Approach

Since the complexity of the above scheme is too high, and thus it could not be of interest for real wireless systems, we also resort to less complex suboptimal solutions. The proposed strategy has two phases: first the power allocation is computed by assuming that all BSs of each supercell can jointly pool their power, i.e., a TPC P_t is imposed instead and the above optimization problem reduces to,

$$\min_{\{p_{k,i,l}\}}\left(\frac{1}{KN_{r_k}N_c}\sum_{k=1}^{K}\sum_{i=1}^{N_{r_k}}\sum_{l=1}^{N_c}Q\left(\sqrt{\frac{p_{k,i,l}\lambda_{k,i,l}}{\sigma^2}}\right)\right)$$
$$\text{s.t.}\begin{cases}\sum_{k=1}^{K}\sum_{i=1}^{N_{r_k}}\sum_{l=1}^{N_c}p_{k,i,l}\left[\mathbf{W}_{k,l}^{H}\mathbf{W}_{k,l}\right]_{i,i}\le P_t\\ p_{k,i,l}\ge 0,\ k=1,..,K,i=1,..,N_{r_k},l=1,..,N_c\end{cases} \tag{4.20}$$

with $\sum_{k=1}^{K}\sum_{i=1}^{N_{r_k}}\sum_{l=1}^{N_c} p_{k,i,l}\left[\mathbf{W}_{k,l}^{H}\mathbf{W}_{k,l}\right]_{i,i} = \sum_{k=1}^{K}\sum_{i=1}^{N_{r_k}}\sum_{l=1}^{N_c} p_{k,i,l}$, note that the N_{r_k} columns of $\mathbf{W}_{k,l}$ have unit norm. Using the Lagrange multipliers method [21], the following cost function with μ Lagrange multiplier is minimized,

$$J_{c,1} = \frac{1}{KN_{r_k}N_c}\sum_{k=1}^{K}\sum_{i=1}^{N_{r_k}}\sum_{l=1}^{N_c} Q\left(\sqrt{\frac{p_{k,i,l}\lambda_{k,i,l}}{\sigma^2}}\right) + \mu\left(\sum_{k=1}^{K}\sum_{i=1}^{N_{r_k}}\sum_{l=1}^{N_c} p_{k,i,l} - P_t\right) \tag{4.21}$$

The powers $p_{k,i,l}$ can be determined by setting the partial derivatives of $J_{c,1}$ to zero and as shown in [1], the solution is (see appendix A for proof),

$$p_{k,i,l} = \frac{\sigma^2}{\lambda_{k,i,l}} W_0\left(\frac{\lambda_{k,i,l}^2}{8\pi\mu^2\left(KN_{r_k}N_c\right)^2\sigma^4}\right) \tag{4.22}$$

It is also straightforward to obtain power elements in diversity mode

$$p_{k,l} = \frac{\sigma^2}{\alpha_{k,l}} W_0\left(\frac{\alpha_{k,l}^2}{8\pi\mu^2K^2N_c^2\sigma^4}\right) \tag{4.23}$$

where W_0 stands for Lambert's W function of index 0 [22]. This function $W_0(x)$ is an increasing function. It is positive for $x > 0$, and $W_0(0) = 0$. Therefore, μ^2 can be determined iteratively to satisfy $\sum_{k=1}^{K}\sum_{i=1}^{N_{r_k}}\sum_{l=1}^{N_c} p_{k,i,l} = P_t$. The optimization problem of (4.20) is similar to the single cell power allocation optimization problem, where the users are allocated the same total multicell power, which may serve as a lower bound of the average BER for the multicell with per-BS power constraint.

The second phase consists in scaling the power allocation matrix $\mathbf{P}_l$ by a factor of η in order to satisfy the individual per-BS power constraints as discussed in [9] which can be given by

$$\eta = \frac{P_{tb}}{\max_{b=1,\ldots,B}\left(\sum_{k=1}^{K}\sum_{i=1}^{N_{r_k}}\sum_{l=1}^{N_c} p_{k,i,l}\left[\mathbf{W}_{b,k,l}^{H}\mathbf{W}_{b,k,l}\right]_{i,i}\right)} \tag{4.24}$$

In diversity mode the scaling factor is simplified to

$$\eta = \frac{P_{tb}}{\max_{b=1,..,B}\left(\frac{1}{N_{r_k}} \sum_{k=1}^{K} \sum_{l=1}^{N_c} p_{k,l} \sum_{i=1}^{N_{r_k}} \left[\mathbf{W}_{b,k,l}^{H} \mathbf{W}_{b,k,l} \right]_{i,i} \right)} \tag{4.25}$$

This scaled power factor assures that the transmit power per-BS is less or equal to P_{tb}. Note that this factor is less than one and thus the SNR given by (4.14) has a penalty of $10\log(\eta)$ dB. This scheme is referred as centralized per-BS suboptimal iterative power allocation (Cent. per-BS SOIPA).

4.4.3 Suboptimal Closed-from Power Allocation Approach

Although this suboptimal solution significantly reduces the complexity relative to the optimal one, it still needs an iterative search. To further simplify we propose an alternative power allocation method based on minimizing the sum of inverse of SNRs, and a closed-form expression can be obtained. Note that minimizing the sum of inverse of SNRs is similar to the maximization of the harmonic mean of the SINRs discussed in [23]. In this case, the optimization problem is written as,

$$\begin{aligned} &\min_{\{p_{k,i,l}\}} \left(\sum_{k=1}^{K} \sum_{i=1}^{N_{r_k}} \sum_{l=1}^{N_c} \frac{\sigma^2}{p_{k,i,l} \lambda_{k,i,l}} \right) \\ &\text{s.t.} \begin{cases} \sum_{k=1}^{K} \sum_{i=1}^{N_{r_k}} \sum_{l=1}^{N_c} p_{k,i,l} \left[\mathbf{W}_{k,l}^{H} \mathbf{W}_{k,l} \right]_{i,i} \le P_t \\ p_{k,i,l} \ge 0,\ k = 1,..,K, i = 1,..,N_{r_k}, l = 1,..,N_c \end{cases} \end{aligned} \tag{4.26}$$

Since the objective function is convex in $p_{k,i,l}$, and the constraint functions are linear, (4.26) is also a convex optimization problem. To solve it we follow the same suboptimal two phases approach as for the first problem. First, we impose a total power constraint and the following cost function, using again the Lagrangian multipliers method, is minimized,

$$J_{c,2} = \sum_{k=1}^{K} \sum_{i=1}^{N_{r_k}} \sum_{l=1}^{N_c} \frac{\sigma^2}{p_{k,i,l} \lambda_{k,i,l}} + \mu \left(\sum_{k=1}^{K} \sum_{i=1}^{N_{r_k}} \sum_{l=1}^{N_c} p_{k,i,l} - P_t \right) \tag{4.27}$$

Now, setting the partial derivatives of $J_{c,2}$ to zero and after some mathematical manipulations, the powers $p_{k,i,l}$ are given by (proof similar to appendix B),

$$p_{k,i,l} = \frac{P_t}{\sqrt{\lambda_{k,i,l}} \sum_{j=1}^{K} \sum_{n=1}^{N_{r_k}} \sum_{p=1}^{N_c} \frac{1}{\sqrt{\lambda_{j,n,p}}}} \tag{4.28}$$

Again the expression above form diversity mode can be written as

$$p_{k,l} = \frac{P_t}{\sqrt{\alpha_{k,l}} \sum_{i=1}^{K} \sum_{j=1}^{N_c} \frac{1}{\sqrt{\alpha_{i,j}}}} \tag{4.29}$$

The second phase consists in scaling the power allocation matrix $\mathbf{P}_l$ by a factor of η, using (4.29) or (4.29) instead (4.22) or (4.23), in order to satisfy the individual per-BS power constraints. This scheme is referred as centralized per-BS suboptimal closed-form power allocation (Cent. per-BS SOCPA).

4.5 Results and Discussions

4.5.1 Simulation Parameters

In order to evaluate the proposed full centralized multicell cooperation schemes, we assume ITU pedestrian channel model B [24], with the modified taps' delays, used according to the sampling frequency defined on LTE standard [25]. This time channel model was extended to space-time by assuming correlated or uncorrelated channels. To evaluate proposed centralized schemes, we consider two scenarios:

- Scenario 1, where we assume a single supercell with 2 BSs, $B = 2$, which are equipped with 2 antennas, $N_{t_b} = 2$, and 2 UTs, $K = 2$, equipped with 2 antennas, $N_{r_k} = 2$.
- Scenario 2, where we assume a single supercell with 4 BSs, $B = 4$, which are equipped with 2 antennas, $N_{t_b} = 2$, and 2 UTs, $K = 2$, equipped with 2 antennas, $N_{r_k} = 2$.

The main parameters used in the simulations are summarized in the Table 4-1. In order to simplify the channel model we used the same correlation matrices for all the taps. We also assume that each UT is placed on each cell. The long-term channel powers are assumed to be $\Phi_{PL_{b,k}} = 1,\ b = k$ for the intra-cell links, and $\Phi_{PL_{b,k}},\ b \neq k$ are uniformly distributed on the interval $[0.2\ ,\ 0.6]$ for the inter-cell links. All the results are presented in terms of the average BER as a function of per-BS SNR defined as $SNR = P_{tb} / N_c \sigma^2$.

Table 4-1 LTE-based Simulation Parameters

FFT size	1024
available subcarriers (N_c) shared by the *K* users	16
sampling frequency	15.36 MHz
useful symbol duration	66.6 μs
cyclic prefix duration	5.21 μs
overall OFDM symbol duration	71.86 μs
subcarrier separation	15 kHz
modulation	QPSK
average angle of arrival (AoA)	67.5^0
receiver angle spread (AS)	68^0
average angle of departure (AoD)	50^0
transmitter angle spread (AS)	12^0
antenna spacing	half wavelength

4.5.2 Performance Evaluation

This section presents the performance results of proposed centralized precoding and power allocation approaches considering Per-subcarrier power constraint (PC) and Joint-subcarrier PC where the powers are constrained on each subcarrier or on total subcarriers, respectively. We compare the performance results of four centralized precoding schemes: one with non power allocation, which is obtained for the single cell systems by setting $\mathbf{P}_l = \mathbf{I}_{N_r}$, i.e., the power per data symbol is constrained to one. For multicell systems the power matrix $\mathbf{P}_l = \mathbf{I}_{N_r}$ should be scaled by η as defined in (4.24) or (4.25) (setting $p_{k,i,l} = 1, \forall k,i,l$), i.e., $\mathbf{P}_l = \eta \mathbf{I}_{N_r}$ ensuring a per-BS power constraint instead. This scheme is referred as centralized per-BS non-power allocation (Cent. per-BS NPA). The two suboptimal approaches are Cent. per-BS SOCPA and Cent. per-BS SOIPA; and the optimal one is Cent. per-BS OPA. Also, we present results for optimal approach considering total power allocation (Cent. TPC OPA), as formulated in (4.20), which may serve as a lower bound of the average BER for the centralized multicell system with per-BS power constraint.

Fig 4-2 shows the performance results of all considered precoding schemes in diversity mode for scenario 1 and correlated channel, considering a *Per-subcarrier PC* strategy (where the power elements are allocated on each subcarrier independently) and *Joint-subcarrier PC* (where the power elements are allocated jointly on all subcarriers). For case of *Per-subcarrier PC,* the performances of the two proposed suboptimal Cent. per-BS SOIPA and Cent. per-BS SOCPA, and the optimal Cent. per-BS OPA approaches, are very close together. Also the penalty of the Cent. per-BS OPA against the lower bound given by the Cent TPC OPA is approximately 0.7 dB considering a BER=10^{-3}. The results show that the proposed precoding schemes with *Joint-subcarrier PC*, clearly outperform those of *Per-subcarrier PC*. For this case the performance of the suboptimal Cent. per-BS SOIPA and Cent. optimal per-BS OPA is also very close (penalty less than 0.2dB), but the gap between these two schemes and the suboptimal Cent. per-BS SOCPA increases for the *Joint-subcarrier PC* approach. These results show that the Cent. per-BS SOIPA only outperforms the Cent. per-BS SOCPA for large number of sub-channels. Another important issue that should be emphasized is that the penalty of the Cent. per-BS OPA against the Cent. TPC OPA is approximately of 0.7 dB for the *Per-subcarrier PC*, but reduced to less than 0.2 dB with *Joint-subcarrier PC* (BER=10^{-3}), because the number of DoF to minimize the average BER is increased. Intuitively, the penalty decreases as the number of sub-channels increases, i.e., the performance of the Cent. per-BS OPA tends to the performance of the Cent. TPC OPA when the number of sub-channels tends to infinity.

Fig 4-3 depicts the performance of the proposed schemes in diversity mode for scenario 1 in terms of the average BER as function of cross power gain setting the per-BS SNR to 14dB. For this case the long term channel powers are defined as $\Phi_{PL_{b,k}}=1,\ \ b=k$; $\Phi_{PL_{b,k}}=\delta,\ \ b\neq k$, where α is the cross-power gain. As can be seen the lowest BER is corresponding to $\delta=0$ which is expected since this assumption ensures that each BS only transmit to one UT and the system is equivalent to two parallel single user systems without inter-cell interference. As the cross power gain increases, the interference level also increases which degrades the performance. But as can be seen in the figure the curves start to decline slightly for higher values of δ , which can be explained by the fact that as the power gain increases the order of diversity and antenna gain increases too, which mainly compensates the system degradation caused by higher level of interference that is why the curves tend to be flat with just a slight decline.

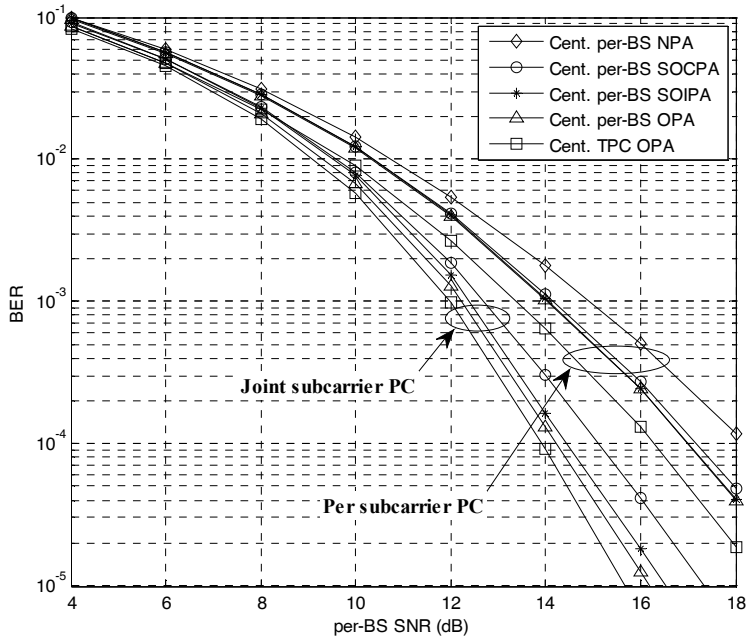

Fig 4-2 Performance evaluation of the proposed centralzed multicell schemes for scenario 1, diversity mode and correlated channels.

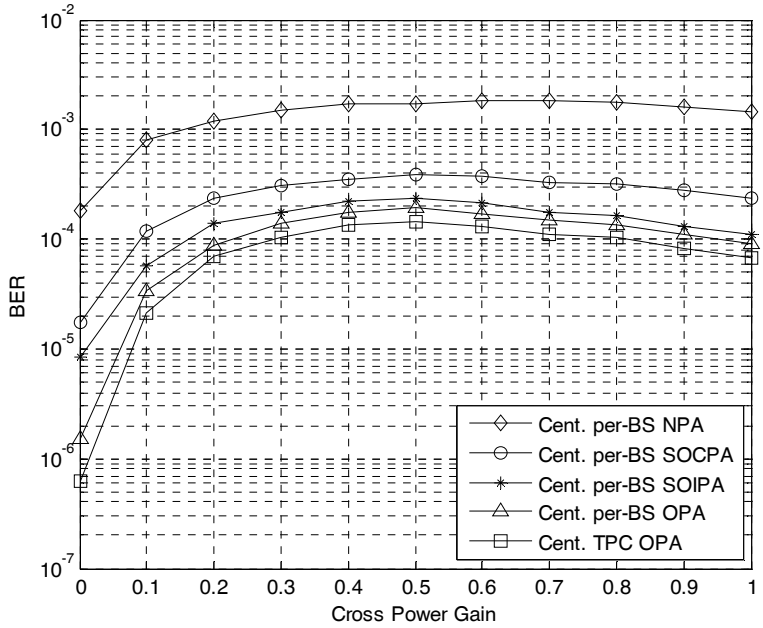

Fig 4-3 BER vs Cross power gain (δ) for proposed schemes for joint subcarrier PC and correlated channels.

The rest of rest of figures in this chapter show the evaluation results for scenarios 1 and 2 with uncorrelated channel and for *Joint-subcarrier PC,* since it provides more degrees of freedom (DoF) and is more practical.

Fig 4-4 shows the performance results of all considered precoding schemes for defined scenario, considering multiplexing mode. It can be observed that the Cent. per-BS SOCPA, Cent. per-BS SOIPA and Cent. per-BS OPA schemes have significant outperformance comparing to the Cent. per-BS NPA approach, because they redistribute the powers across the different sub-channels more efficiently. Comparing the two suboptimal approaches we can see that the iterative one, Cent. per-BS SOIPA, outperforms the closed-form, Cent. per-BS SOCPA because the former is obtained by explicitly minimizing average probability of error. The performance of the proposed suboptimal Cent. per-BS SOIPA and Cent. per-BS SOCPA approaches is close, a penalty less than 0.7 dB for a BER=10^{-2} can be observed. Also, the penalty of the Cent. per-BS SOIPA against the lower bound given by the Cent. TPC OPA is only about 0.5 dB considering also a target BER=10^{-2}.

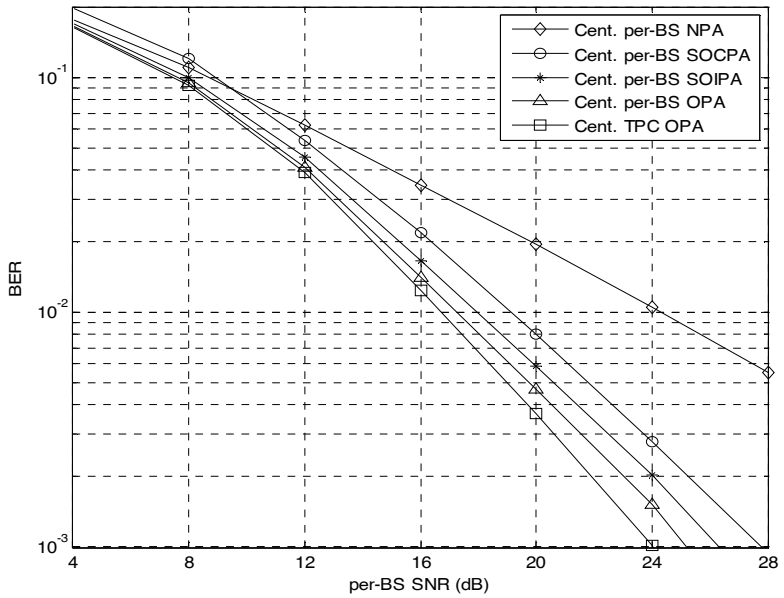

Fig 4-4 Performance evaluation of the proposed multicell schemes for scenario 1, multiplexing mode and uncorrelated channels.

Fig 4-5 shows the performance results of all considered precoding schemes for the same scenario, considering diversity mode. Comparing these results with the last ones, it can be easily seen that there is a large gain due to operating in diversity mode. Since now each data symbol is collected by each receive antenna of each UT. From this figure we basically can point out the same conclusions as for the results obtained in the previous one. However, one important thing that can

be found out by comparing multiplexing and diversity modes is that the difference between Cent. per-BS NPA curves and power allocation based curves (e.g. Cent. per-BS SOIPA) is bigger in multiplexing mode (approximately 4dB) than diversity mode (1.5dB) considering a BER=10^{-2}. This can be explained by the fact that in the diversity mode the equivalent channel gain of each data symbol is the addition of N_{r_k} individual channel gains and thus the dynamic range of the SNRs of the different data symbols is reduced, i.e., somewhat leads to an equalization of the SNRs.

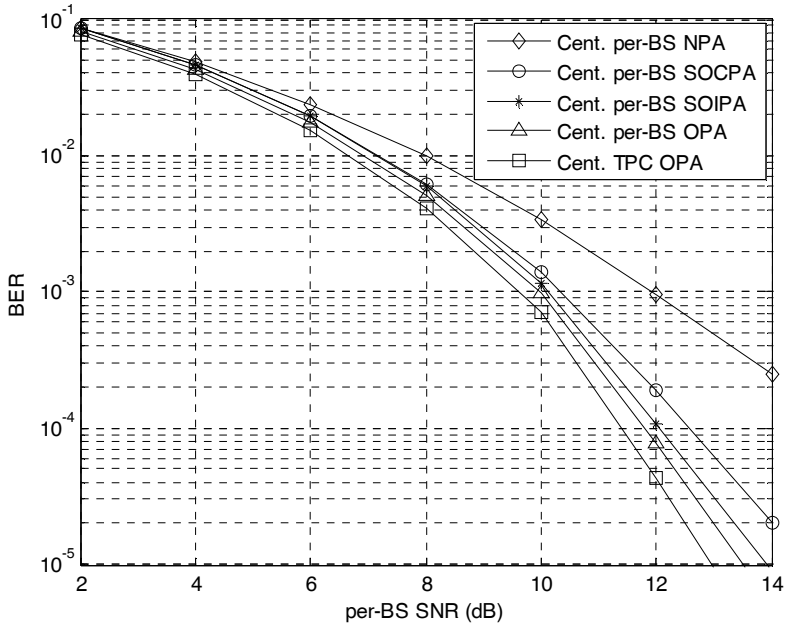

Fig 4-5 Performance evaluation of the proposed centralized multicell schemes for scenario 1, diversity mode and uncorrelated channels.

Fig 4-6 and Fig 4-7 show the performance results of scenario 2 in multiplexing and diversity modes, respectively. As can be seen in the figures, basically the same previous conclusions can be pointed out for this scenario. Here there is a significant gain in both diversity and multiplexing modes comparing to the first scenario which is because of existing more BSs transmitting to the same number of users. For example at target BER=10^{-4}, the gain for diversity curves is almost 8dB. As can be seen the gap between per-BS OPA and TPC OPA curves is larger than in scenario 1 (almost 1 dB for both modes at target BER=10^{-2} against 0.5dB in scenario1). This can be explained due to the fact that the number of BSs is increased which results in more constraints than scenario 1.

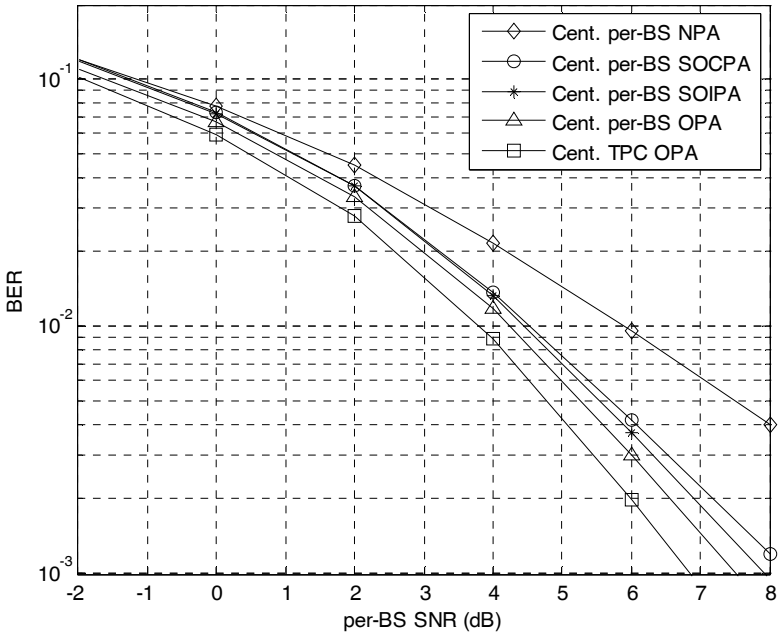

Fig 4-6 Performance evaluation of the proposed multicell schemes for scenario 2, multiplexing mode and uncorrelated channels.

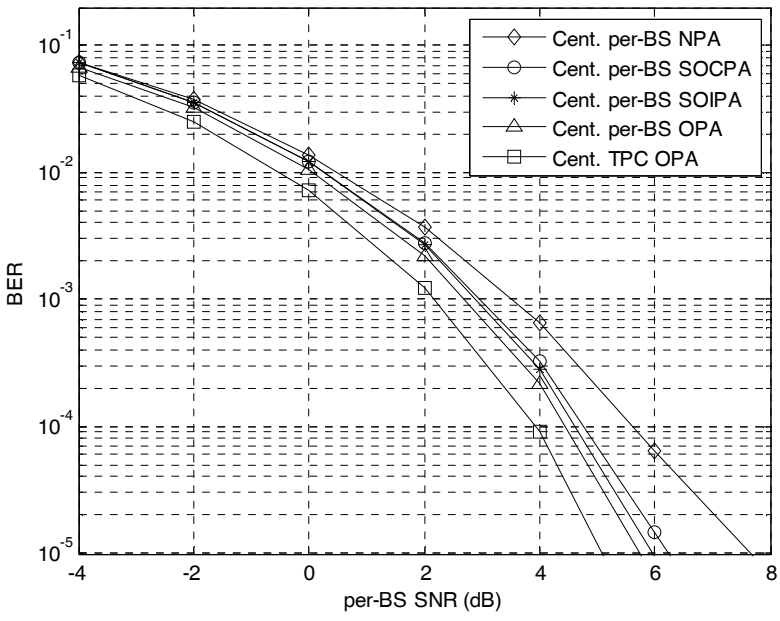

Fig 4-7 Performance evaluation of the proposed multicell schemes for scenario 2, diversity mode and uncorrelated channels.

4.6 Conclusion

In this chapter we proposed and evaluated centralized multicell multiuser precoding and power allocation schemes for MIMO OFDM based systems. The proposed precoder vectors were computed jointly and centrally at JPU benefiting from high DoF, and then the power elements were computed in a centralized fashion at JPU.

The criteria considered was the minimization of the BER and two centralized power allocation algorithms with per-BS power constraint: one optimal that can be achieved at the expense of some complexity and one suboptimal with lower complexity aiming at practical implementations. In both the optimal (per-BS OPA) and the suboptimal (per-BS SOIPA), the computation of the transmitted powers required an iterative approach. To circumvent the need for iterations further proposed another suboptimal scheme (per-BS SOCPA), where the power allocation was computed in order to minimize the sum of inverse of SNRs of each UT allowing us to achieve a closed-form solution.

The results have shown that the proposed multiuser multicell schemes improve the system performance significantly, in comparison with the case where no power allocation is used. Also the performance of the proposed suboptimal algorithms, namely the per-BS SOIPA and per-BS SOCPA approaches, is very close to the optimal with the advantage of lower complexity.

4.7 Bibliography

[1] R. Holakouei, A. Silva e A. Gameiro, "Multiuser precoding techniques for a distributed broadband wireless system," *Telecommunication System Journal, special issue in WMCNT, Springer,* 2011.

[2] R. Holakouei, A. Silva e A. Gameiro, "Precoded Multiuser Distributed MIMO OFDM Systems," em *international Symposium on Wireless Communication Systems (ISWCS)*, 2009.

[3] R. Holakouei, A. Silva e A. Gameiro, "Multi-User Precoding and Power Allocation Techniques for Distributed MIMO OFDM Systems," em *IEEE International Conference on Advanced Networking and Application (AINA)* , 2010.

[4] R. Holakouei, A. Silva e A. Gameiro, "Power Allocation Strategies for SVD Multicell MIMO-OFDM Based Systems," em *Wireless Telecommunications Symposium (WTS)*, 2011.

[5] R. Holakouei, A. Silva e A. Gameiro, "Linear Precoding for Centralized MultiCell MIMO Networks," em *IEEE symposium on Computers and Communications (ISCC)*, 2011.

[6] S. Jing, D. N. C. Tse, J. B. Sorianga, J. Hou, J. E. Smee e R. Padovani, "Multicell downlink capacity with coordinated processing," *EURASIP Journal of Wireless Communicaion Network,* 2008.

[7] O. Somekh, B. Zaidel e S. Shamai, "Sum rate characterization of joint multiple cell-site processing," *IEEE Transaction of Information Theory,* vol. 53, n.º 12, pp. 4473- 4497, 2007.

[8] F. Boccardi e H. Huang, "Limited downlink network coordination in cellular networks," em *Proeeding IEEE PIMRC'07*, 2007.

[9] J. Zhang, R. Chen, J. G. Andrews, A. Ghosh e R. W. J. Heath, "Networked MIMO with Clustered Linear Precoding," *IEEE Transaction on Wireless Communication,* vol. 8, n.º 4, pp. 1910-1921, 2009.

[10] P. Marsch e G. Fettweis, "On Downlink network MIMO under a constrained backhaul and imperfect channel knowledge," em *Proceeding of IEEE GLOBECOM*, 2009.

[11] A. G. Armada, M. S. Fernándes e R. Corvaja, "Waterfilling schemes for zero-forcing coordinated base station transmissions," em *Proceeding of IEEE GLOBECOM*, 2009.

[12] M. Kobayashi, M. Debbah e J. Belfiore, "Outage efficient strategies in network MIMO with partial CSIT," em *Proceeding of IEEE ISIT*, 2009.

[13] R. Zhang, "Cooperative multi-cell block diagonalization with per-base-station power constraints," em *Proceeding of IEEE WCNC*, 2010.

[14] E. Bjornson, R. Zakhour, D. Gesbert e B. Ottersten, "Cooperative multi-cell precoding: rate region characterization and distributed strategies with instantaneous and statistical CSI," *IEEE Transaction on Signal Processing,* vol. 58, n.º 8, pp. 4298-4310, 2010.

[15] M. H. M. Costa, "Writing on dirty paper," *IEEE Transaction on Information Theory,* vol. 29, n.º 3, p. 439–441, 1983.

[16] D. Gesbert, S. Hanly, H. Huang, S. Shamai, O. Simeone e W. Yu, "Multi-cell MIMO cooperation networks: A new look at interference," *IEEE Journal on Selected Areas in Communications,* vol. 28, n.º 9, pp. 1380-1408, 2010.

[17] K. Yu, M. Bengtsson, B. Ottersten, D. McNamara e P. Karlsson, "Modeling of wide-band MIMO radio channels based on NLoS indoor measurements," *IEEE Transactions on Vehicular Technology,* vol. 3, n.º 3, pp. 655- 665, 2004.

[18] A. Goldsmith, Wireless Communications, Cambridge University Press, 2005.

[19] J. Proakis, Digital Communications, New York: McGrraw-Hill, 1995.

[20] S. Boyd e L. Vandenberghe, Convex optimization, Cambridge: Cambridge University Press, 2004.

[21] S. Haykin, Adaptive Filter Theory, Prentice Hall, 1996.

[22] R. Corless, G. H. Gonnet, D. E. G. Hare, D. J. Jeffrey e D. E. Knuth, "On the Lambert W function," *Advances in Computer & Mathematics,* vol. 5, p. 329–359, 1996.

[23] D. P. Palomar, J. M. Cioffi e M. A. Lagunas, "Joint Tx-Rx beamforming design for multicarrier MIMO channels: A unified framework for convex optimization," *IEEE Transactions on Signal Processing,* vol. 51, n.º 9, pp. 2381-2401, 2003.

[24] "Guidelines for the evaluation of radio transmission technologies for IMT-2000," Recommendation ITU-R M.1225, 1997.

[25] "LTE Physical Layer - General Description, no 3. 3GPP TS 36.201 v8.1.0," Third Generation Partnership Project, 2007.

5 Distributed Cooperation for Multicell MIMO OFDM Systems

In this chapter we propose distributed precoding techniques to mitigate inter-cell interference and improve user fairness at cell edges for downlink of multicell systems. To further improve the system performance we propose centralized and distributed power allocation schemes (semi-distributed and full-distributed, respectively). The precoders are designed in two phases: first the precoder vectors are computed in a distributed manner at each BS considering some criteria; then the system is optimized through centralized and distributed power allocation schemes. The results show that the proposed full-distributed schemes are promising when the amount of information exchange over the backhaul is limited, although slightly degraded from semi-distributed ones but for high DoF both methods have similar performance. This chapter is based on contributions from [1], [2], [3], [4], [5], [6], [7] *which are the publications from the thesis author where full-centralized schemes were proposed and evaluated for different conditions.*

5.1 Introduction

Distributed precoding approaches, where the precoder vectors are computed at each BS in a distributed fashion, have been proposed in [8] for the particular case of two UTs and generalized for *K* UTs in [9]. It is assumed that each base station has only the knowledge of local CSI and based on that a parameterization of the beamforming vectors used to achieve the outer boundary of the achievable rate region was derived. In [8], [9] some distributed power allocation algorithms, for the derived precoder vectors, were proposed to further improve the sum rate. In [8] a very simple channel power splitting was considered and no optimization metric was assumed. In [9], a heuristic power allocation based on maximization of a metric related with the sum rate was derived. In [10], each BS performs ZF locally to remove the channel interference and based on the statistical knowledge of the channels, the CU performs a centralized power allocation that jointly minimizes the outage probability of the UTs. A promising distributed precoding scheme based on zero-forcing criterion with several centralized power allocation approaches, which minimize the average BER and sum of inverse of SNIR was proposed in [5]. These distributed schemes were evaluated and compared with some full centralized multicell schemes in [2]. In [11], the performance of various reduced-complexity multicell preprocessing structures in terms of their achievable outage rate over conventional single cell preprocessing schemes was investigated.

In this chapter we propose joint distributed ZF (DZF) precoder and power allocation schemes for downlink of multicell MISO-OFDM systems. The joint scheme design involves in two phases: first the precoder vectors are computed based on DZF. The precoder vectors are computed by assuming that the BSs have only knowledge of local CSI and share the knowledge of the data symbols intended for all UTs. Then the system is further optimized by proposing either centralized or distributed power allocation algorithms. The centralized schemes are based on minimization of the instantaneous average BER and minimization of the sum of inverse of SINR, for which a closed form solution is derived. In this approach, the powers are computed in two phases. First the powers are derived under TPC. Then, the final powers are computed to satisfy the individual per-BS power constraint. Finally the results are compared against maximal ratio combing (MRT) and distributed *virtual* SINR (DVSINR) precoding schemes, recently proposed.

By considering the multicell system as a superposition of single cell systems we define the average *virtual* BER of one single cell system. This allows us to compute the power allocation in a distributed manner at each BS. Basically, the system is optimized by proposing a new distributed power allocation algorithm that minimizes the average *virtual* bit error rate (VBER), under per-BS power constraint. With the proposed strategy both the precoder vectors and the power allocation

are computed at each BS in a distributed manner. The considered criterion for power allocation essentially leads to a redistribution of powers among users and subcarriers, and therefore provides users fairness mainly at the cell edges, which in practical cellular systems may be for the operators a goal as important as throughput maximization.The remainder of this chapter is organized as follows: Section 5.2 presents the considered multicell system model. Section 5.3 describes distributed precoder vectors design considering several criteria. In Section 5.4 centralized and distributed power allocation schemes are derived for the different precoder vectors. Section 5.5 presents the main simulation results and comparing them with the results of full centralized schemes which was presented in chapter 4. The conclusions will be drawn in Section 5.6.

5.2 System Model

We consider B BSs, each equipped with N_{t_b} antennas, transmitting to K single antenna UTs, as shown in Fig 5-1 and Fig 5-2 for semi-distributed and full-distributed scenarios, respectively. Under the assumption of linear precoding, the signal in frequency domain transmitted by the BS b on sub-carrier l is given by

$$\mathbf{z}_{b,l} = \sum_{k=1}^{K} \sqrt{p_{b,k,l}}\, \mathbf{w}_{b,k,l} x_{k,l} \tag{5.1}$$

where $p_{b,k,l}$ represents the power allocated to UT k on sub-carrier l and BS b, $\mathbf{w}_{b,k,l} \in \mathrm{C}^{N_{t_b} \times 1}$ is the precoder of user k at BS b on sub-carrier l with unit norms, i.e., $\left\|\mathbf{w}_{b,k,l}\right\| = 1,\ b = 1,...,B,\ k = 1,...,K, l = 1,...,N_c$. The data symbol $x_{k,l}$, with $\mathrm{E}\left\{\left|x_{k,l}\right|^2\right\} = 1$, is intended for UT k and is assumed to be available at all BSs. The average power transmitted by the BS b is then given by

$$\mathrm{E}\left\{\left\|\mathbf{z}_b\right\|^2\right\} = \sum_{l=1}^{N_c} \sum_{k=1}^{K} p_{b,k,l} \tag{5.2}$$

where $\mathbf{z}_b$ is the signal transmitted over the N_c subcarriers. The received signal in frequency domain at the UT k on sub-carrier l , $y_{k,l} \in \mathrm{C}^{1\times 1}$ can be expressed as

$$y_{k,l} = \sum_{b=1}^{B} \mathbf{h}_{b,k,l}^{H} \mathbf{z}_{b,l} + n_{k,l} \tag{5.3}$$

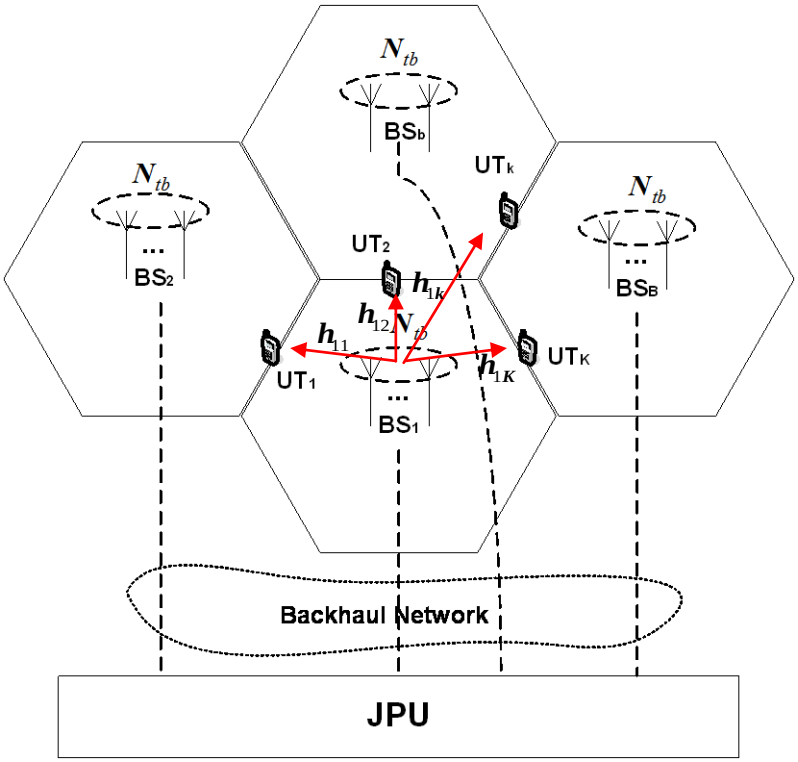

(Only power allocation computation at JPU)

Fig 5-1 Multicell system model with K UTs (illustrated for $B=4$ base stations equipped with N_{t_b} antennas) and with JPU, the subcarrier script is omitted for simplicity.

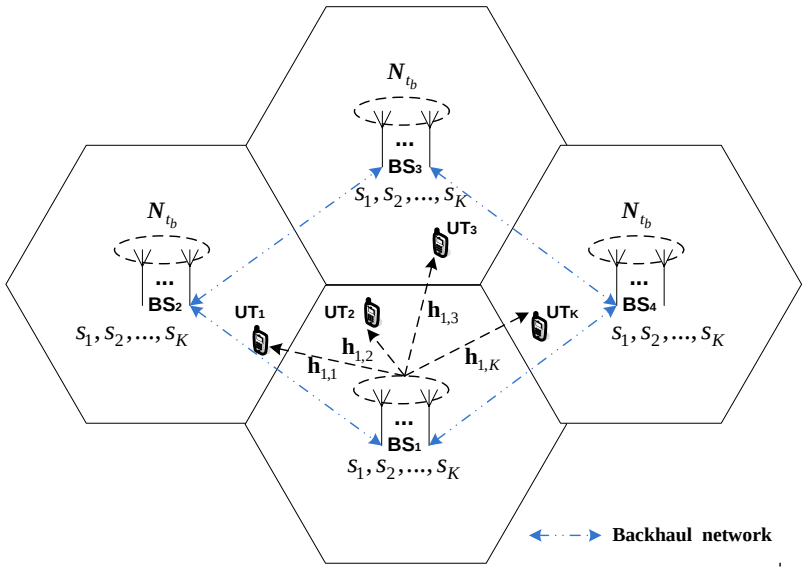

Fig 5-2 Multicell system model with K UTs (illustrated for $B=4$ base stations equipped with N_{t_b} antennas) and without JPU, the subcarrier script is omitted for simplicity.

where $\mathbf{h}_{b,k,l} \sim CN\left(0, \Phi_{PL\,b,k}\mathbf{I}_{N_{t_b}}\right)$ of size $N_{t_b} \times 1$, represents the channel between user k and BS b on subcarrier l and $\Phi_{PL\,b,k}$ is the long-term channel power gain between BS b and UT k, and $n_{k,l} \sim CN\left(0, \sigma^2\right)$ is the noise. The antenna channels from BS b to user k are assumed to be uncorrelated as the BSs.

From (5.1) and (5.3) the received signal in frequency domain at UT k on sub-carrier l can be decomposed in

$$y_{k,l} = \underbrace{\sum_{b=1}^{B} \sqrt{p_{b,k,l}}\,\mathbf{h}_{b,k,l}^{H}\mathbf{w}_{b,k,l}x_{k,l}}_{Desired\ Signal} + \underbrace{\sum_{b=1}^{B}\mathbf{h}_{b,k,l}^{H}\sum_{j=1,\,j\neq k}^{K}\sqrt{p_{b,j,l}}\,\mathbf{w}_{b,j,l}x_{j,l}}_{Multiuser\ Multicell\ Interference} + \underbrace{n_{k,l}}_{Noise} \tag{5.4}$$

assuming that the cyclic prefix is long enough to account for different overall channel impulse responses between the BSs and the UTs. From (5.4) the instantaneous SINR of user k on sub-carrier l can be written as

$$\mathrm{SINR}_{k,l} = \frac{\left|\sum_{b=1}^{B}\sqrt{p_{b,k,l}}\,\mathbf{h}_{b,k,l}^{H}\mathbf{w}_{b,k,l}^{(type)}\right|^2}{\sum_{\substack{j=1\\ j\neq k}}^{K}\left|\sum_{b=1}^{B}\sqrt{p_{b,j,l}}\,\mathbf{h}_{b,k,l}^{H}\mathbf{w}_{b,j,l}^{(type)}\right|^2 + \sigma^2} \tag{5.5}$$

where $type \in \{DZF, MRT, DVSINR\}$. Assuming a M-ary QAM constellations and a Gaussian approximation of the overall interference plus noise, the instantaneous probability of error for user k and data symbol transmitted on subcarrier l is given by [12]

$$P_{e,k,l} = \psi Q\left(\sqrt{\beta SINR_{k,l}}\right) \tag{5.6}$$

where $Q(x) = \left(1/\sqrt{2\pi}\right)\int_{x}^{\infty} e^{-\left(t^2/2\right)}dt$, $\beta = 3/\left(M-1\right)$ and $\psi = \left(4/\log_2 M\right)\left(1-1/\sqrt{M}\right)$.

5.3 Distributed Precoder Vectors

In this section we describe proposed distributed ZF (DZF) precoding vectors. Also we present MRT and DVSINR precoders, proposed recently. To design the distributed precoder vectors we assume that the BSs share the data symbols and have only knowledge of local CSI, i.e., BS b

knows the instantaneous channel vectors $\mathbf{h}_{b,k,l}, \forall k,l$, reducing the feedback load over the backhaul network as compared with the full centralized precoding approach. Hence, there is no exchange of CSI between BSs, thus allowing the scalability of multicell cooperation to large and dense networks. Each BS has CSI for its links to all receivers, which is nonscalable when the resources for CSI acquisition are limited. However, it is still a good model for large networks as most terminals will be far away from any given transmitter and thus have negligibly weak channel gains, as discussed in [9]. Recently, a simple and versatile limited CSI feedback scheme from UTs to the BSs has been proposed in the context of multipoint coordination based systems [13].

5.3.1 Distributed Zero Forcing (DZF)

In this section we describe the proposed DZF, which is a classic beamforming strategy which removes the co-terminal interference. In this case, $\mathbf{w}_{b,k,l}^{(DZF)}$ in (5.5) is a unit-norm zero forcing vector orthogonal to $K-1$ channel vectors, $\left\{\mathbf{h}_{b,j,l}^{H}\right\}_{j\neq k}$. Let $\tilde{\mathbf{H}}_{b,k,l}=\left[\mathbf{h}_{b,1,l} \;\cdots\; \mathbf{h}_{b,k-1,l} \;\; \mathbf{h}_{b,k+1,l} \;\cdots\; \mathbf{h}_{b,K,l}\right]^{H}$ of size $(K-1)\times N_{t_b}$ contain the channels of all users except the *k*th. The SVD of $\tilde{\mathbf{H}}_{b,k,l}$ can be partitioned as follows,

$$\tilde{\mathbf{H}}_{b,k,l}=\mathbf{U}_{b,k,l}\boldsymbol{\Sigma}_{b,k,l}\left[\dddot{\mathbf{W}}_{b,k,l} \;\; \bar{\mathbf{W}}_{b,k,l}\right]^{H} \tag{5.7}$$

where $\mathbf{U}_{b,k,l}$ is an unitary matrix of size $(K-1)\times(K-1)$, $\Omega_{b,k,l}$ is a rectangular diagonal matrix of size $(K-1)\times N_{t_b}$ with the singular values, $\dddot{\mathbf{W}}_{b,k,l}$ contains the first $r=\operatorname{rank}\left\{\tilde{\mathbf{H}}_{b,k,l}\right\}$ columns of $\mathbf{W}_{b,k,l}$ and $\bar{\mathbf{W}}_{b,k,l}\in \mathrm{C}^{N_{t_b}\times\left(N_{t_b}-K+1\right)}$ holds the $\left(N_{t_b}-K+1\right)$ singular vectors in the null space of $\left\{\mathbf{h}_{b,j,l}^{H}\right\}_{j\neq k}$.The columns of $\bar{\mathbf{W}}_{b,k,l}$ are candidates for *k*'s precoding vector since they will produce zero interference at the other UTs. An optimal linear combination of these vectors can be given by [2].

$$\mathbf{w}_{b,k,l}^{(DZF)}=\bar{\mathbf{W}}_{b,k,l}\frac{\left(\mathbf{h}_{b,k,l}^{H}\bar{\mathbf{W}}_{b,k,l}\right)^{H}}{\left\|\mathbf{h}_{b,k,l}^{H}\bar{\mathbf{W}}_{b,k,l}\right\|}. \tag{5.8}$$

As shown in appendix C, the solution given by (5.8) is equivalent to the one based on the orthogonal matrix projection onto the column space of $\tilde{\mathbf{H}}_{b,k,l}$ discussed in some works (e.g., [9], [14]). It should be emphasized that the precoder vectors given by (5.8) only holds for $N_{t_b} \geq K$.

The equivalent channel between BS b and UT k, on sub-carrier l can be expressed as

$$\mathbf{h}_{b,k,l}^{H}\mathbf{w}_{b,k,l}^{(DZF)} = \mathbf{h}_{b,k,l}^{H}\bar{\mathbf{W}}_{b,k,l}\frac{\left(\mathbf{h}_{b,k,l}^{H}\bar{\mathbf{W}}_{b,k,l}\right)^{H}}{\left\|\mathbf{h}_{b,k,l}^{H}\bar{\mathbf{W}}_{b,k,l}\right\|} = \left\|\mathbf{h}_{b,k,l}^{H}\bar{\mathbf{W}}_{b,k,l}\right\|. \tag{5.9}$$

From (5.10) we can observe that the equivalent channel, $\mathbf{h}_{b,k,l}^{H}\mathbf{w}_{b,k,l}^{(DZF)}$ is a positive real number, which means that the signals arriving at a given UT from different BSs will add coherently, and it can be shown that $\mathbf{h}_{b,k,l}^{H}\mathbf{w}_{b,k,l}^{(DZF)} \sim \chi^2_{2\left(N_{t_b}-K+1\right)}$ [15]. So it is a chi-square random variable with $2\left(N_{tb}-K+1\right)$ degrees of freedom. Once the $h_{b,k,l}^{eq}$ variables are independent, each user is expected to achieve a diversity order of $B\left(N_{tb}-K+1\right)$ (assuming that all channels have the same average power, i.e., $\Phi_{PL_{b,k,l}} = \Phi_{PL},\ \forall(b,k,l)$ and $p_{b,k,l} = 1,\ \forall(b,k,l)$). Also, because the received signals from different BSs have the same phase, they are added coherently at the UTs, and thus an additional antenna gain is achieved.

By using the precoding vectors defined in (5.8) and considering (5.9), the received signal in (5.4) reduces to,

$$y_k = \sum_{b=1}^{B}\sqrt{p_{b,k}}h_{b,k}^{eq}x_k + n_k \tag{5.10}$$

It should be mentioned that at the UT, to allow high order modulations, only the $\sqrt{p_{b,k,l}}h_{b,k,l}^{eq}$ coefficients are needed to be estimated instead of all the complex coefficients of the channel, leading to a low complexity UT design.

5.3.2 Distributed Maximal Ratio Transmission (MRT)

MRT is a classical and very simple precoder. Although, it does not explicitly remove the interference, it maximizes the received signal power at each UT. The precoding vector $\mathbf{w}_{b,k,l}^{(MRT)},\ \forall b,k,l$ is given by

$$\mathbf{w}_{b,k,l}^{(MRT)} = \frac{\mathbf{h}_{b,k,l}}{\left\|\mathbf{h}_{b,k,l}\right\|} \tag{5.11}$$

Using these precoder vectors there is no limit on the number of users served by the multicell system but of course we do not expect a good performance at high SNR regime.

5.3.3 Distributed Virtual SINR (DVSINR)

Intuitively, MRT is the asymptotically optimal strategy at low SNR, while ZF has good performance at high SNR or as the number of antennas increases. As discussed in [9], the optimal strategy lies in between these two precoders and cannot be determined without global CSI. However, inspired by the uplink-downlink duality for broadcast channels, the authors of [9] have derived a novel distributed VSINR precoder. The precoder vectors are achieved by maximizing the SINR-like expression in (5.12) where the signal power that BS *b* generates at UT k is balanced against the noise and interference power generated at all other UTs. It was named DVSINR as it originates from the dual *virtual* uplink and does not directly represent the SINR of any of the links in the downlink. Basically it represents the SINR that would be observed for the uplink at the BSs at the output of the reception filter $\mathbf{w}$ [16]. It should be mentioned that the DVSINR in (5.12) is fundamentally identical to a signal to leakage and noise ratio (SLNR) expression discussed in [17]. The precoder vectors are computed by

$$\mathbf{w}_{b,k,l}^{(DVSINR)} = \arg\max_{\|\mathbf{w}\|^2=1} \frac{\left|\mathbf{h}_{b,k,l}^H \mathbf{w}\right|^2}{\sum_{\bar{k}\neq k}\left|\mathbf{h}_{b,\bar{k},l}^H \mathbf{w}\right|^2 + \frac{\sigma^2}{P_{t_b}}} \tag{5.12}$$

where P_{t_b} is the per-BS power constraint. The solution to (5.12) is not unique, since the *virtual* SINR is unaffected by the phase shifts in $\mathbf{w}$. One possible solution can be written as [9]

$$\mathbf{w}_{b,k,l}^{(DVSINR)} = \frac{\mathbf{C}_{b,k,l}^{-1}\mathbf{h}_{b,k,l}}{\left\|\mathbf{C}_{b,k,l}^{-1}\mathbf{h}_{b,k,l}\right\|} \tag{5.13}$$

where

$$\mathbf{C}_{b,k,l} = \frac{\sigma^2}{P_{t_b}}\mathbf{I}_{N_{t_b}} + \sum_{\bar{k}\neq k}\mathbf{h}_{b,\bar{k},l}\mathbf{h}_{b,\bar{k},l}^H. \tag{5.14}$$

As for the DZF, the expression above was selected to make $\mathbf{h}_{b,k,l}^{H}\mathbf{w}_{b,k,l}^{(DVSINR)}$ positive and real valued, which means that the signals arriving at a given terminal from different BSs will also add constructively.

5.4 Power Allocation Strategies

The power allocation strategies considered in this chapter can be divided into two main categories: centralized where base stations need to exchange partial information to perform power allocation and distributed where only local CSI are used at each BS to compute the transmit powers. Also in all derivations, we assumed joint-subcarrier PC.

5.4.1 Centralized Power Allocation Strategies

In this section we propose centralized power allocation schemes for the scenario with distributed precoding; one optimal power strategy, to minimize the average BER, and two suboptimal ones are considered. Similar to what presented in section 4.4 of chapter 4, the criteria used to design centralized power allocation are minimization of the average BER and sum of inverse of SINRs, which essentially lead to a redistribution of powers among users and therefore provide users fairness.

5.4.1.1 Optimal Minimum BER Power Allocation

The power allocation problem with per-BS power constraint can be formulated as,

$$\min_{\{p_{b,k,l}\geq 0\}}\left(\frac{\psi}{KN_c}\sum_{l=1}^{N_c}\sum_{k=1}^{K}Q\left(\sqrt{\beta\, SINR_{k,l}}\right)\right)\ \text{s.t.}\ \sum_{l=1}^{N_c}\sum_{k=1}^{K}p_{b,k,l}\leq P_{t_b},\forall b \tag{5.15}$$

Since the objective function is convex in $p_{b,k,l}$, and the constraint functions are linear, this is a convex optimization problem. Therefore, it may be solved numerically by using for example the interior-point method. This scheme is referred as per-BS optimal power allocation (*Cent. per-BS OPA*).

5.4.1.2 Suboptimal Minimum BER Power Allocation

It is possible to resort to a suboptimal power allocation method with lower complexity for the case of DZF precoding. The proposed strategy has two phases: first the power allocation is

computed by assuming that all BSs of each supercell can jointly pool their power, i.e., a TPC $P_t = \sum_{b=1}^{B} P_{tb}$ is imposed instead and the above optimization problem reduces to,

$$\min_{\{p_{b,k,l}\geq 0\}} \left(\frac{\psi}{KN_c} \sum_{l=1}^{N_c} \sum_{k=1}^{K} Q\left(\sqrt{\beta} \frac{\sum_{b=1}^{B} \sqrt{p_{b,k,l}} h_{b,k,l}^{eq}}{\sigma} \right) \right) \quad \text{s.t.} \quad \left\{ \sum_{b=1}^{B} \sum_{l=1}^{N_c} \sum_{k=1}^{K} p_{b,k,l} \leq P_t \right. \tag{5.16}$$

using the Lagrange multipliers method, the following cost function is minimized,

$$L\left(p_{b,k,l}, \mu\right) = \frac{\psi}{KN_c} \sum_{l=1}^{N_c} \sum_{k=1}^{K} Q\left(\sqrt{\beta} \frac{\sum_{b=1}^{B} \sqrt{p_{b,k,l}} h_{b,k,l}^{eq}}{\sigma} \right) + \mu \left(\sum_{b=1}^{B} \sum_{l=1}^{N_c} \sum_{k=1}^{K} p_{b,k,l} - P_t \right) \tag{5.17}$$

where $\mu \geq 0$ is the Lagrange multiplier. Since the problem (5.16) is convex, it is necessary and sufficient to solve the Karush-Kuhn-Tucker (KKT) conditions [18], [19]. It can be shown that the powers $p_{b,k,l}$ as function of the Lagrange multiplier μ, are given by (proof similar to appendix A),

$$p_{b,k,l} = \frac{\sigma^2 \left(h_{b,k,l}^{eq} \right)^2}{\left(\sum_{i=1}^{B} \left(h_{i,k,l}^{eq} \right)^2 \right)^2} W_0 \left(\frac{\psi^2 \left(\sum_{i=1}^{B} \left(h_{i,k,l}^{eq} \right)^2 \right)^2}{8\pi\mu^2 K^2 N_c^2 \sigma^4} \right), \tag{5.18}$$

where W_0 stands for Lambert's *W* function of index 0 as discussed in chapter 4. Therefore, μ^2 can be determined iteratively, using TPC constraint..

The second phase consists of replacing μ^2 by μ_b^2, $b = 1, ..., B$ in (5.18), and then computing iteratively different μ_b^2 to satisfy the individual per-BS power constraints instead, i.e., μ_b^2 are computed to satisfy $\sum_{l=1}^{N_c} \sum_{k=1}^{K} p_{b,k,l} \leq P_{t_b}$. This scheme is referred as per-BS sub-optimal iterative power allocation (*Cent. per-BS SOIPA*).

5.4.1.3 Minimization of Sum of Inverse of SINRs

Although this suboptimal solution significantly reduces the complexity relatively to the optimal one, it still needs an iterative search. To further simplify we propose an alternative power allocation method based on minimizing the sum of inverse of SINRs under per-BS power constraint. Note

that minimizing the sum of inverse of SINRs is similar to the maximization of the harmonic mean of the SINRs discussed in [20]. In this case, the optimization problem is written as,

$$\min_{\{p_{b,k,l}\geq 0\}}\left(\sum_{l=1}^{N_c}\sum_{k=1}^{K}\frac{1}{SINR_{k,l}}\right)\ \text{s.t.}\ \sum_{l=1}^{N_c}\sum_{k=1}^{K}p_{b,k,l}\leq P_{t_b},\forall b \tag{5.19}$$

The objective function is convex in $p_{b,k,l}$, and the constraint functions are linear, this is also a convex optimization problem, and thus it may be solved as (5.15). To the best of our knowledge, closed-form solution for problem (5.19) cannot be achieved. Thus we also propose an alternative two step sub-optimal strategy: first the power allocation is computed by assuming that all BSs can jointly pool their power, i.e., a TPC is imposed instead and the above optimization problem reduces to

$$\min_{\{p_{b,k,l}\geq 0\}}\left(\sum_{l=1}^{N_c}\sum_{k=1}^{K}\frac{1}{SINR_{k,l}}\right)\ \text{s.t.}\ \left\{\sum_{b=1}^{B}\sum_{l=1}^{N_c}\sum_{k=1}^{K}p_{b,k,l}\leq P_t \right. \tag{5.20}$$

with $P_t=\sum_{b=1}^{B}P_{t_b}$. Even for this simplified problem, using the MRT or VSINR precoders, to the best of our knowledge a closed-form solution cannot be achieved. However, considering the DZF precoder, a closed-form solution can be derived since the interference part of (5.5) is eliminated. Therefore, the optimization problem of (5.20), using (5.8) reduces to,

$$\min_{\{p_{b,k,l}\geq 0\}}\left(\sum_{l=1}^{N_c}\sum_{k=1}^{K}\frac{\sigma^2}{\left(\sum_{b=1}^{B}\sqrt{p_{b,k,l}}h_{b,k,l}^{eq}\right)^2}\right)\ \text{s.t.}\ \left\{\sum_{b=1}^{B}\sum_{l=1}^{N_c}\sum_{k=1}^{K}p_{b,k,l}\leq P_t \right. \tag{5.21}$$

The Lagrangian associated with this problem is given by,

$$L\left(p_{b,k,l},\mu\right)=\sum_{l=1}^{N_c}\sum_{k=1}^{K}\frac{\sigma^2}{\left(\sum_{b=1}^{B}\sqrt{p_{b,k,l}}h_{b,k,l}^{eq}\right)^2}+\mu\left(\sum_{b=1}^{B}\sum_{l=1}^{N_c}\sum_{k=1}^{K}p_{b,k,l}-P_t\right) \tag{5.22}$$

where $\mu\geq 0$ is the Lagrange multiplier. Since the problem (5.21) is convex, it is necessary and sufficient to solve the KKT conditions. It can be shown that the powers $p_{b,k,l}$ as function of the Lagrange multiplier μ, are given by,

$$p_{b,k,l} = \frac{\left(h_{b,k,l}^{eq}\right)^2}{\phi\sqrt{\left(\sum_{i=1}^{B}\left(h_{i,k,l}^{eq}\right)^2\right)^3}} \tag{5.23}$$

where $\phi = \sqrt{\mu/\sigma^2}$. The second phase consists in replacing ϕ by ϕ_b, $b = 1,...,B$ in (5.23), and then computing different ϕ_b, to satisfy the individual per-BS power constraints instead, and the closed-form solution achieved is then given by (see appendix B for proof),

$$p_{b,k,l} = \frac{P_{t_b}\left(h_{b,k,l}^{eq}\right)^2}{\sqrt{\left(\sum_{i=1}^{B}\left(h_{i,k,l}^{eq}\right)^2\right)^3}\sum_{p=1}^{N_c}\sum_{j=1}^{K}\frac{\left(h_{b,j,p}^{eq}\right)^2}{\sqrt{\left(\sum_{i=1}^{B}\left(h_{i,j,p}^{eq}\right)^2\right)^3}}} \tag{5.24}$$

This scheme is referred as centralized per-BS sub-optimal closed-form power allocation (*Cent. per-BS SOCPA*). Note that for the MRT and VSINR the powers are obtained by solving directly(5.19), using the interior-point method.

5.4.1.4 Simplified Approaches for MRT and VSINR

Considering centralized power allocation proposed, the MRT and DVSINR precoders have two main drawbacks: first, since the inference part of (5.5) is not fully eliminated no closed form solution can be derived; second this interference part should be known at the CU. This means that all the equivalent complex channels coefficients $\mathbf{h}_{b,k,l}^H \mathbf{w}_{b,k,l}^{(MRT,DVSINR)}$, $\forall b,k,l$ should be sent to the CU through the backhaul network, i.e., approximately the same information required by the fully centralized approach. For the proposed DZF each BS should send only the equivalent real channels coefficients $h_{b,k,l}^{eq}$, $\forall b,k,l$, i.e., a real vector of size KN_c to the CU, while for MRT or DVSINR a vector of size BKN_c is required.

One possible way to avoid these drawbacks is to compute the powers, for the MRT and DVSINR precoders, by assuming that the interference part of (5.5) is negligible, i.e.,

$$\mathrm{SINR}_{k,l} = \frac{\left|\sum_{b=1}^{B}\sqrt{p_{b,k,l}}\mathbf{h}_{b,k,l}^H \mathbf{w}_{b,k,l}^{(type)}\right|^2}{\sigma^2} \tag{5.25}$$

where $type \in \{MRT, DVSINR\}$. In this case the optimization problems are identical to the DZF case and the approaches are referred as centralized per-BS SOIPA/SOCPA worst-case power allocation. (*Cent. per-BS SOIPA/SOIPA WC)*.

All the distributed precoder vectors are designed by assuming that BSs have only knowledge of local CSI. However, since here we have considered centralized power allocation schemes, to compute all powers the $h_{b,k,l}^{eq},\ b=1,...,B, k=1,...,K, l=1,...,N_c$ coefficients should be available at the JPU. In our multicell system each BS should send a real vector of size KN_c to the JPU. Note that if the precoder vectors were computed in a centralized manner at the JPU, each BS should send to the JPU a complex vector of size $N_{tb}KN_c$, i.e. $2N_{tb}$ more information.

5.4.2 Distributed Power Allocation

In this section we derive a new distributed power allocation algorithm, computed locally at each BS and using only the knowledge of local CSI (Fig 5-2), which minimizes the average VBER over the available subcarriers. Note that when minimizing the VBER over the available subcarriers we have more DoF to improve the system's performance as discussed in [20], for point-to-point communications.

Minimization of Average VBER for DZF

To derive the distributed power allocation we assume that the interference is negligible even for the DVSINR. Thus the same strategy can be used to deduce the power allocation for both precoders (DZF and DVSINR). This approach has been followed by some other works, where the power allocation strategy used for the ZF based precoders can be also employed for the non-ZF based ones [21]. Assuming an interference free system, for both precoders, (5.5) can be simplified as,

$$\mathrm{SNR}_{k,l} = \frac{\left| \sum_{b=1}^{B} \sqrt{p_{b,k,l}}\, \mathbf{h}_{b,k,l}^{H} \mathbf{w}_{b,k,l}^{(type)} \right|^2}{\sigma^2} \tag{5.26}$$

The above expression cannot be used to derive distributed power allocation because it would imply the knowledge of nonlocal channel gains, i.e., the equivalent channel gains between all BSs and the user *k*, at BS *b*. Therefore, we define a *virtual* $\mathrm{SNR}_{b,k,l}$ as the power of the equivalent channel between BS *b* and the UT *k* on subcarrier *l* plus a parameter (which account for the nonlocal contribution) over the noise, given by

$$\mathrm{VSNR}_{b,k,l} = \left| \sqrt{p_{b,k,l}} \frac{\mathbf{h}_{b,k,l}^{H} \mathbf{w}_{b,k,l}^{(type)}}{\sigma} + d_{b,k,l} \right|^2 \tag{5.27}$$

For $d_{b,k,l} = \sum_{j=1, j\neq b}^{B} \sqrt{p_{j,k,l}} \frac{\mathbf{h}_{j,k,l}^{H} \mathbf{w}_{j,k,l}^{(type)}}{\sigma}$ the $\mathrm{VSNR}_{b,k,l}$ expression corresponds to the $\mathrm{SNR}_{k,l}$ one given by (5.26). To avoid the exchange of the instantaneous CSI information between the BSs two strategies can be considered to compute $d_{b,k,l}$, namely, it can be set to zero $d_{b,k,l} = 0$ or using long-term values of the equivalent channels. When the parameter $d_{b,k,l} = 0$, the powers at each BS are computed ignoring the contributions from the others BSs on the desired received signal, i.e., the powers are computed at each BS using only local information. This strategy can be seen as the worst case (WC). When $d_{b,k,l} \neq 0$ the powers are computed taking into account some channel information from the others BSs, i.e., there is some cooperation between BSs to compute the powers.

Based on (5.27) we define the average VBER as

$$P_{av,b}^{virtual} = \frac{\psi}{KN_c} \sum_{l=1}^{N_c} \sum_{k=1}^{K} Q\left(\sqrt{\beta\, \mathrm{VSNR}_{b,k,l}^{d}} \right). \tag{5.28}$$

Note that (5.28) does not represent any real average BER. Considering the multicell system as a superposition of B single cell systems, as shown in Fig 5-3, the overall average VBER can be seen as average *virtual* BER of the *b*th single cell system.

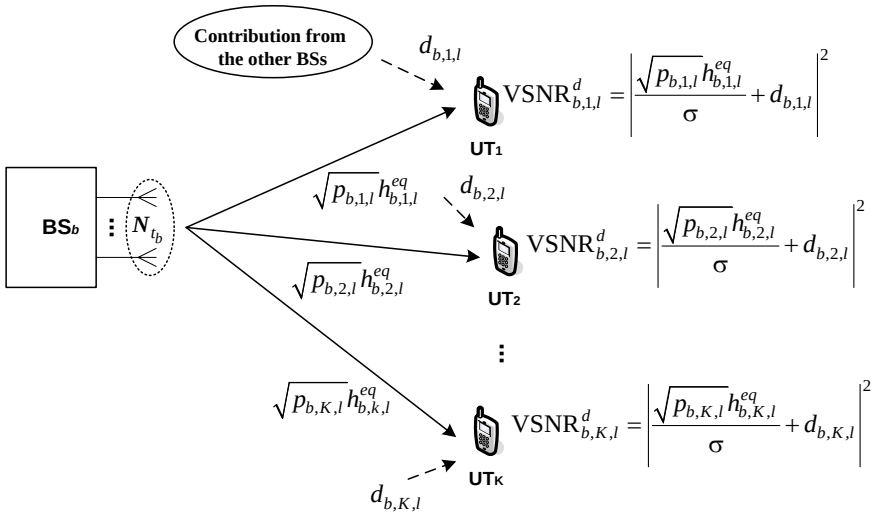

Fig 5-3 A block diagram depicting the *b*th superposed interference-free single cell system.

The motivation to use (5.28) is that the minimization of the average VBER reduces the dynamic range of the VSNRs between the different UTs and subcarriers, i.e., leads to an equalization of the VSNRs over all UTs and subcarriers (more power is allocated to the weaker links and less to the stronger ones as compared to equal power allocation approach), which implicitly leads to an equalization of the SINRs and therefore provides user fairness at the cell edges. The power allocation problem at each BS *b*, with per-BS power constraint, can be formulated as

$$\min_{\left\{p_{b,k,l}\geq 0\right\}}\left(\frac{\psi}{KN_c}\sum_{l=1}^{N_c}\sum_{k=1}^{K}Q\left(\sqrt{\beta\,\mathrm{VSNR}_{b,k,l}^{d}}\right)\right)\ \text{s.t.}\ \left\{\sum_{l=1}^{N_c}\sum_{k=1}^{K}p_{b,k,l}\leq P_{t_b},\ b=1,...,B.\right. \tag{5.29}$$

The Lagrangian associated with this problem can be written by

$$L\left(p_{b,k,l},\mu_b\right)=\frac{\psi}{KN_c}\sum_{l=1}^{N_c}\sum_{k=1}^{K}Q\left(\sqrt{\beta\mathrm{VSNR}_{b,k,l}^{d}}\right)+\mu_b\left(\sum_{l=1}^{N_c}\sum_{k=1}^{K}p_{b,k,l}-P_{t_b}\right)-\sum_{l=1}^{N_c}\sum_{k=1}^{K}\lambda_{b,k,l}\,p_{b,k,l} \tag{5.30}$$

where $\mu_b\geq 0$ and $\lambda_{b,k,l}\geq 0$ are the Lagrange multipliers [22]. Since the objective function is convex in $p_{b,k,l}$, and the constraint functions are linear, this is a convex optimization problem. It is necessary and sufficient to solve KKT conditions, given by

$$\begin{cases}\dfrac{\partial L\left(p_{b,k,l},\mu_b\right)}{\partial p_{b,k,l}}=\dfrac{-1}{KN_c}\dfrac{\psi\sqrt{\beta}\,\dfrac{h_{b,k,l}^{eq}}{\sigma}e^{-\frac{\beta}{2}\left(\frac{h_{b,k,l}^{eq}}{\sigma}\sqrt{p_{b,k,l}}+d_{b,k,l}\right)^2}}{2\sqrt{2\pi}\sqrt{p_{b,k,l}}}+\mu_b-\lambda_{b,k,l}=0\\ \left(\sum_{l=1}^{N_c}\sum_{k=1}^{K}p_{b,k,l}-P_{t_b}\right)\mu_b=0,\ \mu_b\geq 0,\ \sum_{l=1}^{N_c}\sum_{k=1}^{K}p_{b,k,l}\leq P_{t_b}\\ \lambda_{b,k,l}\,p_{b,k,l}=0,\ \lambda_{b,k,l}\geq 0,\ p_{b,k,l}\geq 0\end{cases} \tag{5.31}$$

with $h_{b,k,l}^{eq}=\mathbf{h}_{b,k,l}^{H}\mathbf{w}_{b,k,l}^{(type)}$. Let us assume that $\mu_b=0$. Therefore, from the first equation of (5.31) we see that $\lambda_{b,k,l}<0$. However, by the third line of equation (5.31) we know that $\lambda_{b,k,l}\geq 0$, a contradiction. Consequently, μ_b is always positive ($\mu_b>0$) and the power constraint, at each BS b, is always active $\sum_{l=1}^{N_c}\sum_{k=1}^{K}p_{b,k,l}=P_{t_b}$. Additionally, by removing the positivity constraint of $p_{b,k,l}$ and solving optimization problem (5.29) we get an optimal solution with all $p_{b,k,l}\geq 0$. Henceforth, the optimal solution of problem (5.29) is independent of

constraints $p_{b,k,l} \geq 0$ and $\lambda_{b,k,l} = 0$. Assuming $d_{b,k,l} = 0$ and $\lambda_{b,k,l} = 0$, i.e., for the worst-case, the powers $p_{b,k,l}$ as function of the Lagrange multiplier μ_b are given by (proof similar to appendix A),

$$p_{b,k,l} = \frac{\sigma^2}{\beta\left(h_{b,k,l}^{eq}\right)^2} W_0\left(\frac{\bar{\mu}_b \psi^2 \beta^2 \left(h_{b,k,l}^{eq}\right)^4}{8\pi\sigma^4 K^2 N_c^2}\right) \tag{5.32}$$

where $\bar{\mu}_b = \frac{1}{\mu_b^2}$ and W_0 stands for Lambert's W function of index 0 . Therefore, $\bar{\mu}_b$ can be efficiently determined iteratively to satisfy $\sum_{l=1}^{N_c}\sum_{k=1}^{K} p_{b,k,l} = P_{tb}$, by using the bisection method. For that a sub-interval in which the root $\bar{\mu}_b$ must lie should be provided. It can be shown that the Lambert's $W_0(x)$ function is bounded by, $\alpha Log(x) \leq W_0(x) \leq x$, $x > 0, \forall \alpha \in \left[0, \frac{e}{1+e}\right]$, (see the appendix D). Thus, we can derive a lower bound for the root $\bar{\mu}_b$, given by

$$\bar{\mu}_{b_{LB}} = \frac{P_{t_b}}{\sum_{k=1}^{K}\sum_{l=1}^{N_c} \frac{\psi^2 \beta\left(h_{b,k,l}^{eq}\right)^2}{8\pi K^2 N_c{}^2 \sigma^2}} \tag{5.33}$$

and for faster algorithm's convergence the upper bound should be as close to as the lower bound, thus α should be chosen as $\frac{e}{1+e}$ and therefore the upper bound is given by

$$\bar{\mu}_{b_{UB}} = Exp\left(\frac{P_{t_b} - \left(\frac{e}{1+e}\right)\sum_{k=1}^{K}\sum_{l=1}^{N_c} \frac{\sigma^2}{\beta\left(h_{b,k,l}^{eq}\right)^2} \mathrm{Log}\left(\frac{\psi^2\beta^2\left(h_{b,k,l}^{eq}\right)^4}{8\pi K^2 N_c{}^2 \sigma^4}\right)}{\left(\frac{e}{1+e}\right)\sum_{k=1}^{K}\sum_{l=1}^{N_c} \frac{\sigma^2}{\beta\left(h_{b,k,l}^{eq}\right)^2}}\right) \tag{5.34}$$

thus the root $\bar{\mu}_b \in \left[\bar{\mu}_{b_{LB}} \quad \bar{\mu}_{b_{UB}}\right]$. This scheme is referred as minimum VBER worst case power allocation (MVBER WC). The corresponding algorithm can be described, in pseudo code, as follows:

Algorithm 1: MVBER WC ($d_{b,k,l} = 0$)

For $b = 1$ to B

1. Compute the precoder vectors using (5.8), (5.11) or (5.13).
2. Set $\bar{\mu}_{b_{LB}}$ and $\bar{\mu}_{b_{UB}}$ according to (5.33) and (5.34), respectively.
3. Determine the optimal $\bar{\mu}_b$ value that satisfies the power constraint $\sum_{l=1}^{N_c}\sum_{k=1}^{K} p_{b,k,l} = P_{t_b}$ using the bisection method and bounds calculated into step 2.
4. Obtain the optimum power values, according to equation (5.32), using the pre-calculated value of $\bar{\mu}_b$.

For the case where $d_{b,k,l} \neq 0$, to the best of our knowledge no solution based on Lambert's W function can be derived, but the precoders can be computed by solving directly (5.29) using for example the interior-point method [23]. However, as discussed in next section, for this case the complexity to compute the powers is much higher than for $d_{b,k,l} = 0$. One possible selection for $d_{b,k,l}$ could be

$$d_{b,k,l} = \sqrt{\frac{P_{t_b}}{N_{t_b} N_c}} \sum_{j=1, j\neq b}^{B} \sqrt{\frac{\mathrm{E}\left\{\left|\mathbf{h}_{j,k,l}^H \mathbf{w}_{j,k,l}^{(type)}\right|^2\right\}}{\sigma^2}} \tag{5.35}$$

Considering the DZF precoder the average power of the equivalent channels, $\mathbf{h}_{j,k,l}^H \mathbf{w}_{j,k,l}^{(type)}$, is given by

$$\mathrm{E}\left\{\left|\mathbf{h}_{j,k,l}^H \mathbf{w}_{j,k,l}^{(DZF)}\right|^2\right\} = \left(N_{t_b} - K + 1\right)\Phi_{PL\ j,k,l} \tag{5.36}$$

In this case the long-term channel powers, $\Phi_{PL\ j,k,l}$, $j \neq k$ should be either feedbacked from the UTs to the BS b or shared by the backhaul network. This scheme is referred as minimum VBER long term channel power allocation (MVBER LTC). Note that for the VSINR precoder it is difficult to obtain a closed-form expression for the average power of the equivalent channels $\mathrm{E}\left\{\left|\mathbf{h}_{j,k,l}^H \mathbf{w}_{j,k,l}^{(DVSINR)}\right|^2\right\}$.

Algorithm 2: MVBER ($d_{b,k,l} \neq 0$)

For b = 1 to B

1. Compute the precoder vectors using (5.8), (5.11) or (5.13).
2. Set $d_{b,k,l}$ using (5.35) or others.
3. Obtain the optimum power values by solving (5.29) using for example the interior-point method.

5.5 Numerical Results

In this section, the performance of the different centralized and distributed power allocation strategies for proposed distributed precoding vectors (DZF) is obtained numerically and compared against results from MRT and DVSINR precoders. Two types of scenarios are defined:

- Scenario 1: where we consider 2 or 4 BSs, $B=2$ which are equipped with 2 or 4 antennas, $N_{t_b}=2,4$ and 2 or 4 single antenna UTs, $K=2,4$. As in chapter 4, we assume that each UT is placed on each cell. The long-term channel powers are assumed to be $\Phi_{PL_{b,k}}=1,\ b=k$ for the intra-cell links, and $\Phi_{PL_{b,k}},\ b\neq k$ are uniformly distributed on the interval $[0.2,\ 0.6]$ for the inter-cell links. In this scenario the results are presented in terms of per-BS SNR defined as $SNR=P_{tb}/N_c\sigma^2$.
- Scenario 2: which consists of K uniformly distributed single antenna UTs in a square with BSs in each of the corners. The power decay is proportional to $1/r^4$, where r is the distance from a transmitter. In this scenario the results are presented in terms of SNR at the cell edge defined as $SNR_{cell\text{-}edge}=P_{tb}\Phi_{PL_c}/N_c\sigma^2$, where the Φ_{PL_c} represented the long-term channel power in the centre of the square. This represents a scenario where terminals are moving around in the area covered by B=4 base stations each equipped with 4 antennas ($N_{t_b}=4$).

The main parameters used in the simulations are based on LTE standard and according to Table 5-1 [24]. Also, we used the LTE extended typical urban (ETU) channel model with 9 taps [25].

Table 5-1 LTE-based Simulation Parameters

FFT size	1024
available subcarriers (N_c) shared by the *K* users	128
sampling frequency	15.36 MHz
useful symbol duration	66.6 μs
cyclic prefix duration	5.21 μs
overall OFDM symbol duration	71.86 μs
subcarrier separation	15 kHz
Modulation	QPSK
channel code	CTC block size of (6144, 3072)/No coding
channel code block size	6144, 3072
Code rate	1/2
Max Log MAP algorithm	8 iterations

5.5.1 Evaluation of Semi-distributed Schemes for DZF precoder

In this section first we present the performance results of proposed centralized power allocation schemes for scenario 1 considering DZF precoder. To this end we present the results for per-BS equal power allocation (Cent. per-BS EPA), in this case $p_{b,k,l} = P_{tb} / K, \forall (b,k,l)$; the two suboptimal approaches Cent. per-BS SOIPA and Cent. per-BS SOCPA and the optimal one Cent. per-BS OPA. We present results for two different approaches as in chapter 4: for the case where the power is constrained per-subcarrier, i.e. the power per-subcarrier is fixed to P_{tb} but may vary from user to user, these curves are referred as per-subcarrier power constraint, *Per subcarrier PC*. In this approach the powers of each user are computed individually on each subcarrier. In the second one, the powers are computed jointly for all the available subcarriers, i.e., the overall power is fixed to $P_{tb} N_c$ and may vary from subcarrier to subcarrier and from user to user. These curves are referred as joint subcarrier power constraint, *Joint subcarrier PC*. Also, we present results for optimal approach considering total power allocation (Cent. TPC OPA), as formulated in (5.16). This is similar to the single cell scenario where the powers are computed to satisfy the overall power constraint, i.e., $\sum_{b=1}^{B} \sum_{k=1}^{K} p_{b,k} \le P_t / N_c$ and $\sum_{b=1}^{B} \sum_{k=1}^{K} \sum_{l=1}^{Nc} p_{b,k,l} \le P_t$ if the powers are computed individually

per subcarrier and jointly for all subcarriers, respectively. This serves as lower bound for the multicell scenario under per-BS power constraint. All the results are presented in terms of the average BER as a function of per-BS SNR defined as $SNR = P_{tb} / N_c\sigma^2$.

Fig 5-4 shows the performance results of all considered precoding schemes for per-BS scenario with $B = 2; N_{t_b} = 2; K = 2$ and uncorrelated channels, i.e., $\mathbf{R} = \boldsymbol{I}_{N_{tb}}$. It can be observed that the Cent. per-BS SOCPA, Cent. per-BS SOIPA and Cent. per-BS OPA schemes outperform the Cent. per-BS EPA approach, because they redistribute the powers across the different sub-channels more efficiently. Considering a *Per subcarrier PC* strategy, the performance of the two proposed suboptimal per-BS approaches is very close. Moreover, the performance penalty of the two suboptimal schemes against the optimal one is low, less than 0.2 dB for a BER=10^{-3}. Also, the penalty of the Cent. per-BS OPA against the lower bound given by the Cent. TPC OPA is approximately 0.3 dB considering also a BER=10^{-3}. The results show that the proposed precoding schemes with *Joint subcarrier PC* clearly outperform the same ones with *Per subcarrier PC*. For this case the performance of the suboptimal Cent. per-BS SOIPA and optimal Cent. per-BS OPA is also very close (penalty less than 0.1dB), but the gap between these two schemes and the suboptimal Cent. per-BS SOCPA increases for the *Joint subcarrier PC* approach. These results show that the Cent. per-BS SOIPA only outperforms the Cent. per-BS SOCPA for large number of subchannels. We can observe a penalty of approximately 0.6 dB of the Cent. per-BS SOCPA scheme against the Cent. per-BS SOIPA for a BER=10^{-3}. Also, a gain of approximately 1.2dB and 4.2 dB of the suboptimal Cent. per-BS SOIPA scheme against the Cent. per-BS EPA is obtained (BER=10^{-3}) for *Per subcarrier PC* and *Joint subcarrier PC* approaches, respectively.

The simulations leading to Fig 5-4 were obtained for per-BS scenario with $B = 4; N_{t_b} = 4; K = 4$ and uncorrelated channels. Comparing the results obtained for this scenario with the ones shown in last figure we can observe a considerable gain. This is because now each UT receives the same data from 4 different BSs instead of only 2, increasing the diversity order and also the antenna array gain since the different copies are coherently combined in the receiver. We also can see here that all proposed schemes outperform the Cent. per-BS EPA. Considering a *Per subcarrier PC* strategy, in this scenario the performance of the two proposed suboptimal Cent. per-BS approaches is very close. Moreover, the performance penalty of the two suboptimal schemes against the optimal one is low, less than 0.5 dB for a BER=10^{-3}. Also, the penalty of the Cent. per-BS OPA against the lower bound given by the Cent. TPC OPA is higher than in the first scenario and is approximately 0.5 dB considering also a BER=10^{-3}. This is because in this scenario the number of power constraint is higher than the previous one since the number of BSs is increased to 4.

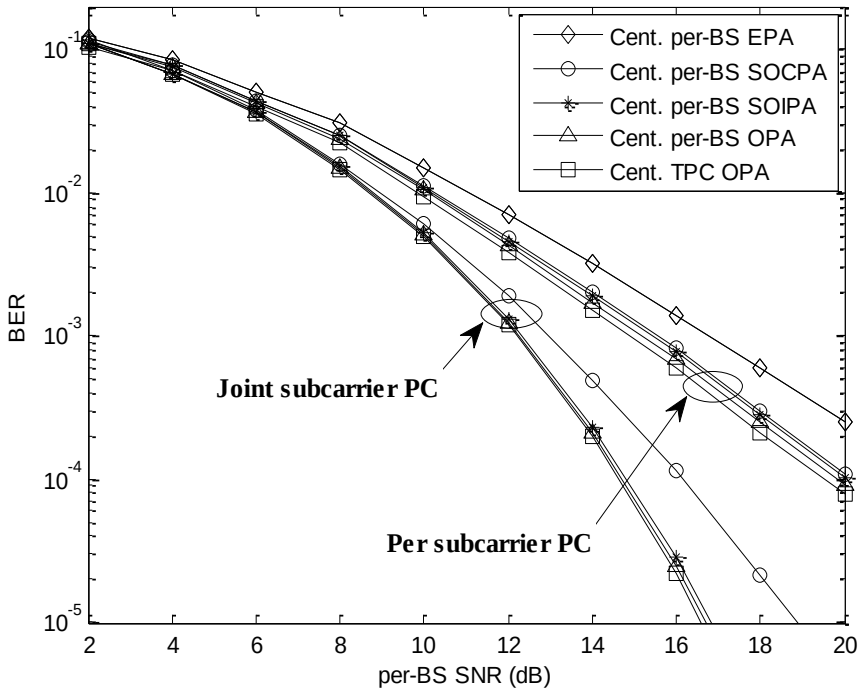

Fig 5-4 Performance evaluation of the DZF semi-distributed schemes for per-BS scenario with $B = 2; N_{t_b} = 2; K = 2$ and uncorrelated channels.

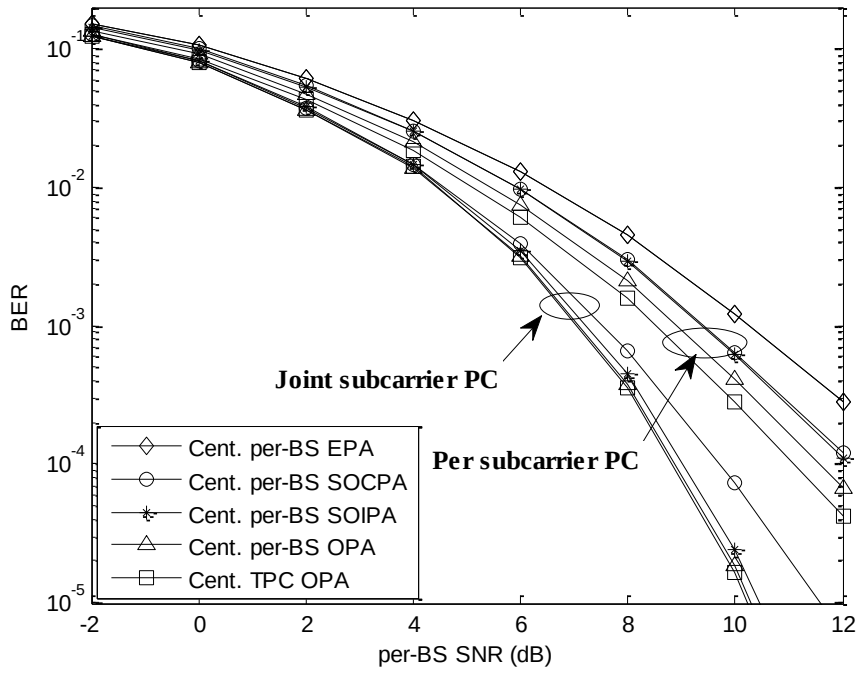

Fig 5-5 Performance evaluation of the DZF semi-distributed schemes for per-BS scenario with $B = 4; N_{t_b} = 4; K = 4$ and uncorrelated channels.

The results also show that the proposed precoding schemes with *Joint subcarrier PC* clearly outperform the same schemes with *Per subcarrier PC* for the same reasons explained for former scenario. Another important issue that should be emphasized is that the penalty of the Cent. per-BS OPA against the Cent. TPC OPA is approximately of 0.5 dB for the *Per subcarrier PC*, but is reduced to less than 0.1 dB with *Joint subcarrier PC* (BER=10^{-3}), because the number of degrees of freedom to minimize the average BER is increased. Intuitively, the penalty decreases as the number of subchannels increases, i.e., the performance of the Cent. per-BS OPA tends to the performance of the Cent. TPC OPA when the number of subchannels tends to infinity.

5.5.2 Comparison of DZF, MRT and DVSINR in Semi-distributed Schemes

In this section we compare the performance results of centralized power allocation schemes for proposed DZF, against the ones for MRT and DVSINR assuming scenario 2. We consider Cent. per-BS equal power allocation (EPA) and the two centralized power allocation techniques, namely Cent. per-BS SOIPA and Cent. per-BS SOCPA. Also, we present results for the DVSINR assuming that the interference part of (5.5) is negligible, referred as Cent. per-BS SOIPA WC and Cent. per-BS SOCPA WC discussed in section 5.4.1.4. The results are presented in terms of the average BER as a function of cell edge SNR defined before.

Error! Reference source not found. shows the performance results considering $K = 4$. As can be seen, the proposed power allocation schemes outperform the Cent. per-BS EPA approach, because they redistribute the powers across the different sub-channels more efficiently. We can see that at high SNR regime the performance of DVSINR tends to DZF while MRT degrades a lot even with power allocation, since the system is interference limited. It can be seen that gap between DVSINR and DZF curves is approximately 6dB, considering a BER=1e-3. However, the amount of information to be transmitted by the backhaul network is higher for the DVSINR approach with power allocation. Also, the performance of the DZF with Cent. per-BS SOCPA approach is close to the one obtained for DZF with Cent. per-BS SOIPA approach, but with lower complexity. The same behaviour can be observed for the DVINR with both Cent. per-BS SOIPA and Cent. per-BS SOCPA. Also, we can observe a penalty of the Cent. per-BS SOIPA WC and Cent. per-BS SOCPA WC (the power allocation is computed neglecting the interference part) against the Cent. per-BS SOIPA and Cent. per-BS SOCPA of approximately 1dB for a BER=1e-3. Nevertheless, we can see a gain of the Cent. per-BS SOIPA WC and Cent. per-BS SOCPA WC curves against the VSINR with Cent. EPA of approximately 1 dB (BER=1e-3).

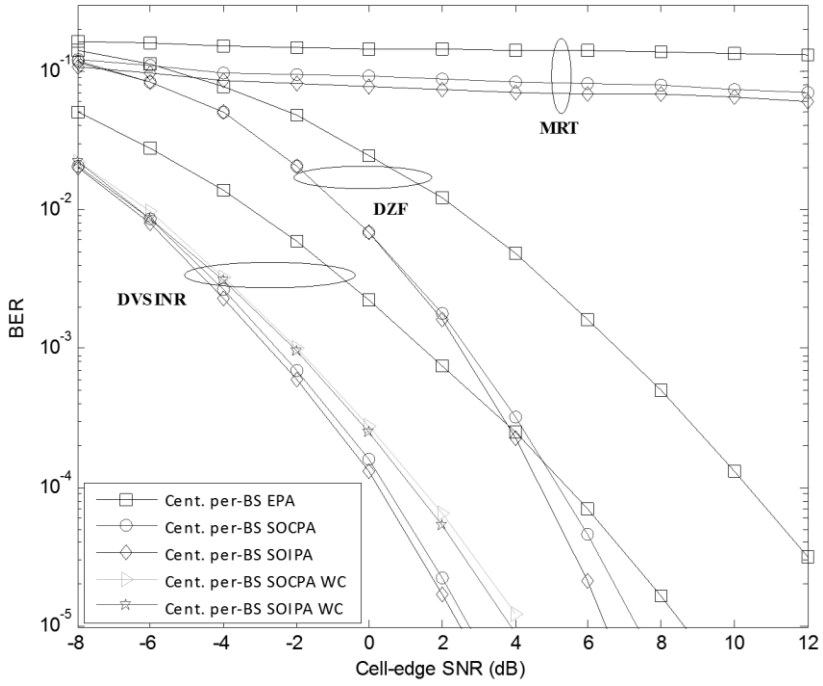

Fig 5-6 Performance evaluation of the distributed multicell precoding with centralized PA for K=4

Fig 5-7 shows the performance results when the number of UTs is reduced to 2. In this scenario the DoF of the equivalent channels variables $h_{b,k,l}^{eq}$, given by $2(N_{tb}-K+1)$, increases from 2 to 6. It can be observed that increasing the DoF, the DZF curves tends to the DVSINR ones. This behaviour is similar to the single cell systems where the precoders based on ZF criterion tends to the ones based on MMSE as the number of transmit antennas (or DoF) increases or at high SNR. It can be observed that for the MRT precoder the gains obtained with the power allocation techniques against the Cent. EPA are much higher for this scenario. However for medium and high SNR the gains are far from the ones obtained with the DZF and VSINR precoders. In this figure, the curves for DVSINR with the approaches Cent. per-BS SOIPA WC and Cent. per-BS SOCPA WC, are omitted for clarity since their performance are approximately the same as Cent. per-BS SOIPA and Cent. per-BS SOCPA, respectively for DVSINR.

Error! Reference source not found. depicts the performance results for 6 UTs and only for the DVSINR precoder with the proposed power allocation techniques. Note that the DZF cannot be used in this scenario since $N_{t_b} < K$ and the performance of the MRT precoder for the scenario with 4 UTs (see **Error! Reference source not found.**) was already very bad. From the results we can

observe that the proposed power allocation schemes outperform the EPA approach. Also, we can see that all the curves have an error floor since in this scenario the system is interference limited, i.e., the interference part cannot be negligible. Another interesting result is that the penalty of the Cent. per-BS SOIPA/SOCPA WC against the Cent. per-BS SOIPA/SOCPA is higher than in the previous scenarios. This is because in this scenario the interference part cannot be negligible as for the previous scenarios. Comparing these results with the ones presented in **Error! Reference source not found.**, we can conclude that even if DVSINR can be used in scenarios with $N_{t_b} < K$, the performance penalty against the scenarios with $N_{t_b} \geq K$ is very high.

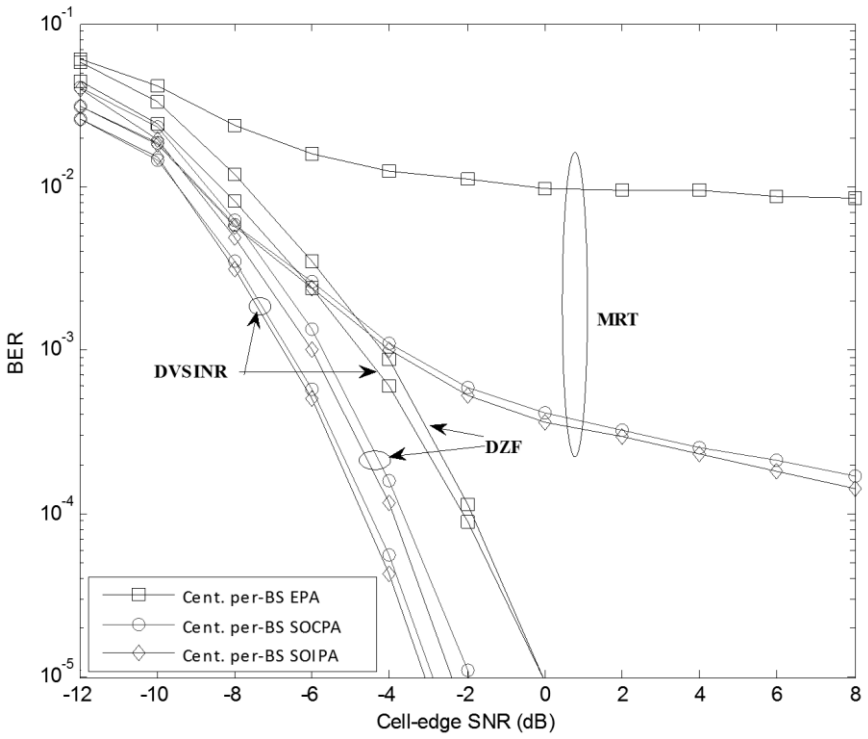

Fig 5-7 Performance evaluation of the distributed multicell precoding with centralized PA for K=2.

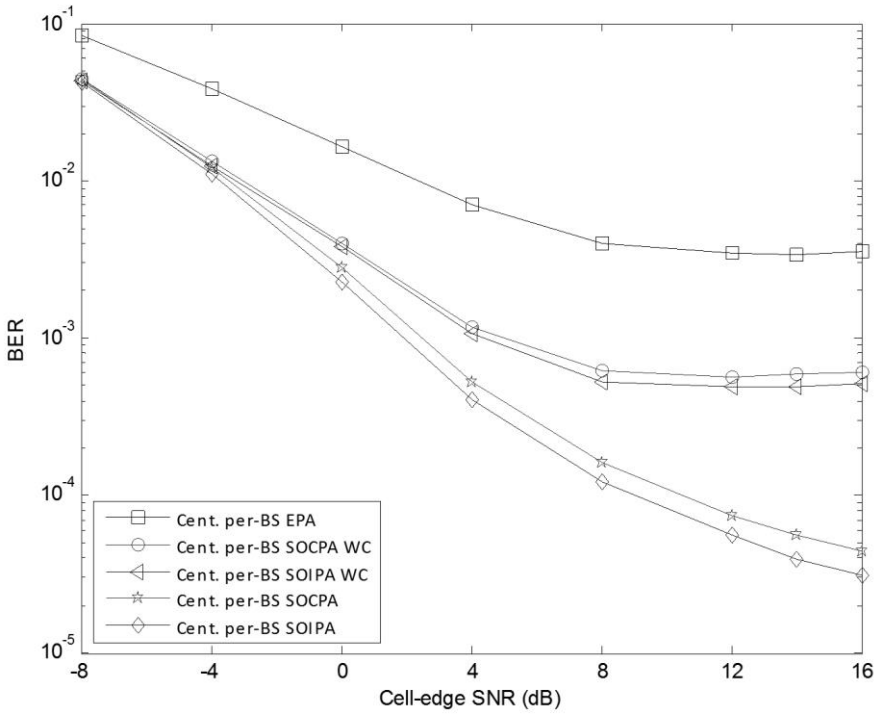

Fig 5-8 Performance evaluation of the distributed multicell VSINR based precoding with centralized PA for K=6.

5.5.3 Performance Comparison of Semi-distributed and Full-centralized Schemes for ZF

In this section, the performance results of semi-distributed and full-centralized schemes for ZF precoder are compared. The latter was presented in chapter 4 where both precoders and power elements were computed centrally at JPU. To this end we assume scenario 1.

Error! Reference source not found. shows the results for per-BS scenario with $B=2;N_{t_b}=2;K=2$, from this figure we can see that the performance of all centralized power allocation schemes with centralized ZF outperforms the one with DZF, because there are more DoF to remove the interference and enhance the system performance. For DZF, the performance of the suboptimal Cent. per-BS SOIPA and optimal Cent. per-BS OPA is very close (penalty less than 0.1dB), but the gap between these two schemes and the suboptimal Cent. per-BS SOCPA is almost increased to 0.8dB (BER=10^{-3}). In the case of centralized ZF, the performances of Cent. per-BS SOIPA and Cent. per-BS OPA are still very close but both are degraded from Cent. TPC OPA (about 0.5dB at BER=10^{-3}) and also there is 0.5dB gap among these curves and Cent. per-BS SOCPA at the same BER. Another important issue that should be emphasized is that the penalty of

the Cent. per-BS OPA against the Cent. TPC OPA is approximately 0.1 dB (BER=10^{-3}) for DZF, against 0.5dB for centralized ZF.

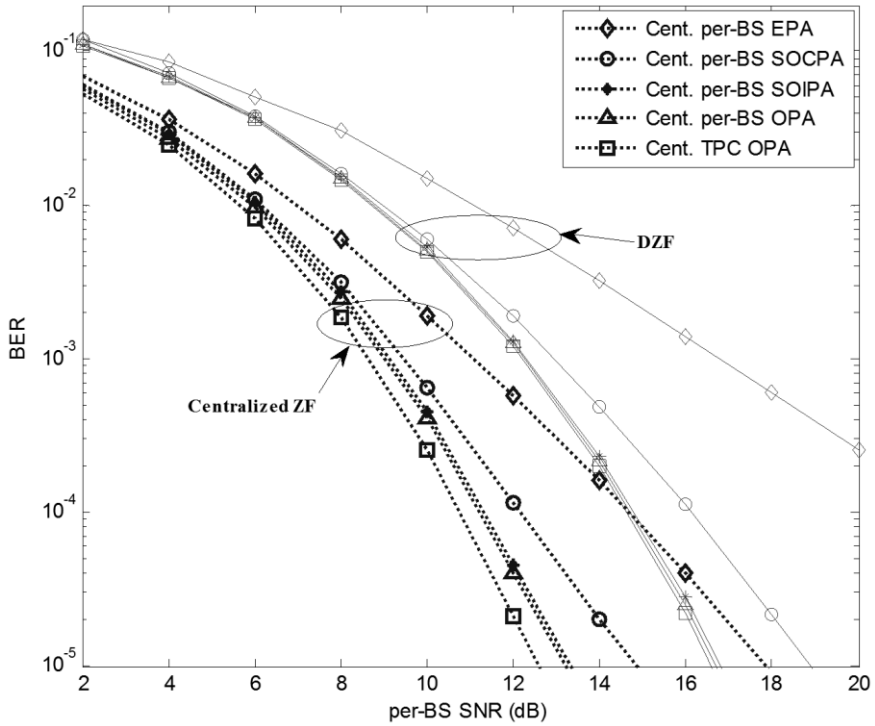

Fig 5-9 Performance comparison of the proposed semi-distributed and full-centralized schemes for $N_{t_b}=2$.

Fig 5-10 compares the performance results of semi-distributed and full-centralized schemes assuming per-BS scenario with $B=2;N_{t_b}=4;K=2$. By observing this figure almost the same conclusions can be drawn. An interesting result is that the performances of both schemes are much closer comparing with the scenario with less transmit antenna per BS. This can be explained by the fact that for the centralized precoding the number of DoF, which is given by the number of total transmit antennas BN_{t_b}, increased from 4 ($N_{t_b}=2$) to 8 ($N_{t_b}=4$); while for the DZF, the number of DoF, which is given by $B\left(N_{t_b}-K+1\right)$ as discussed before; is increased from 2 ($N_{t_b}=2$) to 6 ($N_{t_b}=4$), i.e., the difference in number of DoF of both approaches is smaller comparing to scenario with $N_{t_b}=2$. From the presented results two important facts should be also emphasized: first is that in case of DZF, the performance improvement achieved utilizing three proposed centralized power allocation techniques, is higher than the case of centralized ZF; the second is that in the case

of DZF, the suboptimal techniques are more successful in achieving the lower bound of average BER.

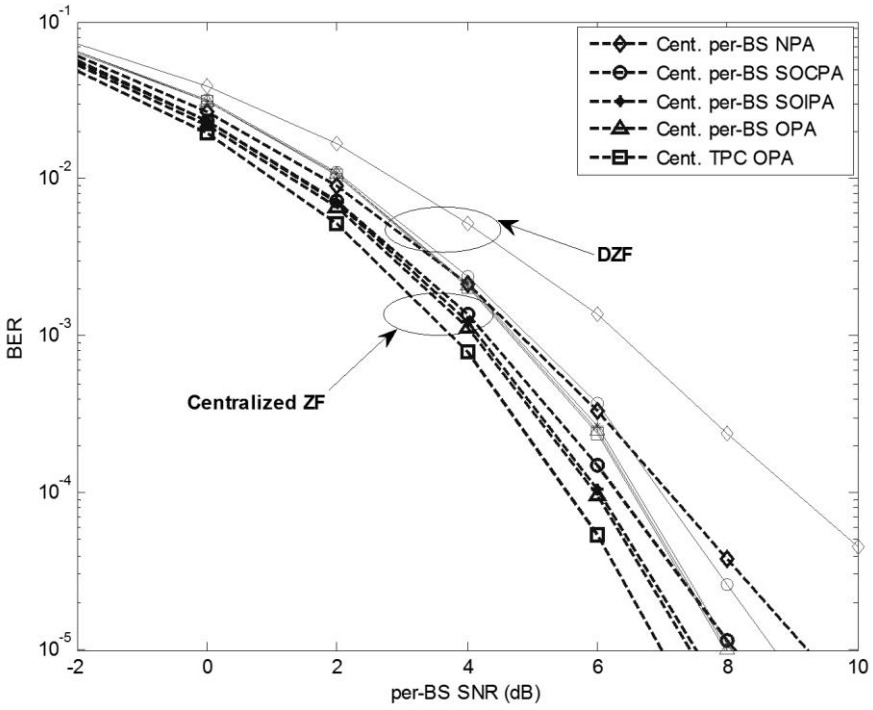

Fig 5-10 Performance comparison of the proposed semi-distributed and full-centralized schemes for $N_{t_b} = 4$.

5.5.4 Evaluation of Full Distributed Scheme

In this section we present and compare the performance results of the proposed distributed power allocation schemes, MVBER WC just for DVSINR and DZF precoders and MVBER LTC for DZF one only for scenario 2. Also, these schemes are compared with two different power allocation strategies: equal power allocation approach, i.e., the power available at each BS is equally divided by the users and subcarrier, referred as EPA; DZF with joint centralized power allocation as proposed in section 5.4.1 and 5.4.2 (under the name per-BS OPA), referred to here as centralized MBER power allocation (CMBER). We also present the curve for the DVSINR with joint centralized power allocation using the same strategy as for the DZF, also referred as (CMBER).

Fig 5-11 shows the performance results considering $K = 4$ and uncoded data. The results are presented in terms of the average BER as a function of cell-edge SNR defined before. From the figure we can see that the performance of the proposed distributed power allocation schemes for

both precoders outperforms their equal power, i.e., the DZF EPA and DVSINR EPA ones, because they redistribute the powers across the different users and sub-channels more efficiently. As can be seen in Fig 5-11, the gain of the MVBER WC power allocation scheme is approximately 1dB for both precoders (BER=10^{-3}) when compared with the equal power strategy. The results show that knowing the non local LTC powers at each BS the performance can be improved namely at high SNR regime, we can observe a gain of approximately 0.5dB of the MVBER LTC against MVBER WC, for BER=10^{-3}. Also, the performance can be improved whether the powers are computed jointly at the JPU to minimize the real average BER (approximately of 3 dB gain of the CMBER against the MVBER WC for DZF precoder at BER=10^{-3}). However, this strategy requires more feedback load over the backhaul network as compared with the full distributed approaches.

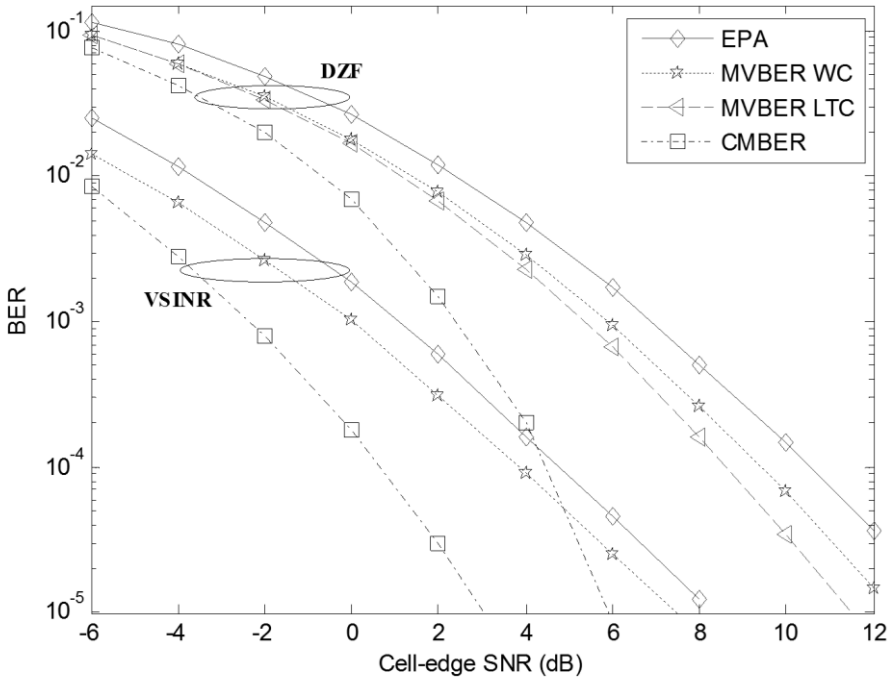

Fig 5-11 Performance evaluation of the distributed power allocation schemes for $K=4$ and uncoded data.

Fig 5-12 shows the performance results when the number of UTs is reduced to 3. In this scenario the number of DoF of the equivalent ZF channels variables, given by $2(N_{tb}-K+1)$, increases from 2 to 4. It can be observed that increasing the DoF, the DZF tends to the DVSINR. This behaviour is similar to the single cell systems where the precoders based on ZF criterion tends to the ones based on MMSE as the number of transmit antennas (or DoF) increases or at high SNR. From these results it is clear that the gains with power allocation schemes relatively to the EPA

case are lower than in the previous scenario. Also, the gain obtained with the centralized power allocation against the full distributed approaches is lower. In this plot, the curve for the approach MVBER LTC is omitted for clarity, since its performance is approximately the same as MVBER WC.

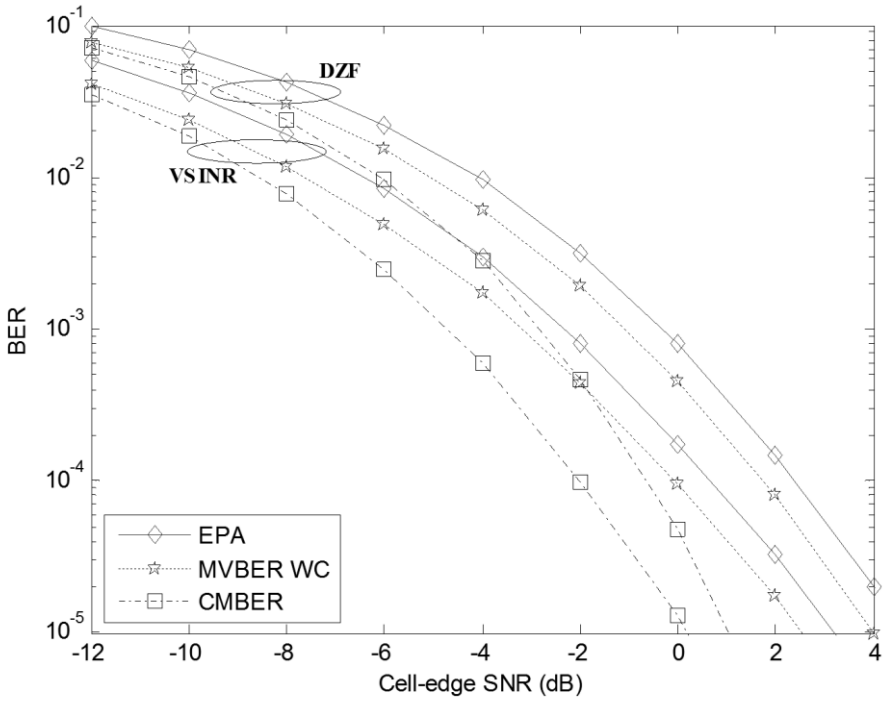

Fig 5-12 Performance evaluation of the distributed power allocation schemes for $K=3$ and uncoded data.

Although our power allocation scheme is based on the minimization of the virtual uncoded BER, we also assess the impact of our scheme on a coded system. In Fig 5-13 and Fig 5-14 we depict the performance results for the same scenarios of Fig 5-11 and Fig 5-12, respectively, but now considering the convolutional turbo code (CTC) specified above. From these figures we basically can point out the same conclusions as for the results obtained for uncoded case. The gain of the MVBER WC power allocation scheme for both precoders is approximately 1dB (BER=10^{-3}) when compared with the equal power strategy. The penalty regarding the joint centralized approach is approximately of 1.2 dB at BER of 10^{-3}. In this plot, the curve for the approach MVBER LTC is also omitted for clarity, since its performance is approximately the same as MVBER WC. This means that for practical scenarios the knowledge of long-term equivalent channel variables does not bring significant improvements regarding the MVBER WC approach.

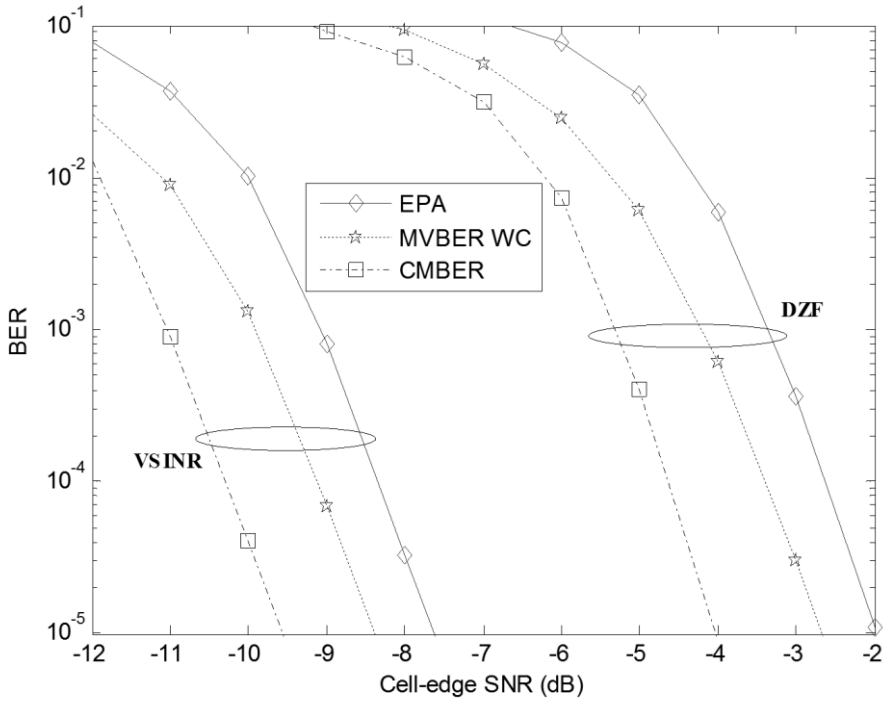

Fig 5-13 Performance evaluation of the distributed power allocation schemes for $K = 4$ and coded data.

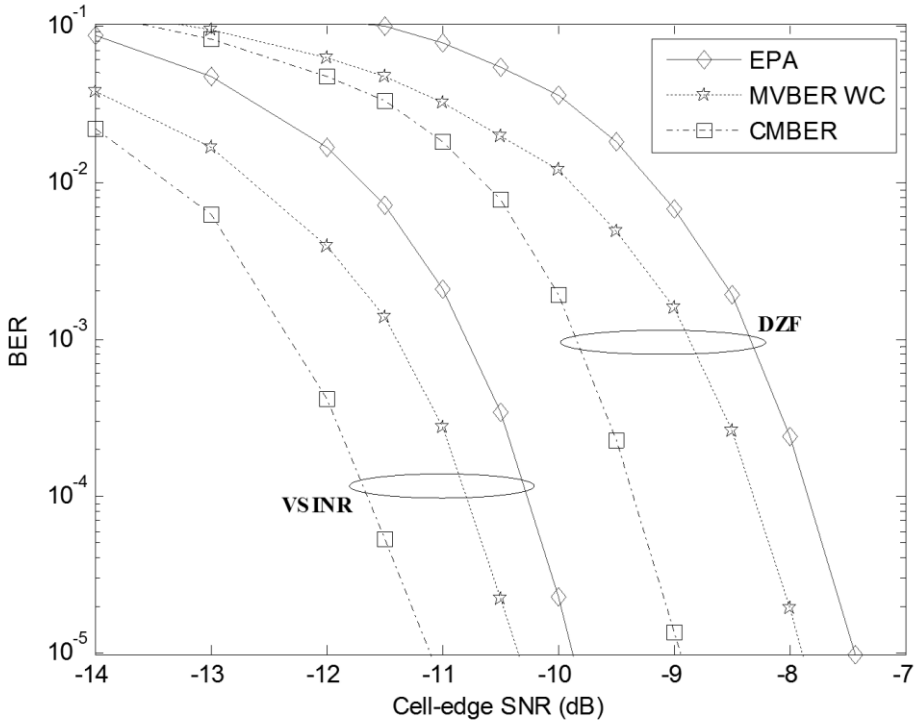

Fig 5-14 Performance evaluation of the distributed power allocation schemes for $K = 3$ and coded data.

5.5.5 Complexity Analysis of Full Distributed Scheme

In this section the complexity of the different distributed approaches for scenario 2, is evaluated numerically. We compare the average running time for the algorithm MVBER WC ($d_{b,k,l}=0$) for the cases where the search interval is restricted to the derived interval $\left[\bar{\mu}_{b_{LB}} \quad \bar{\mu}_{b_{UB}}\right]$ and when there is no a priori bounding of the interval, i.e., the search is over $\left[0 \quad \text{Inf}\right]$, where Inf is the maximum software number representation. We also evaluate the average running time for MVBER WC ($d_{b,k,l}=0$) solving directly (5.29) using the interior-point-method (IPM), here referred as MVBER WC IPM. For this latter case the complexity is approximately the same as the one of the algorithm using $d_{b,k,l}\neq 0$. The stop criterion for the algorithms using the bisection method (MVBER WC $\left[\bar{\mu}_{b_{LB}} \quad \bar{\mu}_{b_{UB}}\right]$ and $\left[0 \quad \text{Inf}\right]$) is formulated as, $\bar{\mu}_b(i-1)-\bar{\mu}_b(i)\leq\varepsilon,\forall b$, where i is the index for the iteration and ε is the chosen convergence threshold. For the one using the IPM the stop criterion is $p_{b,k,l}(i-1)-p_{b,k,l}(i)\leq\varepsilon$,$\forall b,k,l$. The results of Fig 5-15 and Fig 5-16 were obtained setting $\varepsilon=10^{-8}$. This parameter was also used to obtain the curves presented in Fig 5-11 to 5-14.

The results of Fig 5-15 are presented in terms of the ratio between the average running time of the MVBER WC IPM over the one of MVBER WC $\left[\bar{\mu}_{b_{LB}} \quad \bar{\mu}_{b_{UB}}\right]$ (curves A in Fig 5-15) and MVBER WC $\left[0 \quad \text{Inf}\right]$ (curves B in Fig 5-15), as function of the number of users. The average running times of the different algorithms have been measured over 10^3 trials and we obtained results for two operation points: Cell Edge SNR=0 and 12dB. As can be observed from the Fig 5-15, the average running time of the MVBER WC IPM is approximately 120 and 500 times more than the proposed one MVBER WC $\left[\bar{\mu}_{b_{LB}} \quad \bar{\mu}_{b_{UB}}\right]$ for $K=2$ and $K=4$, respectively. Also, we can see that the gain of the MVBER WC $\left[0 \quad \text{Inf}\right]$ against MVBER WC IPM is modest. This means that if the interval for the bisection method is not efficiently computed the gain relatively to the MVBER WC IPM is low.

In Fig 5-16 we present results in terms of the ratio between the average number of iterations required of the MVBER WC $\left[0 \quad \text{Inf}\right]$ over the one of MVBER WC $\left[\bar{\mu}_{b_{LB}} \quad \bar{\mu}_{b_{UB}}\right]$. The curves are shown as function of number of users and the SNRs considered were the same used for Fig 5-15. As can be seen from the figure the average number of iterations required for the MVBER WC

$[0 \quad \text{Inf}]$ to achieve the solution is approximately 9.5 and 6 times more than the ones required by the proposed algorithm MVBER WC $\left[\bar{\mu}_{b_{LB}} \quad \bar{\mu}_{b_{UB}}\right]$ for the cases of 2 and 4 users, respectively (for Cell-edge SNR=12dB). Considering the low SNR regime the gains are slightly lower. We can observe a gain (in terms on number of required iterations) of approximately 7.5 and 5 times of the proposed algorithm against MVBER WC $[0 \quad \text{Inf}]$. Also, we can see that the gain decreases as the number of users increases for the both SNRs regimes.

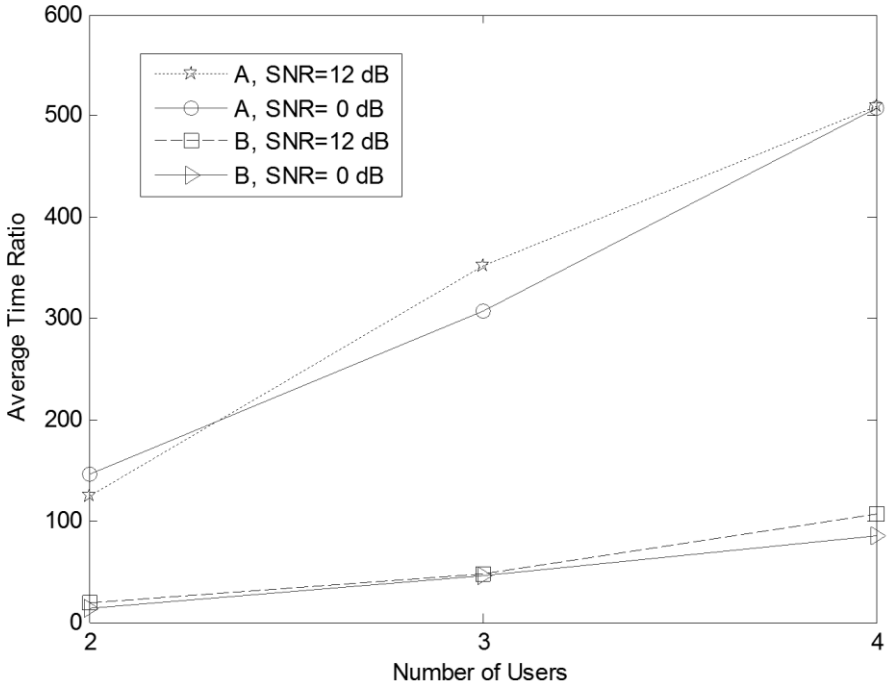

Fig 5-15 Average running time ratio as function of number of users: A (MVBER WC IPM over MVBER WC $\left[\bar{\mu}_{b_{LB}} \quad \bar{\mu}_{b_{UB}}\right]$), B (MVBER WC IPM over MVBER WC $[0 \quad \text{Inf}]$).

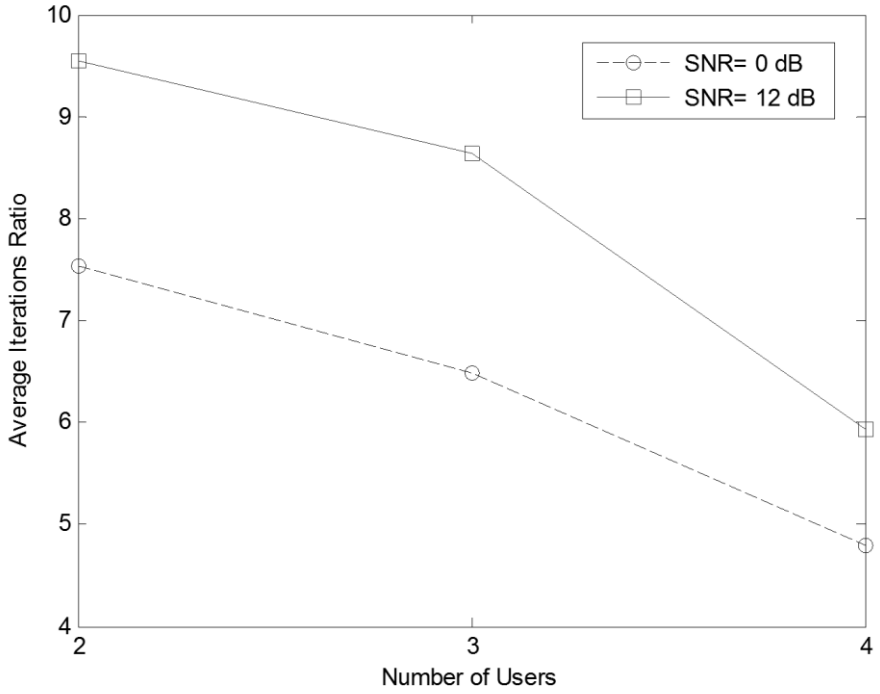

Fig 5-16 Average running time ratio as function of number of users: A (MVBER WC IPM over MVBER WC $\left[\bar{\mu}_{b_{LB}} \quad \bar{\mu}_{b_{UB}}\right]$), B (MVBER WC IPM over MVBER WC $\left[0 \quad \text{Inf}\right]$).

5.6 Conclusion

In this chapter we proposed semi-centralized and full-distributed precoding and power allocation schemes for downlink of multicell MISO OFDM systems. A novel Distributed precoding (DZF) was proposed and the performance for centralized and distributed power allocation, were compared against MRT and DVSINR, which were proposed recently.

The precoders were computed locally at each BS just by assuming the knowledge of local CSI. Then the system performance was further improved by proposing either centralized or distributed power allocation methods. In case of centralized power allocation, the power elements were computed in a centralized fashion at the JPU. The criteria considered was the minimization of the BER and two centralized power allocation algorithms with per-BS power constraint: one optimal that can be achieved at the expense of some complexity and one suboptimal with lower complexity aiming at practical implementations. In both the optimal and the suboptimal, the computation of the transmitted powers required an iterative approach. To circumvent the need for iterations, further proposed another suboptimal scheme, where the power allocation was computed in order to minimize the sum of inverse of SNRs of each UT allowing us to achieve a closed-form solution.

The results have shown that the proposed multiuser multicell schemes cause significant improvement in system performance, in comparison with the case where no power allocation is used. Also for both semi-centralized and full-distributed approaches, the performance of the proposed suboptimal algorithms, namely the per-BS SOIPA approach, is very close to the optimal with the advantage of lower complexity. By further comparison of both approaches it was shown that the semi-centralized approach tends to the one achieved by the full-centralized, when the number of DoF available tends to the number of DoF available in the full-centralized system. It was also shown that the DVSINR outperforms the DZF with the proposed power allocations schemes; although for high SNR regime or high number of DoF the performance of both precoders is close.

We also proposed distributed power allocation where the power elements were also computed locally at each base station just by assuming the knowledge of local CSI or long term equivalent channel non-local statistics. For this purpose we defined the VBER by treating the multicell system as a superposition of interference-free single cell systems. The metric used to derive the power allocation scheme, minimization of VBER, implicitly provides user's fairness at the cell edges. We also obtain upper and lower bounds for the Lambert's W function of index zero that can be used to allow an efficient computation of the power allocation coefficients.

The results have shown that the proposed distributed power allocation scheme outperforms the equal power ones with moderate complexity. When the number of DoF of the equivalent channel variables increases the DZF based approaches tends to the DVSINR ones, and the performance of the distributed power allocation schemes also tends to the joint centralized strategies. Furthermore, the minimization of the *virtual* uncoded BER produces an effective improvement on the performance of coded data. Therefore, semi-centralized and full-distributed schemes can be interesting in practice when the backhaul capacity is limited in some sense.

5.7 Bibliography

[1] R. Holakouei, A. Silva, R. Dinis and A. Gameiro, "Distributed power allocation schemes for precoded multicell MISO-OFDM systems," in *Vehicular Technology Conference (VTC)*, 2012.

[2] R. Holakouei, A. Silva and A. Gameiro, "Performance Evaluation of Distributed Precoding Schemes for Multicell OFDM Systems," in *Vehicular Technology Conference (VTC)*, 2011.

[3] R. Holakouei, A. Silva and A. Gameiro, "Distributed Precoding with Centralized Power Allocation for Multicell OFDM based Systems," in *Wireless Personal Multimedia Communications (WPMC)*, 2011.

[4] R. Holakouei, A. Silva and A. Gameiro, "Distributed Versus Centralized Zero-Forcing Precoding for Multicell OFDM Systems," in *GLOBECOM (GC)*, 2011.

[5] A. Silva, R. Holakouei and A. Gameiro, "Power allocation strategies for distributed precoded multicell based systems," *EURASIP Journal on Wireless Communications and Networking,* vol. 1, 2011.

[6] R. Holakouei, A. Silva and A. Gameiro, "Coordinated Precoding Techniques for Multi-cell MISO-OFDM Networks," *Wireless Personal Communication (WPC) Journal,* 2012.

[7] A. Silva, R. Holakouei, D. Castanheira, A. Gameiro and R. Dinis, "A Novel Distributed Power Allocation Scheme for Coordinated Multicell Systems," *Accepted to EURASIP Wireless Communication and Networking Journal,* 2013.

[8] R. Zakhour and D. Gesbert, "Distributed multicell-MISO precoding using the layered virtual SINR framework," *IEEE Trans. Wireless Commun,* vol. 9, no. 8, pp. 2444-2448, 2010.

[9] E. Bjornson, R. Zakhour, D. Gesbert and B. Ottersten, "Cooperative multicell precoding: rate region characterization and distributed strategies with instantaneous and statistical CSI," *IEEE Trans. Signal Process,* vol. 58, no. 8, pp. 4298-4310, Aug. 2010.

[10] M. Kobayashi, M. Debbah and J. Belfiore, "Outage efficient strategies in network MIMO with partial CSIT," in *Proceeding of IEEE ISIT*, 2009.

[11] R. Zhang and L. Hanzo, "Cooperative downlink multicell preprocessing relying on reduced-rate back-haul data exchange," *IEEE Trans. Veh. Technol.,* vol. 60, no. 2, pp. 539-545, Feb. 2004.

[12] J. Proakis, Digital Communications, McGrraw-Hill: McGrraw-Hill, 1995.

[13] F. Domene, G. Piñero, C. Botella and A. Gonzales, "A limited feedback scheme based on spatially correlated channels for coordinated multipoint systems," *J. Wireless Commun. Netw.,* vol. 2012, p. 176, 2012.

[14] M. Kobayashi, M. Debbah and J. Belfiore, "Outage efficient strategies in network MIMO with partial CSIT," in *Proc. ISIT'09*, 2009.

[15] J. Zhang and J. G. Andrews, "Adaptive spatial intercell interference cancellation in multicell wireless networks," *IEEE J. Sel. Areas Commun.,* vol. 28, no. 9, pp. 1455-1468, Dec. 2010.

[16] M. Schubert and H. Boche, "Solution of the multiuser downlink beamforming problem with individual SINR constraints," *IEEE Trans. Veh. Technol.,* vol. 53, no. 1, pp. 18-28, Jan. 2004.

[17] M. Sadek, A. Tarighat and A. H. Sayed, "A leakage-based precoding scheme for downlink multi-user MIMO channels," *IEEE Trans. Wireless Comm.,* vol. 6, no. 5, pp. 1711-1721, May 2007.

[18] H. W. Kuhn and A. W. Tucker, "Nonlinear programming," in *Proceedings of the Second Berkeley Symposium on Mathematical Statistics and Probability*, 1950.

[19] W. Karush, "Minima of Functions of Several Variables with Inequalities as Side Constraints," 1939.

[20] D. P. Palomar, J. M. Cioffi and M. A. Lagunas, "Joint Tx-Rx beamforming design for multicarrier MIMO channels: A unified framework for convex optimization," *IEEE Trans. Signal Process.,* vol. 51, no. 9, pp. 2381-2401, Set. 2003.

[21] M. Fuchs, G. Galdo and M. Haardt, "Low-Complexity Space-Time-Frequency Scheduling for MIMO Systems with SDMA," *IEEE Trans. Veh. Technol.,* vol. 56, no. 5, pp. 2775-2784, Sep. 2007.

[22] S. Haykin, Adaptive Filter Theory, Adaptive Filter Theory, 1996.

[23] S. Boyd and L. Vandenberghe, Convex optimization, Cambridge: Cambridge University Press, 2004.

[24] "LTE Physical Layer - General Description" , No 3. 3GPP TS 36.201 V8.1," 3GPP, 2007.

[25] "Radio transmission and reception", ETSI TS 136 521-1 version 8.2.1 Release 8, Annex B," 3GPP, 2009.

6 Conclusions and Future Work

6.1 Conclusions

The rapid growth of wireless traffic and the number of devices result in higher interference level and lower spectral efficiency, which significantly degrades the capacity gains promised by the single-cell MIMO systems. An option to improve the system capacity is reducing the cell size. However, the deployment of a large number of small cells has new technical challenges. Most of the interference mitigation challenges originate from the cell-edge users/devices that are increasing as the number of cells increase. Therefore, multicell cooperation or coordination where transmitting nodes cooperate in serving users; is a promising solution for cellular wireless systems to mitigate inter-cell interference, improving system fairness and increasing capacity. The proposed signal processing techniques in this thesis to attain that goal were divided into three main categories depending on the level of cooperation among BSs named as full-centralized, semi-distributed and full-distributed joint precoding and power allocation schemes.

In chapter 4 we proposed centralized precoding and power allocation schemes for downlink of multicell cellular systems. The aim was to propose practical centralized techniques to remove the

inter-cell interference and improve the user's fairness at the cell-edges. The main outcomes of chapter 4 are

- The interference is fully cancelled utilizing centralized schemes such as ZF and SVD based precoding. The precoding is done in JPU using the knowledge of all BSs channels.
- The system performance is further improved by allocating transmit powers to users and OFDM subcarriers optimally with per-BS PC and by minimizing the average BER at UTs (per-BS OPA). The process is also performed centrally in JPU and requires knowledge of global channel.
- In order to reduce the complexity, a suboptimal central power allocation scheme is proposed based on minimizing BER but first by imposing with TPC and finally computing powers with per-BS PC.
- To further reduce the complexity another suboptimal central power allocation is proposed based on minimizing inverse of SNRs of each UT allowing us to achieve a closed-form solution while previous solutions needed an iterative approach.
- The results have showed that the proposed full-centralized schemes for systems with multicell cooperation improve the system performance significantly, in comparison with the case where no precoding or power allocation is used. Also the performance of the proposed suboptimal algorithms, namely the per-BS SOIPA and per-BS SOCPA approaches, is very close to the optimal with the advantage of lower complexity.

In chapter 5 we proposed DZF precoder and power allocation techniques to mitigate inter-cell interference and improve system performance and user fairness at cell edges for downlink of multicell systems. We proposed centralized and distributed power allocation schemes (corresponding to semi-distributed and full-distributed schemes, respectively). The main outcomes of chapter 5 are

- The interference is cancelled or mitigated using proposed DZF precoder, by knowing just local CSI and shared data and for comparison purpose, MRT and DVSINR precoders were used.
- The system performance is further improved by proposing either centralized or distributed power allocation methods
- In case of centralized power allocation, the power elements are computed in a centralized fashion at the JPU by minimizing BER with per-BS power constraint. Two iterative criteria are considered, one optimal (Cent. per-BS OPA) that can be achieved

at the expense of some complexity and one suboptimal (Cent. per-BS SOIPA) with lower complexity aiming at practical implementations.

- To achieve even less complexity a closed-form power allocation scheme is proposed based on minimization of sum of inverse of SNRs of each UT (Cent. per-BS SOCPA).
- The results show significant improvement in system performance for all schemes comparing to the case of no power allocation for multicell system.
- It is shown that performance of semi-centralized approach tends to the one achieved by full-centralized, when the number of DoF available tends to the number of DoF available in the full-centralized system.
- Distributed power locations schemes are also proposed where the power elements are also computed locally at each base station just by assuming the knowledge of local CSI or long term equivalent channel non-local statistics.
- *Virtual* BER is defined by treating the multicell system as a superposition of interference-free single cell systems. The metric then is used to derive the power allocation scheme based on minimization of *virtual* BER, which implicitly provides user's fairness at the cell edges.
- Bounds for the solutions based on Lambert function are derived allowing reduced complexity.
- The results show that when the number of DoF of the equivalent channel variables increases, the proposed DZF approach tends to DVSINR. Also, the performance of the distributed power allocation schemes tends to one of semi-distributed strategies.
- It is also shown that, the minimization of the *virtual* uncoded BER produces an effective improvement on the performance of coded data.

6.2 Future Work

This thesis has focused on interference cancellation and improvement of system performance and providing user fairness, for multicell wireless systems by proposing precoding and power allocation schemes. The work carried out can be divided into three categories (full-centralized, semi-centralize and full-distributed schemes). In this study, some problems are left open for future research.

- In the proposed analysis, it was considered an ideal situation, i.e. fully removal of interference, perfect CSI, no delay between cooperating BSs and no synchronization issues. The study of the impact of each of these imperfections, on cooperated multicell system, is

of special importance, since it will make worse the improvement obtained by the joint or distributed processing, than the one presented.

- The availability of CSI at BSs is always limited, since it implies the existence of feedback channels, whose capacity is limited. Several assumptions can be made about it. Namely, it can be global (i.e. a BS knows the CSI of all users), local (i.e. a BS knows only the CSI of a small set of users) and it can be quantized and estimated (i.e. not exact). In the design of the proposed precoder it was assumed either global or local CSI. An interesting extension is to consider quantized and estimated CSI since it reflects a real-world scenario.
- The proposed semi-distributed and full-distributed algorithms can only be used for single-antenna. The case of multiple receives antennas remained untouched. It is interesting to extend the proposed schemes for this new setup.
- The schemes presented in this work were basically based on *enhanced scenario* of FUTON which was presented in chapter 3. It is also interesting to propose modified and extended schemes for FUTON *advanced scenario*.

Appendix

A. Derivation of MBER Power Coefficients

In this appendix we prove that the solution that minimizes (4.20) is given by (4.22). The problem of (4.20) can be solved by using the Lagrange multipliers method.

The power $p_{k,i,l}$ in (4.20) can be determined by setting the partial derivatives of $J_{c,1}$ with respect to $p_{k,i,l}, k = 1,\ldots,K, i = 1,\ldots,N_{r,k}, l = 1,...,N_c$ to zero, obtaining the following set of $N_c N_r$ equations,

$$\frac{\partial J_{c,1}}{\partial p_{k,i,l}} = -\frac{\lambda_{k,i,l}\, e^{\frac{-\lambda_{k,i,l} p_{k,i,l}}{2\sigma^2}}}{2KN_c N_{r_k}\sigma\sqrt{2\pi\lambda_{k,i,l} p_{k,i,l}}} + \mu = 0 \qquad \text{(A.1)}$$

Then both terms of (A.1) are squared,

$$\left(\frac{\lambda_{k,i,l} e^{\frac{-\lambda_{k,i,l} p_{k,i,l}}{2\sigma^2}}}{2KN_c N_{r_k}\sigma\sqrt{2\pi\lambda_{k,i,l} p_{k,i,l}}}\right)^2 = (\mu)^2 \qquad \text{(A.2)}$$

After some mathematical manipulations, (A.2) can be written as,

$$\underbrace{\frac{\lambda_{k,i,l}p_{k,i}}{\sigma^2}}_{X}e^{\underbrace{\frac{\lambda_{k,i,l}p_{k,i,l}}{\sigma^2}}_{X}}=\underbrace{\frac{\lambda_{k,i,l}^2}{8\pi\mu^2K^2N_c^2N_{r_k}^2\sigma^4}}_{Y} \tag{A.3}$$

Now the problem reduces to solve an exponential equation of type $Xe^X = Y$, and the solution can be given by the Lambert function of index 0,

$$X = W_0(Y) \tag{A.4}$$

Finally, replacing X and Y in (A.4) we obtain the powers $p_{k,i,l}$ that minimize (4.20),

$$p_{k,i,l}=\frac{\sigma^2}{\lambda_{k,i,l}}W_0\left(\frac{\lambda_{k,i,l}^2}{8\pi\mu^2N_r^2N_c^2\sigma^4}\right) \tag{A.5}$$

Also the solution for diversity mode (4.23) can be obtained in a similar way.

B. Derivation of MSINR Power Coefficients

In this appendix we prove that the solution that minimizes (5.21) is given by (5.24). The problem can be solved by using the Lagrange multipliers method.

The power $p_{k,i,l}$ in (5.21) can be determined by setting the partial derivatives of L with respect to $p_{b,k,l}, b=1,\ldots,B, k=1,\ldots,K, l=1,...,N_c$ to zero, obtaining the following set of BKN_c equations,

$$\frac{\partial L}{\partial p_{b,k,l}}=-\frac{\sigma^2h_{b,k,l}^{eq}}{\sqrt{p_{b,k,l}}\left(\sum_{i=1}^{B}\sqrt{p_{i,k,l}}h_{i,k,l}^{eq}\right)^3}+\mu=0 \tag{B.1}$$

By simple manipulation on (B.1) $p_{b,k,l}$ are obtained as,

$$p_{b,k,l} = \frac{\left(h_{b,k,l}^{eq}\right)^2}{\phi\sqrt{\left(\sum_{i=1}^{B}\left(h_{i,k,l}^{eq}\right)^2\right)^3}} \tag{B.2}$$

where $\phi = \sqrt{\mu/\sigma^2}$. The second phase consists in replacing ϕ by ϕ_b, $b = 1,...,B$ in (B.2), and then computing different ϕ_b, to satisfy the individual per-BS power constraints instead which leads to powers given by (5.24).

C. Proof of the Precoder Vectors' Equivalence

Here we prove that the distributed zero-forcing precoder vectors given by (5.8) are equivalent to the ones based on the orthogonal matrix projection discussed in some works (e.g., chapter 5 [13],[20])

$$\mathbf{w}_{b,k,l}^{(DZF)} = \frac{\mathbf{\Pi}_{\mathbf{A}_{b,k,l}}^{\perp}\mathbf{h}_{b,k,l}}{\left\|\mathbf{\Pi}_{\mathbf{A}_{b,k,l}}^{\perp}\mathbf{h}_{b,k,l}\right\|} \tag{C.1}$$

with $\mathbf{A}_{b,k,l} = \tilde{\mathbf{H}}_{b,k,l}^{H}$ and $\mathbf{\Pi}_{\mathbf{A}_{b,k,l}} = \mathbf{A}_{b,k,l}\left(\mathbf{A}_{b,k,l}^{H}\mathbf{A}_{b,k,l}\right)^{-1}\mathbf{A}_{b,k,l}^{H}$ is the orthogonal projection matrix onto the column space of $\mathbf{A}_{b,k,l}$, and that onto its orthogonal complement is $\mathbf{\Pi}_{\mathbf{A}_{b,k,l}}^{\perp} = \mathbf{I}_{N_{t_b}} - \mathbf{\Pi}_{\mathbf{A}_{b,k,l}}$. The precoder vector given by (5.8) can be re-written as

$$\mathbf{w}_{b,k,l}^{(DZF)} = \frac{\bar{\mathbf{W}}_{b,k,l}\bar{\mathbf{W}}_{b,k,l}^{H}\mathbf{h}_{b,k,l}}{\left\|\mathbf{h}_{b,k,l}^{H}\bar{\mathbf{W}}_{b,k,l}\right\|} \tag{C.2}$$

where $\bar{\mathbf{W}}_{b,k,l}\bar{\mathbf{W}}_{b,k,l}^{H}$ of size $N_{t_b} \times N_{t_b}$ is an orthogonal projection into the intersection of the nullspaces of all other users' channel vectors, and thus $\bar{\mathbf{W}}_{b,k,l}\bar{\mathbf{W}}_{b,k,l}^{H} = \mathbf{\Pi}_{\mathbf{A}_{b,k,l}}^{\perp}$. Now we should prove that the denominator of (C.1) and (C.2) are the same.

The square of the dominator of (C.1) can be written as

$$\begin{aligned}\left\|\boldsymbol{\Pi}^{\perp}_{\mathbf{A}_{b,k,l}}\mathbf{h}_{b,k,l}\right\|^2 &= \left(\boldsymbol{\Pi}^{\perp}_{\mathbf{A}_{b,k,l}}\mathbf{h}_{b,k,l}\right)^H\left(\boldsymbol{\Pi}^{\perp}_{\mathbf{A}_{b,k,l}}\mathbf{h}_{b,k,l}\right)\\ &= \mathbf{h}^H_{b,k,l}\left(\boldsymbol{\Pi}^{\perp}_{\mathbf{A}_{b,k,l}}\right)^H\boldsymbol{\Pi}^{\perp}_{\mathbf{A}_{b,k,l}}\mathbf{h}_{b,k,l} = \mathbf{h}^H_{b,k,l}\boldsymbol{\Pi}^{\perp}_{\mathbf{A}_{b,k,l}}\mathbf{h}_{b,k,l}\end{aligned} \tag{C.3}$$

since $\left(\boldsymbol{\Pi}^{\perp}_{\mathbf{A}_{b,k,l}}\right)^H\boldsymbol{\Pi}^{\perp}_{\mathbf{A}_{b,k,l}} = \boldsymbol{\Pi}^{\perp}_{\mathbf{A}_{b,k,l}}$.

The square of the dominator of (C.2) is given by

$$\begin{aligned}\left\|\mathbf{h}^H_{b,k,l}\bar{\mathbf{W}}_{b,k,l}\right\|^2 &= \left(\mathbf{h}^H_{b,k,l}\bar{\mathbf{W}}_{b,k,l}\right)\left(\mathbf{h}^H_{b,k,l}\bar{\mathbf{W}}_{b,k,l}\right)^H\\ &= \mathbf{h}^H_{b,k,l}\bar{\mathbf{W}}_{b,k,l}\bar{\mathbf{W}}^H_{b,k,l}\mathbf{h}_{b,k,l} = \mathbf{h}^H_{b,k,l}\boldsymbol{\Pi}^{\perp}_{\mathbf{A}_{b,k,l}}\mathbf{h}_{b,k,l}\end{aligned} \tag{C.4}$$

and thus both denominators are the same.

D. Derivation of Lamberts' Function Bounds

In this section we prove the following Lambert function bounds

$$\alpha\log(x) \le W_0(x) \le x,\ x \ge 0 \wedge \alpha \in \left[0, \frac{e}{1+e}\right] \tag{D.1}$$

We are only interested in the case of $x \ge 0$, even if $W_0(x)$ is defined in a larger domain. The Lambert function is defined as (chapter 5 [25])

$$W_0(x)e^{W_0(x)} = x,\ x \ge -e^{-1} \tag{D.2}$$

Upper bound

The first derivative is

$$W_0{}'(x) = \frac{W(x)}{x(1+W(x))} \tag{D.3}$$

From the Lambert function definition in (D.3) we can write

$$W_0(x) \geq 0, x \geq 0 \tag{D.4}$$

Therefore, $W_0'(x)$ is always positive and $W_0(x)$ strictly increasing. From (D.4) we have

$$x(1+W(x)) \geq 0,\ x \geq 0 \tag{D.5}$$

Taking the exponent of both sides of (D.4)

$$e^{W_0(x)} \geq 1, x \geq 0 \tag{D.6}$$

If both sides of (D.6) are multiplied by $W_0(x)$ and the inequality of (D.4) is used

$$W_0(x)e^{W_0(x)} \geq W_0(x), x \geq 0 \tag{D.7}$$

From the Lambert function definition, the corresponding upper bound is obtained

$$x \geq W_0(x), x \geq 0. \tag{D.8}$$

Lower bound

Let us define the function $f(x):[0,+\infty[\rightarrow \mathbb{R}$

$$f(x) = W_0(x) - \alpha Log(x) \tag{D.9}$$

whose first derivative is

$$f'(x) = \frac{(1-\alpha)W(x) - \alpha}{x(1+W(x))} \tag{D.10}$$

From (D.5) $f'(x)$ is a strictly increasing function since $W_0(x)$ is also strictly increasing. Therefore, $f'(x)$ has at most one zero (x_0)

$$x_0 = \frac{\alpha}{1-\alpha} Exp\left[\frac{\alpha}{1-\alpha}\right],\ \alpha < 1 \wedge x_0 \neq 0 \tag{D.11}$$

and due to it monotonic properties

$$\begin{aligned} f'(x) &< 0,\ x < x_0 \\ f'(x) &\geq 0,\ x \geq x_0 \end{aligned} \tag{D.12}$$

$f(x_0)$ is the global minimum of $f(x)$

$$f(x_0) = \frac{\alpha}{1-\alpha} - \alpha \log\left(\frac{\alpha}{1-\alpha} Exp\left[\frac{\alpha}{1-\alpha}\right]\right). \tag{D.13}$$

Solving the inequality $f(x_0) \geq 0$ we get

$$0 \leq \alpha \leq \frac{e}{1+e} \tag{D.14}$$

Hence, since $f(x_0)$ is the global minimum of $f(x)$

$$f(x) \geq 0,\ x \geq 0 \wedge \alpha \in \left[0, \frac{e}{1+e}\right] \tag{D.15}$$

As a consequence of (D.15), we obtain the following Lambert function lower bound

$$W_0(x) \geq \alpha \log(x),\ x \geq 0 \wedge \alpha \in \left[0, \frac{e}{1+e}\right] \tag{D.16}$$